LOAN DOCUMENT

PHOTOGRAPH THIS SHEET

AD-A254 037

DTIC ACCESSION NUMBER

LEVEL

INVENTORY

AFWAL-TR-88-4047

DOCUMENT IDENTIFICATION

Dec 88

DISTRIBUTION STATEMENT A
Approved for public release;
Distribution Unlimited

DISTRIBUTION STATEMENT

NTIS GRA&I
DTIC TRAC
UNANNOUNCED
JUSTIFICATION

BY
DISTRIBUTION/
AVAILABILITY CODES

DISTRIBUTION	AVAILABILITY AND/OR SPECIAL
A-1	

DISTRIBUTION STAMP

DTIC ELECTE
AUG 7 1992
S C

DATE ACCESSIONED

DTIC QUALITY INSPECTED 5

DATE RETURNED

92 8 05 030

DATE RECEIVED IN DTIC

92-21372

REGISTERED OR CERTIFIED NUMBER

PHOTOGRAPH THIS SHEET AND RETURN TO DTIC-FDAC

HANDLE WITH CARE

DTIC FORM 70A JAN 90 DOCUMENT PROCESSING SHEET PREVIOUS EDITIONS MAY BE USED UNTIL STOCK IS EXHAUSTED.

LOAN DOCUMENT

UNCLASSIFIED

SECURITY CLASSIFICATION OF THIS PAGE

REPORT DOCUMENTATION PAGE

Form Approved OMB No. 0704-0188

1a. REPORT SECURITY CLASSIFICATION UNCLASSIFIED	1b. RESTRICTIVE MARKINGS None
2a. SECURITY CLASSIFICATION AUTHORITY	3. DISTRIBUTION/AVAILABILITY OF REPORT Approved for public release; distribution is unlimited.
2b. DECLASSIFICATION/DOWNGRADING SCHEDULE	
4. PERFORMING ORGANIZATION REPORT NUMBER(S) FR-19528	5. MONITORING ORGANIZATION REPORT NUMBER(S) AFWAL-TR-88-4047
6a. NAME OF PERFORMING ORGANIZATION United Technologies Corp. Pratt & Whitney Engineering 6b. OFFICE SYMBOL (If applicable)	7a. NAME OF MONITORING ORGANIZATION Materials Laboratory (AFWAL/MLLM) Air Force Wright Aeronautical Laboratories
6c. ADDRESS (City, State, and ZIP Code) P.O. Box 109600 West Palm Beach, FL 33410-9600	7b. ADDRESS (City, State, and ZIP Code) Wright-Patterson AFB, OH 45433-6533
8a. NAME OF FUNDING/SPONSORING ORGANIZATION AFWAL Materials Laboratory 8b. OFFICE SYMBOL (If applicable) AFWAL/MLLM	9. PROCUREMENT INSTRUMENT IDENTIFICATION NUMBER F33615-82-C-5066
8c. ADDRESS (City, State, and ZIP Code) AFWAL/MLLM Wright-Patterson AFB, OH 34322-6533	10. SOURCE OF FUNDING NOS. PROGRAM ELEMENT NO.: 62102F PROJECT NO.: 2420 TASK NO.: 02 WORK UNIT ACCESSION NO.: 20
11. TITLE (Include Security Classification) Effect of Cyclic Strain/Temperature Exposure on Fatigue Life of Coated Turbine Alloys	
12. PERSONAL AUTHOR(S) Barkalow, R.H.	
13a. TYPE OF REPORT Final 13b. TIME COVERED FROM August 83 TO March 87	14. DATE OF REPORT (Year, Month, Day) 1988 December 15. PAGE COUNT 99
16. SUPPLEMENTARY NOTATION	

17. COSATI CODES			18. SUBJECT TERMS (Continue on reverse if necessary and identify by block number)
FIELD	GROUP	SUB. GR.	Coatings; Coated Turbine Alloys; Coated Superalloys; Fatigue Life; Cyclic Strain; Temperature Exposure
11	06	00	
11	03	00	

19. ABSTRACT (Continue on reverse if necessary and identify by block number)

This program sought basic information about the behavior of coated superalloys versus strain-temperature history in high-temperature, thermal-mechanical exposure. The test plan was based on the observation that test cycle shape strongly impacts the thermal-mechanical-fatigue (TMF) behavior. We found that increasing T_{max} of the Type 1 cycle from 1900 to 2100°F shortened the initiation period for TMF cracking and reduced cycles to specimen failure by about 30 to 50 percent. A more radical change in cycle shape, namely a four-sided shaped cycle, was less mechanically damaging (a factor of two) but more severely oxidizing than Type 1 cycles between the same temperature and strain limits. Cyclic speed experiments showed that crack initiation and cycles-to-failure data were not strongly sensitive to testing speed in the range of 1 to 4 cycles per minute. Lower N_f values for slow speed tests are believed to reflect crack growth in the substrate rather than coating effects. Shut-down steps and hold times at T_{max} and during cool-down from T_{max} generally decreased N_f values.

20. DISTRIBUTION/AVAILABILITY OF ABSTRACT ☒ UNCLASSIFIED/UNLIMITED ☐ SAME AS RPT. ☐ DTIC USERS	21. ABSTRACT SECURITY CLASSIFICATION UNCLASSIFIED

22a. NAME OF RESPONSIBLE INDIVIDUAL	22b. TELEPHONE (Include Area Code)	22c. OFFICE SYMBOL
Norman M. Geyer	(513) 255-9822	AFWAL/MLLM

DD Form 1473, JUN 86 *Previous editions are obsolete.* UNCLASSIFIED

SECURITY CLASSIFICATION OF THIS PAGE

R19888/12

CONTENTS

CONTENTS (Continued)

ILLUSTRATIONS

ILLUSTRATIONS (Continued)

ILLUSTRATIONS (Continued)

ILLUSTRATIONS (Continued)

ILLUSTRATIONS (Continued)

ILLUSTRATIONS (Continued)

TABLES

SECTION 1.0
INTRODUCTION

1.0 OVERALL OBJECTIVE

The intent of this program was to seek basic information about the behavior of coated superalloys versus strain-temperature history in high-temperature thermal mechanical exposure. It was hoped that the data would be sufficiently detailed and quantified to impact future alloy/coating development efforts and to permit a qualitative or semi-quantitative prediction of the durability of various coating/substrate combinations as a function of design and mission of the engine. The incentive for such information is that thermal mechanical fatigue rather than oxidation or hot corrosion is often the life-limiting degradation mechanism of coated engine components. Further advances in overall component durability may thus depend primarily on achieving better thermal fatigue resistance while maintaining the already adequate oxidation protection afforded by current generation overlay coatings.

1.1 THERMAL MECHANICAL FATIGUE — BACKGROUND DISCUSSION

The term thermal mechanical fatigue (TMF) implies a unique degradation mechanism due to simultaneously varying temperature and strain cycles (refs. 1 through 7). The temperature cycles are imposed by start-up, thrust change, and shutdown of the engine, while the resultant mechanical strains are induced by temperature differences on the airfoil surface. Material behavior under these conditions can be influenced by oxidation and interdiffusion effects in the high-temperature portion of the thermal cycle. In addition, it is vastly more complex than isothermal fatigue because the temperature dependent mechanical properties, i.e., elastic modulus, yield strength, creep resistance, and ductility, are continuously changing as the material is mechanically strained or loaded.

While the possible combinations of temperature and strain cycles are indeed infinite, the simplified limiting cases are as sketched in Figure 1. Cycle 1 is characterized by maximum tensile strain at minimum temperature and is representative of more rapidly cooled sections of the airfoil (the leading and trailing edges) which are placed in tension on cooling. Cycle 2 involves tensile strain at high temperatures and is generally representative of more slowly cooled portions of the airfoil.

Figure 1 also shows qualitatively the effect of stress relaxation and thermal expansion mismatch on elastic strain range in the coating. Basically, the relaxation effect is that elastic strain in the coating relaxes to zero at the maximum temperature of the cycles because the coating is very weak at high temperatures. Superimposed on the relaxation effect is a difference in slope of the strain-temperature curve due to thermal expansion mismatch, where the point of greatest practical significance is the increased Cycle 1 strain in the coating if $\alpha_c > \alpha_s$ (which is the case for current generation overlay coatings and superalloy substrates).

The combination of stress relaxation and thermal expansion mismatch renders Type 1 cycles particularly damaging to coated systems, since the direction of both effects is to increase tensile strain at low temperatures where coating ductility is low. Type 2 cycles are much less damaging because the coating is relatively ductile under high-temperature tension and sufficiently strong to resist the low temperature compression.

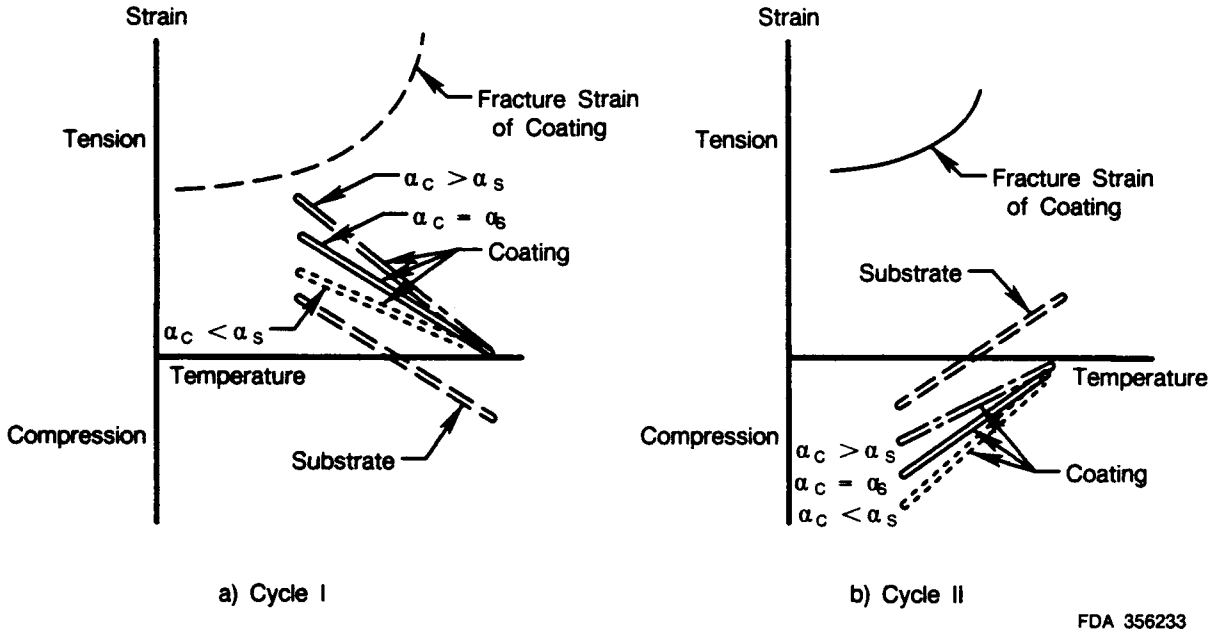

Figure 1. Definition of Idealized TMF Cycles, Including Effect of Stress Relaxation and Thermal Expansion Mismatch on Elastic Strain in the Coating

Although simplified as far as possible, the straight-line cycles still involve at least five major test variables: (1) T_{min}, (2) T_{max}, (3) strain range, (4) mean strain, and (5) speed of the cycle. The latter might be further expanded to include isothermal soaking to simulate steady-state cruise conditions between the thrust change transients which induce the thermal and mechanical strains. Since this number of variables can easily become unmanageable, it has generally been necessary to fix T_{min}, T_{max}, mean strain, and cyclic rate and present TMF data as cycles to failure versus strain range for the material or material/coating combination being evaluated.

Hence, most of the TMF testing to date — at least that performed at Pratt & Whitney — has involved Type 1 cycles between temperature limits of 800 to 1900°F (427 to 1038°C). These points represent a compromise between realism and experimental convenience. The 1900°F endpoint was representative of maximum metal temperatures in turbine airfoils at the time the test was developed. It is readily attainable experimentally and presents no testing difficulties, i.e., the material is not excessively weak or heavily oxidized at this temperature. Likewise the 800°F minimum can be justified from metal temperatures during powerdown but also facilitates testing since lower temperatures would increase cycle time because cooling rates become much slower as temperature decreases.

Strain ranges of the order of 0.3 to 0.5 percent are believed to be most representative of service conditions, although much testing has been done at higher strain limits (0.5 to 0.9 percent) to accelerate failure.

Type 1 TMF behavior between temperature limits of 800 to 1900°F and strain ranges of 0.3 to 0.9 percent has been extensively documented and analyzed (refs. 6 and 8 through 12). Relative durability of various materials and alloy/coating systems in Type 1 TMF tests is generally correlatable with static mechanical properties (strength, modulus, ductility) and microstructure (particularly columnar versus equiaxed grains). However, the straight-line cycle and 1900°F maximum temperature do not reproduce the contribution of oxidation and coating/substrate interdiffusion processes to engine-induced degradation, particularly in the case of advanced

engines where maximum metal temperatures are much higher than 1900°F. Further, the strain/temperature history of an airfoil segment is not the idealized straight line of Type 1 cycles.

The deviation between the Type 1 cycle and the actual strain/temperature history of turbine airfoils becomes especially pronounced in the case of military fighter engines, where the rapid acceleration capability required for combat maneuverability imposes a more severe fatigue environment on fighter (as opposed to transport) aircraft. The higher strain range and more open cycle characteristic of the former are shown by the comparison of typical cycles, as sketched in Figure 2.

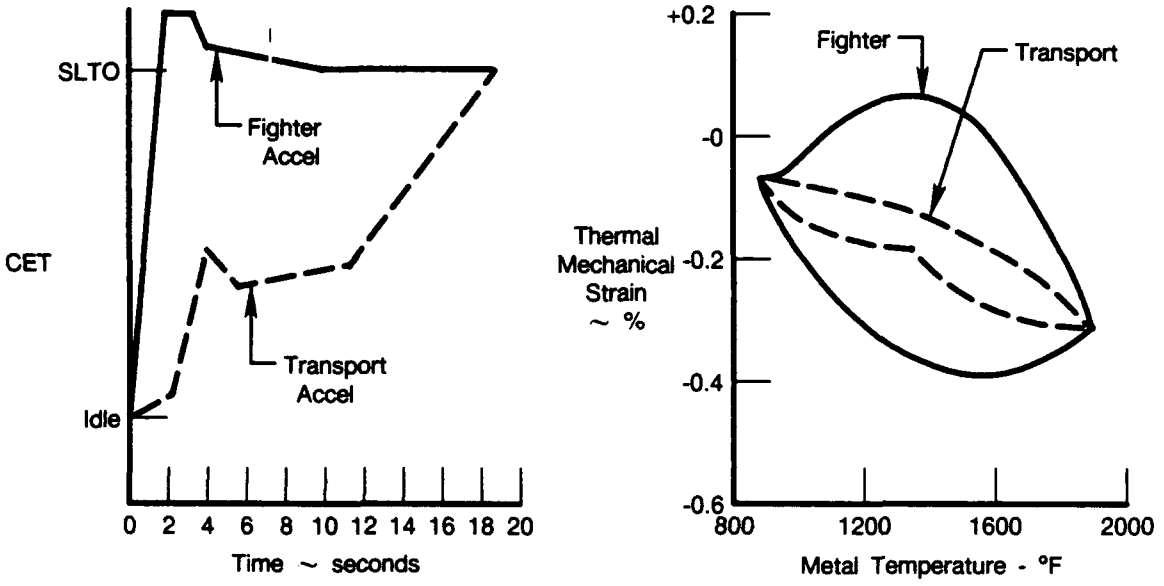

Figure 2. Schematic Diagram of Strain/Temperature History of Fighter Versus Transport Engines

To insure relevance of TMF data to these conditions, i.e., higher temperatures and complex cycle shapes, it is necessary to define the effect of maximum temperature and the nature of material degradation produced by Type 1 versus more realistic cycles.

An idealized cycle of the form shown in Figure 3 is believed to represent the life limiting TMF conditions encountered in high pressure turbine airfoils of fighter aircraft engines (ref. 13). The minimum temperature (800°F) and small compressive strain at T_{min} are characteristic of critical airfoil locations while the engine operates at idle power. During power excursion to takeoff thrust, thermal transients effect an increase in compressive strain because expansion is constrained by adjacent cooler material. Maximum compressive strains of the order of 0.4 to 0.6 percent are reached at temperatures near 1800°F.

As temperatures continue to increase and stabilize, thermal gradients decrease and strain relaxes to an intermediate level at a maximum metal temperature of about 2000°F. A hold time at high temperature may occur as engine power remains at rated thrust during steady-state cruise; the hold time may be included in the test cycle to simulate this condition and the resultant oxidation/interdiffusion of the coating substrate system.

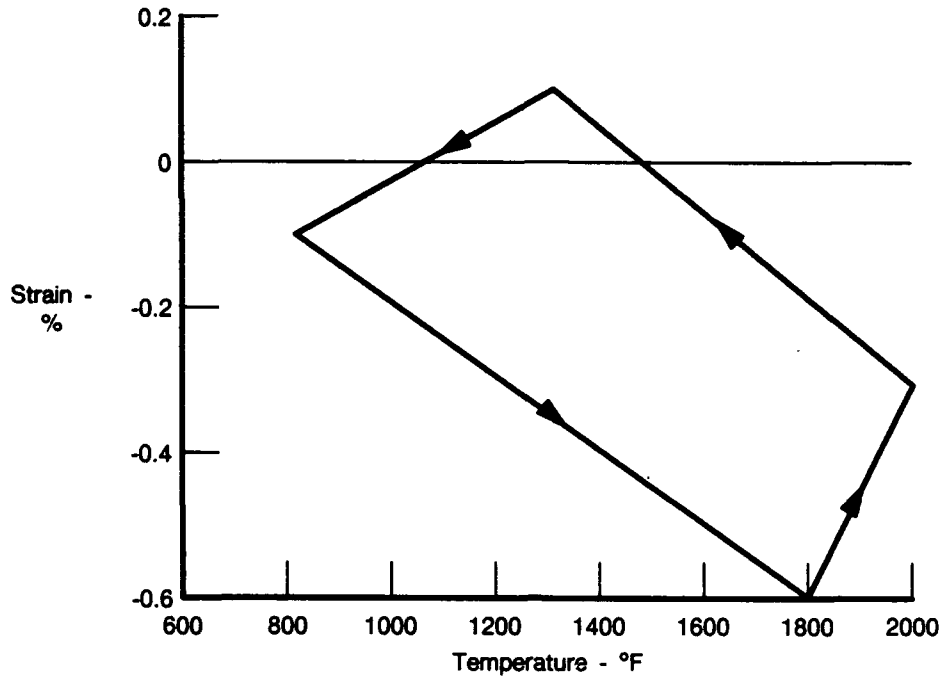

FDA 356232

Figure 3. Quadrilateral TMF Cycle for Optimum Simulation of Strain Temperature History of Turbine Airfoils in Fighter Aircraft

Conversely on engine deceleration, the critical airfoil site is rapidly cooled and held in tension by adjacent hotter material. Maximum tensile strain is predicted to be approximately +0.1 percent at 1300°F. With further cooling toward idle power level, metal temperature again stabilizes and tensile strain relaxes to a slight compression at 800°F.

This cycle presents the possibility of fatigue damage to coated airfoils by several mechanisms:

- Lack of ductility in low temperature, tensile strainportions of the cycle where the coating is strong but relatively brittle
- Excessive plastic and/or creep deformation in the high temperature portion of the cycle where the coating material is ductile but very weak
- Effects of oxidation and/or interdiffusion due to time-at-temperature exposure.

These processes are not mutually exclusive, and the ultimate effect is probably an interaction between all three (e.g., low temperature cracking can lead to increased oxidation because the cracks provide a path for surface diffusion of oxygen; and, vice versa, oxide particles can provide sites for crack initiation). Coating/substrate interdiffusion can contribute to failure via loss of oxidation resistance or ductility with change in coating composition, or by decrease in load-bearing cross section if the substrate superalloy is weakened by dilution with elements of the coating.

1.2 EXPERIMENTAL APPROACH

The overall technical objective of this work was reduced to a test plan intended to establish the following:

- Effect of higher maximum temperatures (since advanced engines are running hotter than T_{max} of most available thermal mechanical data)
- Effect of mean strains during test (since the engine cycle involves a net compressive strain)
- Effect of hold time at or near T_{max} (to increase the role of oxidation /interdiffusion processes in component degradation)
- Comparison of Type 1 versus more realistic test cycles (to observe the metallurgical effects of different strain/temperature histories and facilitate correlation of laboratory data with service experience
- Effect of type of coating on fatigue behavior of the coating/substrate combination in Type 1 and quadrilateral-shaped cycles (to observe the effect of different microstructure and properties of the coating at fixed strain/temperature parameters).

As discussed in detail when presenting the data, a midprogram modification of the test plan provided for additional study of quadrilateral cycle shape effects and characterization of a two-layer strain isolator system made by air-spraying of a porous underlayer.

SECTION 2.0
PROGRAM PLAN AND SUMMARY

As originally conceived, this program consisted of four technical tasks and their correlation into a cyclic damage model. The test plan was based on observations in a preceding contract (Advanced Coating Research and Development, ref. 10) that cycle shape strongly impacts TMF behavior and that major changes in composition and microstructure of overlay coatings result from time-at-temperature interdiffusion. It was hypothesized that such changes in coating composition (and, consequently, in mechanical properties and thermal expansion coefficient of the coating material) might be a factor in determining the TMF durability of the coating/substrate system. Hence the experimental approach was to study cycles to initiation/failure versus cycle shape in Task 1 for the purpose of selecting an optimum cycle and material. In the remaining tasks of the program, coated samples were to be exposed to various percentages of expected cyclic lifetime to determine if fatigue behavior could be related to degradation of the composition and microstructure of the coating during TMF exposure.

Key results of Task I were that increasing T_{max} of the Type 1 cycle from 1900 (as in most of the previous work) to 2100°F shortened the initiation period for TMF cracking and reduced cycles to specimen failure by a factor of about 30 to 50 percent. A more radical change in cycle shape — namely a four-sided quadrilateral or quad-shaped cycle — was found to be less mechanically damaging (cycles to initiation and failure were approximately a factor of two greater) but more severely oxidizing than Type 1 cycles between the same temperature and strain limits.

Although the longer testing times of the quad cycle maximized the opportunity for documenting the anticipated metallurgical changes in the coating, metallography of short-time specimens suggested coating cracks were developing and propagating into the substrate long before the composition and microstructure of the coating were significantly altered by time-at-temperature exposure. Further, a direct attempt to measure the effect of TMF exposure on coating ductility by acoustic emission during tensile testing and fluorescent penetrant inspection was not successful. Major acoustic events occurred at approximately the same tensile strains in both as-processed and TMF-exposed coatings, and severe rumpling of the TMF-exposed coatings precluded documentation of tensile cracks by fluorescent penetrant.

Since these results rendered the rest of the test plan untenable, Tasks II and III of the original contract were terminated, and Tasks IV and V were redirected toward a more extensive investigation of cycle shape effects, comparison of aluminide versus overlay coatings, and layered microstructure effects. The new Task IV was considered appropriate because prior work had demonstrated the critical importance of cycle shape but had not thoroughly investigated the multiplicity of cyclic variables — e.g., cyclic speed, shutdown steps, hold time, and mean strain effects — which might influence the initiation and propagation of TMF cracks. Task V was formulated to study multilayer coatings and incorporate a novel strain isolation concept suggested by personnel at United Technologies Research Center.

The cyclic speed experiments showed that crack initiation and cycles to failure data were not strongly sensitive to testing speed in the range of approximately 1 to 4 cycles per minute. A major consequence of this result was that remaining tests in the program were routinely run at 4 cpm, with significant savings in time and cost of the test. Lower Nf values for slow speed tests (½ to ¼ cycles per minute) are believed to reflect crack growth in the substrate rather than coating effects.

Shutdown steps were found to decrease N_f values, but their utility in defining mechanisms or relative coating performance has yet to be demonstrated. A basis for recommending a shutdown step for evaluation of coatings effects in TMF was not established by this work.

As in the case of the shutdown steps, hold times inposed at T_{max} and during cool-down from T_{max} of the quad cycle generally decreased N_f values, but post-test metallography did not relate this to coating effects. Even in prolonged holds at T_{max}, oxidation of the coating was not significantly increased. Coating microstructures were indeed affected, but the loss of loadbearing cross section was not significant and the samples contained numerous secondary cracks much deeper than the interdiffusion effects.

Some of the data on mean stress effects are not readily interpretable, probably because of typical scatter encountered in fatigue testing. An overall subjective interpretation is that cycle shape — particularly the length of the high-temperature Type 2 leg of the quad cycle — is far more important than mean stress.

Practical advantages of a strain-isolating layer were not demonstrated. Although examples of a crack stopping at large pores in an air-sprayed compliant layer were documented, most of the cracks continued to propagate, and the compliant layer tended to debond when intersected by a TMF crack.

Modified quad cycles run late in the program sometimes showed a crystallographic effect. The form of this effect was a striking four-fold symmetry of the fracture surface (with maximum crack growth along <100> and minimum growth in <110> directions) and sometimes a symmetrical oxidation pattern on uncoated material (heavier oxidation near normals to <100> directions). The observation is considered interesting because engine-induced TMF damage of aluminide coatings often takes the form of herringbone cracks delineating the octahedral planes of directionally solidified single crystals or columnal grains. This role of crystallographic effects in TMF behavior has not been well reproduced in testing machine TMF experiemnts, and further study might lead to interesting developments.

SECTION 3.0
MATERIALS AND PROCEDURE

The number of test variables inherent in TMF behavior necessitated restriction of the number of materials to be studied in this program. The substrate alloy for all specimens was PWA 1480 single crystal (nominal composition (weight percent): Ni-5Co-10Cr-5Al-1.5Ti-4W-12Ta). The material was cast in 10-bar clusters and solutionized at 2350°F for 2 hours. Single crystal microstructure and satisfactory orientation (bar axis within 10 degrees of <100>) were confirmed by macroetching and Laue patterns prior to machining of specimens.

The overlay coating material for most of the program was electron beam vapor deposited (EB-PVD) or low pressure plasma sprayed (LPPS) NiCoCrAlY (nominal composition: Ni-23Co-18Cr-12.5Al-0.5Y), chosen because of extensive Pratt & Whitney experience with processing and service performance of these coatings. Except as discussed for the experimental strain isolating layer in Task V, the coatings were applied by standard EB-PVD and LPPS processes per specifications PWA 270 and PWA 276, respectively. The LPPS samples (used exclusively except for initial testing to compare crack initiation in EB-PVD versus LPPS microstructures) were annealed 1 hour at 1975°F, peened at 19N, annealed 3 hours at 1975°F, tumble-finished to 30μ in AA, and aged 32 hours at 1600°F.

To acquire data on another coating and gain longer exposure times for the accumulation of microstructural damage prior to crack initiation, Type 1 and quad cycle tests were run on a tantalum-strengthened coating of nominal composition Ni-9.6Cr-11.7Al-6.1Ta-0.22Hf-0.50Y. This composition was formulated per results and rationalizations on Advanced Coating Research that stronger coatings of low thermal expansion mismatch offered potential for an improved balance of oxidation life and fatigue resistance.

When the test plan was modified to compare diffusion coatings with NiCoCrAlY overlays, the system selected was PWA 275 gas phase aluminide. This coating is bill-of-material in the F100 engine.

The extensive testing and experimentation required in this program are rendered cost effective by the load-adjusted thermal mechanical fatigue test described in references 8 and 10. The test equipment is a conventional low cycle fatigue test machine (Figure 4) modified to simultaneously ramp and control temperature. The machine contains two electronically controlled servosystems. One is a hydraulic system for closed-loop control of load, strain, or displacement; the other servosystem is used concurrently for closed-loop control of specimen temperature. The command waveforms for each parameter are independent and can be programmed to conduct any load-temperature cycle within the ramp rate capacity of the hydraulic and thermal servosystems.

The temperature control system uses direct resistance heating from a low-voltage, high-current transformer. Temperature is measured and controlled by an infrared pyrometer sighted on the specimen gage section. A heated sample is shown in Figure 5, where the sharpness of the temperature gradients and efficiency of the cooling system are demonstrated by the operator's unprotected fingers less than an inch from the 2000°F gage section of the sample.

FC 81676

Figure 4. Load Controlled Thermal Mechanical Fatigue Test Machine

The initial quad cycle experiments required strain controlled calibration tests using the hollow tube specimen illustrated in Figure 6; the specimen design for load-adjusted TMF testing and post-test ductility measurements is shown in Figure 7.

FE 229805

Figure 5. TMF Specimen Under Test

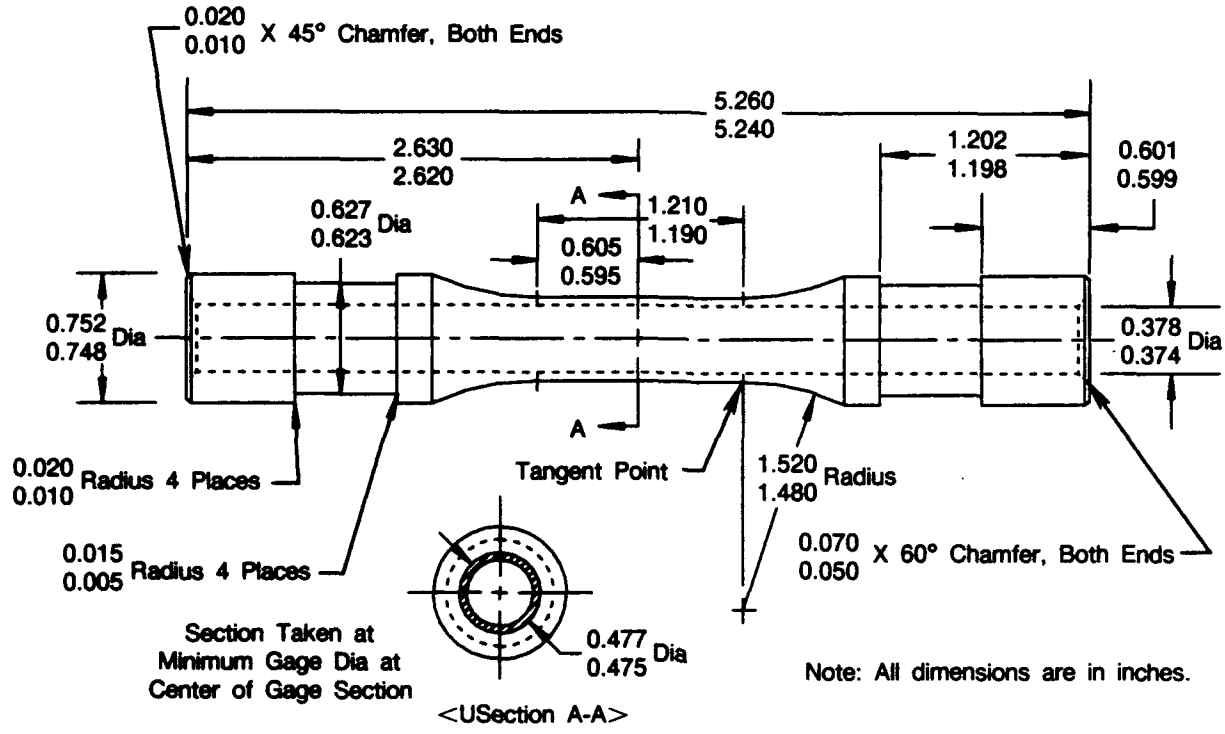

Figure 6. Hollow Tube Sample for Strain Controlled TMF Testing

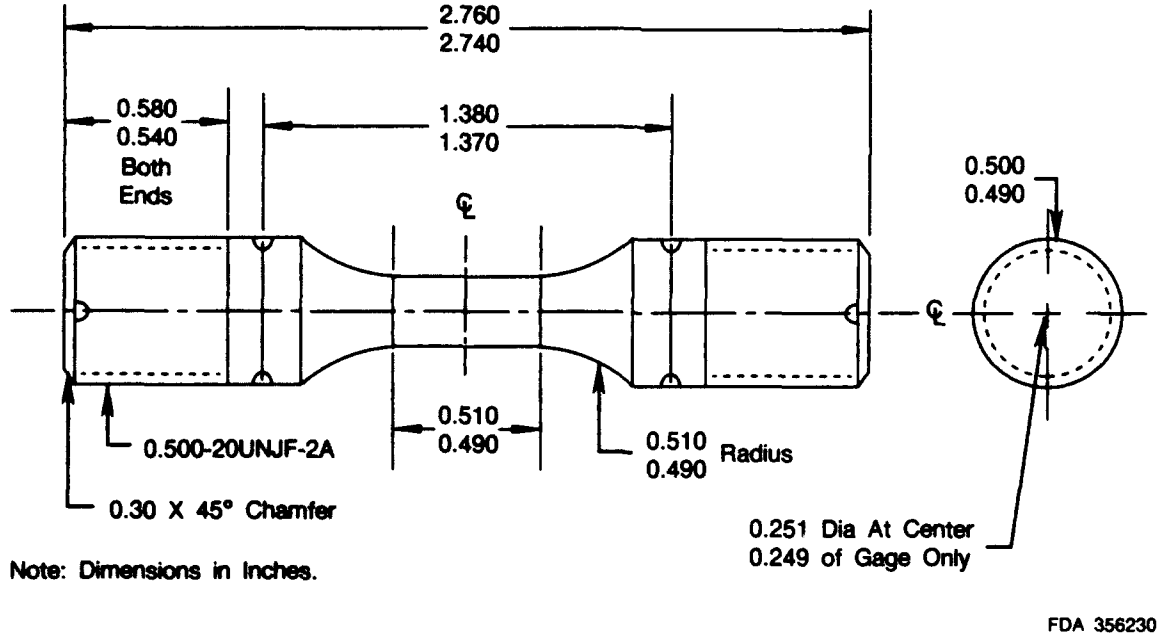

Figure 7. Load Control TMF/Coating Ductility Specimen

SECTION 4.0
TASK I — EFFECTS OF STRAIN-TEMPERATURE CYCLE ON TMF LIFE

4.1 OBJECTIVE

The purpose of this task was to generate basic thermal mechanical fatigue data (i.e. cycles to initiation and failure versus strain range) for the selected materials and cyclic variables.

4.2 RESULTS AND DISCUSSION

4.2.1 Crack Initiation in Short-Time Type 1 Cycles

There are two basic aspects to fatigue degradation: (1) time to crack initiation and (2) crack growth rate. To examine the initial stages of these mechanisms, a series of Type 1 tests, all at 0.6 percent strain range and 800 to 1900°F temperature limits, was run with hourglass samples left over from a preceding contract. Cyclic exposure was terminated prior to failure to document the extent, depth, and morphology of TMF cracks.

The initial test of LPPS NiCoCrAlY was run to 2179 cycles and stopped at that point due to visual observation of numerous short cracks; typical depth and morphology are shown in Figure 8. All of the cracks were wide but shallow; metallographic examination on two planes of polish revealed none extending into the substrate.

Figure 8. LPPS NiCoCrAlY (PWA 276) Coating on PWA 1480 TMF Sample (Exposure Time = 2179 Cycles)

Scanning microscopy of the polished section was conducted to attempt definition of the crack path. However, the photomicrographs are not easily interpreted, perhaps because of the

width of the crack. Figure 9, for example, includes evidence of separation at $\gamma - \beta$ interfaces, but also shows cracking through γ.

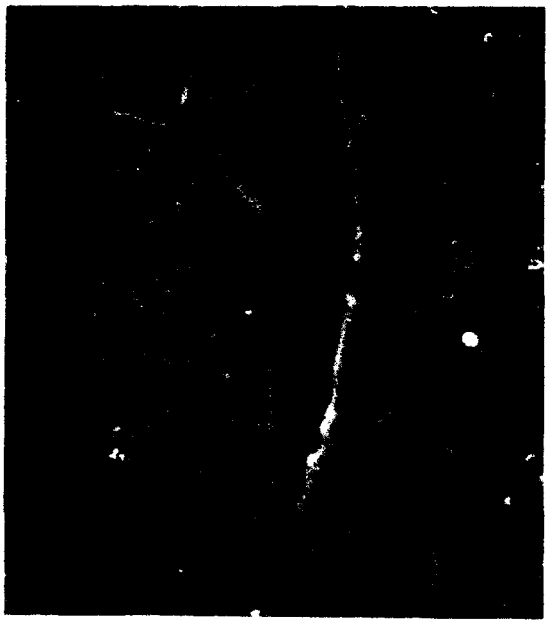

Figure 9. SEM Image of Crack Tip in Sample of Figure 8

Testing of EB-PVD NiCoCrAlY was terminated at 1000 cycles due to the surface condition illustrated in Figure 10; metallography showed that most of the cracks were attributable to leaders. There were 37 cracks on the plane of polish examined; 12 propagated into the substrate.

Since cracking was extensive after 1000 cycles, the next two samples were characterized after 500. Cracking of the EB-PVD coating at this point is illustrated in Figure 11. The cracks were short (<1 mm), wavy, and relatively wide in the center. Some were initiated at corn kernels, while others were not readily traced to structural defects.

Crack morphology in the longitudinal section was consistent with the wide, ductile appearance typical of binocular microscope and SEM characterization results. Some of the cracks were obviously related to leaders in the columnar microstructure (Figure 12). Since these features are unavoidable in the vapor deposited microstructure, it appears impossible to establish a meaningful value of cycles-to-crack initiation for an EB-PVD coating.

For LPPS NiCoCrAlY (PWA 276) of the same nominal composition, no cracks were detected by binocular microscope, SEM, or metallography after 500 cycles. At 1000 cycles, cracking was discernable by careful binocular microscope examination, although the cracks were not nearly as evident as those on EB-PVD NiCoCrAlY after the same cyclic exposure. Again the cracks appeared relatively wide in polished cross sections (Figure 13), but none were observed to penetrate the coating. Scanning microscopy of the crack tip suggested a tendency to follow grain boundaries and $\gamma - \beta$ interfaces (Figure 14).

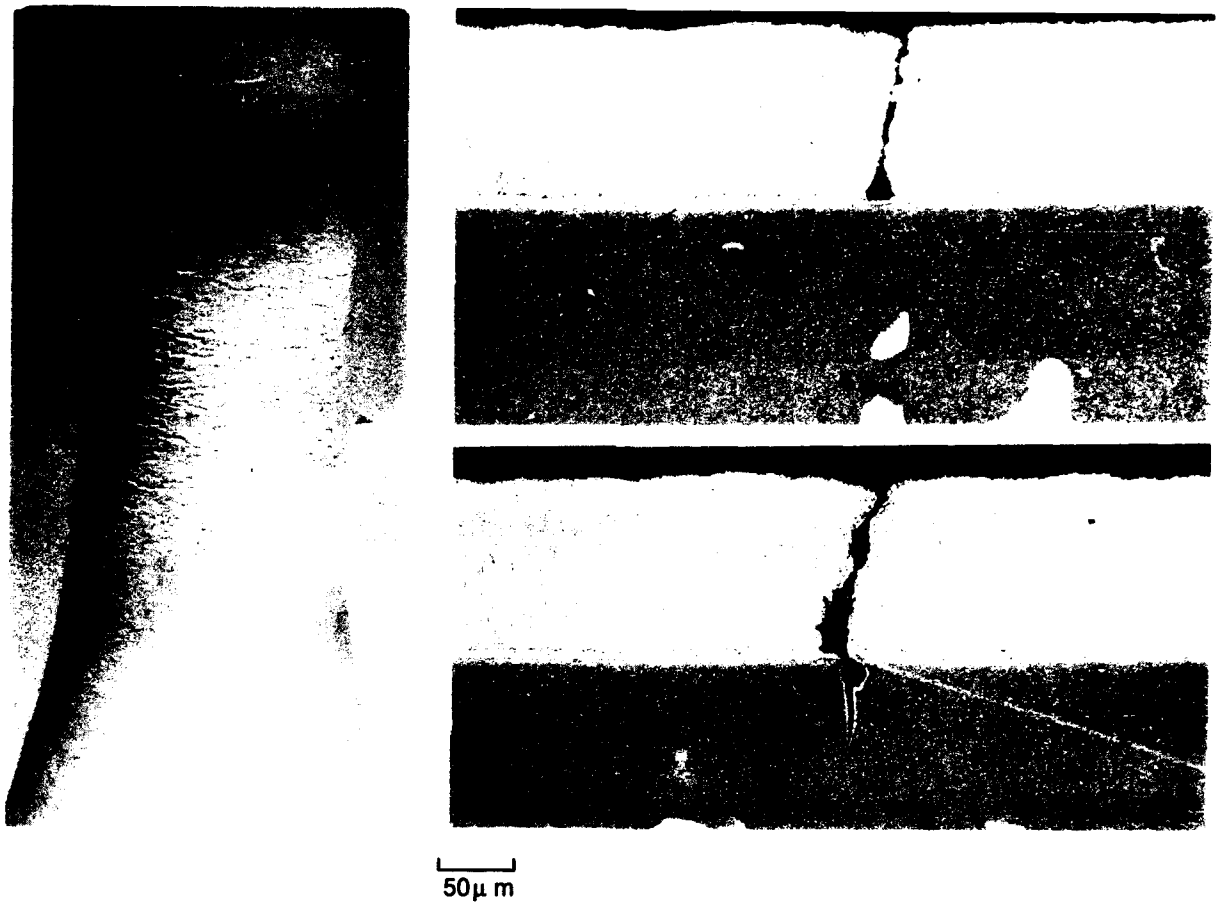

Figure 10. Surface Condition and Corresponding Microstructure of EB-PVD NiCoCrAlY After 1000 TMF Cycles

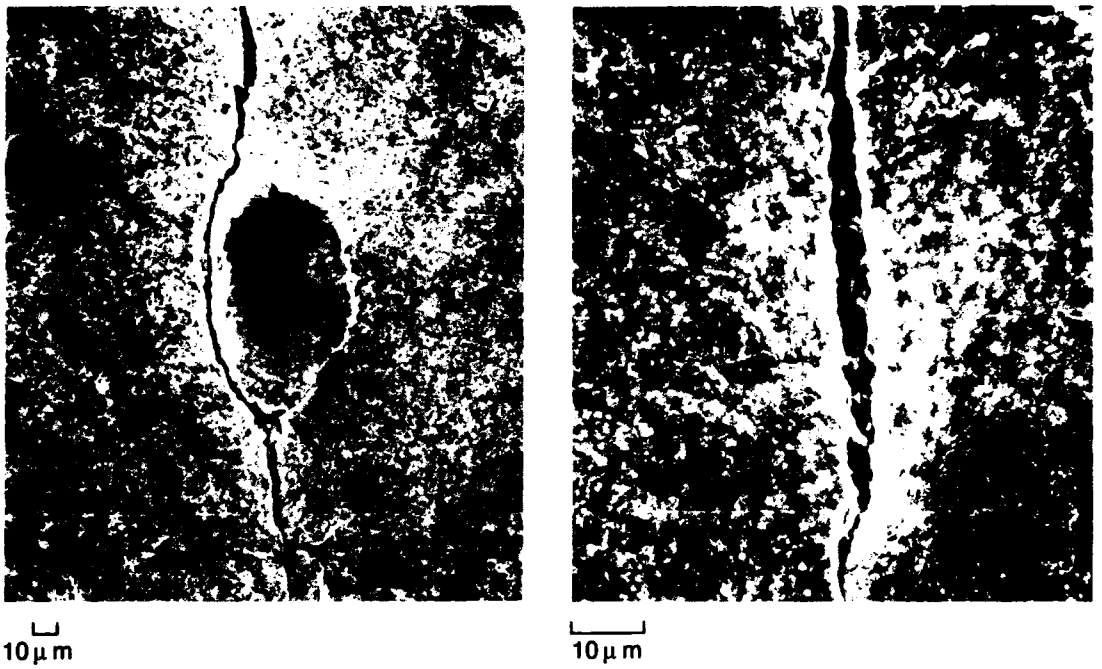

Figure 11. TMF Cracks in EB-PVD NiCoCrAlY (Exposure Time = 500 Cycles)

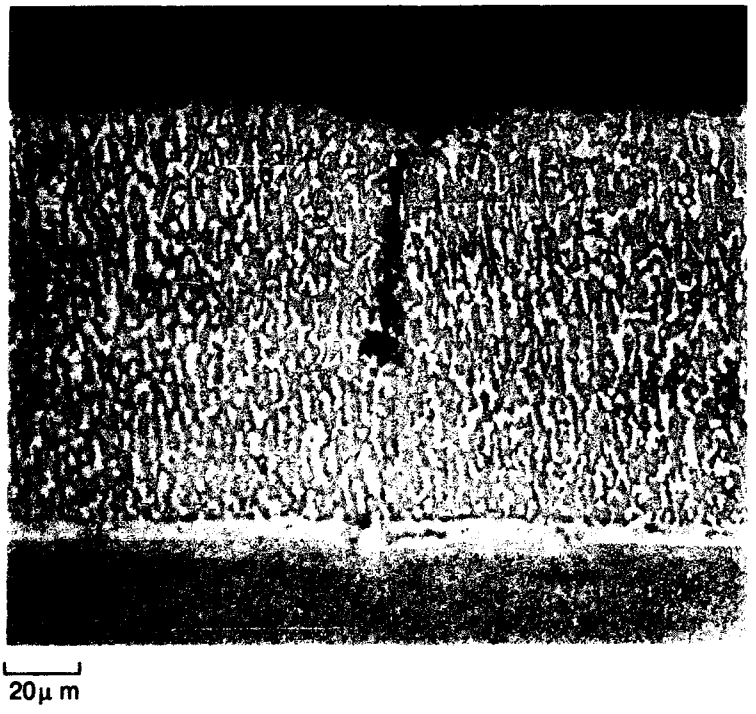

Figure 12. Longitudinal Section of Cracks in EB-PVD NiCoCrAlY

FD 357888

Figure 13. TMF Cracks in LPPS NiCoCrAlY After 1000 Cycles

FD 357889

Figure 14. Crack Tip in LPPS NiCoCrAlY

The observation of cracks in EB-PVD NiCoCrAlY after only 500 cycles suggests that the coating — for all practical purposes — can be considered cracked as-coated, and the TMF test at this strain range (0.6 percent) is exclusively a measure of crack propagation rates. For LPPS microstructures, which are not susceptible to the type of through-thickness features (corn kernels or leaders) typical of EB-PVD deposits, there does appear to be a short initiation period (probably of the order of 1000 cycles) for development of metallographically definable cracks in the coating. However the shortness of the initiation period renders it highly unlikely that oxidation or interdiffusion processes contribute significantly to crack initiation.

4.2.2 Cycles to Initiation/Failure Versus Strain Range and T_{max}

Type 1 tests were run with the cylindrical gage sample (Figure 7) to evaluate the suitability of the specimen design and generate basic information on behavior of the coating/substrate systems. Table 1 is a complete listing of tests performed, and cycles to failure data are plotted versus strain range and T_{max} in Figure 15. Cycles to initiation were based on in-test inspection with a telescope sight; failure criterion was fracture of the specimen. Mean strain, except where noted, was zero, and T_{min} in all tests was 800°F. Speed of the test was 1 cycle per minute except for later experiments run after the quad cycle tests (as discussed in the next section) indicated the need for a faster rate of cycling.

Table 1. *Cycles to Initiation and Failure in Type 1 Thermal Mechanical Fatigue of PWA 1480/LPPS NiCoCrAlY*

	T_{max} = 1900°F		T_{max} = 2100°F	
Strain Range	*Cycles to Initiation*	*Cycles to Failure*	*Cycles to Initiation*	*Cycles to Failure*
0.60	1,332	5,445	181	4,874
0.60	1,200	6,862		
0.60*	410	5,445		
0.60*			395	(1)
0.50	2,140	9,966	260	6,762
0.40	4,894	16,032	2,763	1,0831
0.40**	5,610	14,814		9,296
0.40**			2,910	9,296
0.35	5,046	(2)		
0.35	3,059	10,600***		
0.30			1,242	(3)

*mean strain = −0.2 percent
**2 cycles per minute
***premature failure due to overtemp

(1) terminated at 1037 cycles due to control problems
(2) terminated at 5445 cycles for metallography
(3) terminated at 9106 cycles due to control problems

R19528/10

The tabulated results show more scatter in crack initiation than in cycles to failure data. Earlier crack initiation in the test at $\bar{\varepsilon}$ = −0.2 percent and at higher T_{max} appears conclusively established, however. Cycles to failure data for those tests continued to breakage of the specimen show a consistent dependence on strain range and maximum temperature. The magnitude of the temperature effect at a given strain range is approximately a factor of 1.5 in cycles to failure on changing T_{max} from 1900 to 2100°F.

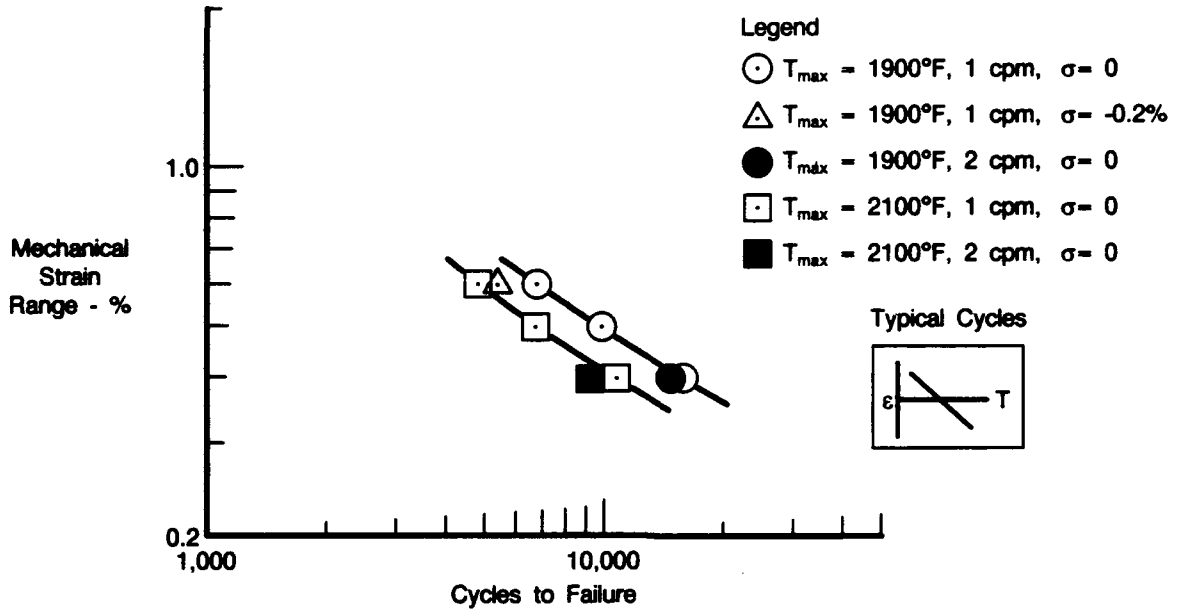

Figure 15. Cycles to Failure Versus Strain Range Data From Table 1

4.2.2.1 T_{max} = 1900°F, $\bar{\varepsilon}$ = 0

Metallography of the 1900°F samples is summarized in Figures 16 through 25, beginning with the initial test of the cylindrical gage sample which was examined in particular detail due to the new specimen design. In-test visual examination showed good uniformity of heating in the half-inch gage section. A short, defect-initiated crack was observed at about 300 cycles. The isolated crack did not appear to propagate, however, and the specimen accumulated approximately 1300 cycles before additional cracks were nucleated. These cracks exhibited the short, wavy appearance typical of NiCoCrAlY.

The specimen failed in center gage. Surface condition and extent of secondary cracking (Figure 16) were consistent with previous observations of this coating/substrate system (ref. 10).

Continuing the microstructural characterization, Figure 17 shows coarsening of the coating microstructure in center gage in comparison with the cooler section toward the threads. The extent of microstructural change is noticeable but not drastic, and it is apparent that cracking can also occur in areas which experienced negligible effects of time-at-temperature exposure.

Scanning microscopy of a short secondary crack about halfway between center gage and the radius indicated it was completely surrounded by γ phase (Figure 18a), and the crack seems to stop at an area of β (Figure 18b). However it is difficult to find a continuous γ path of comparable length, suggesting that transformation of β to γ occurred either during crack growth or due to oxidation of the crack surface.

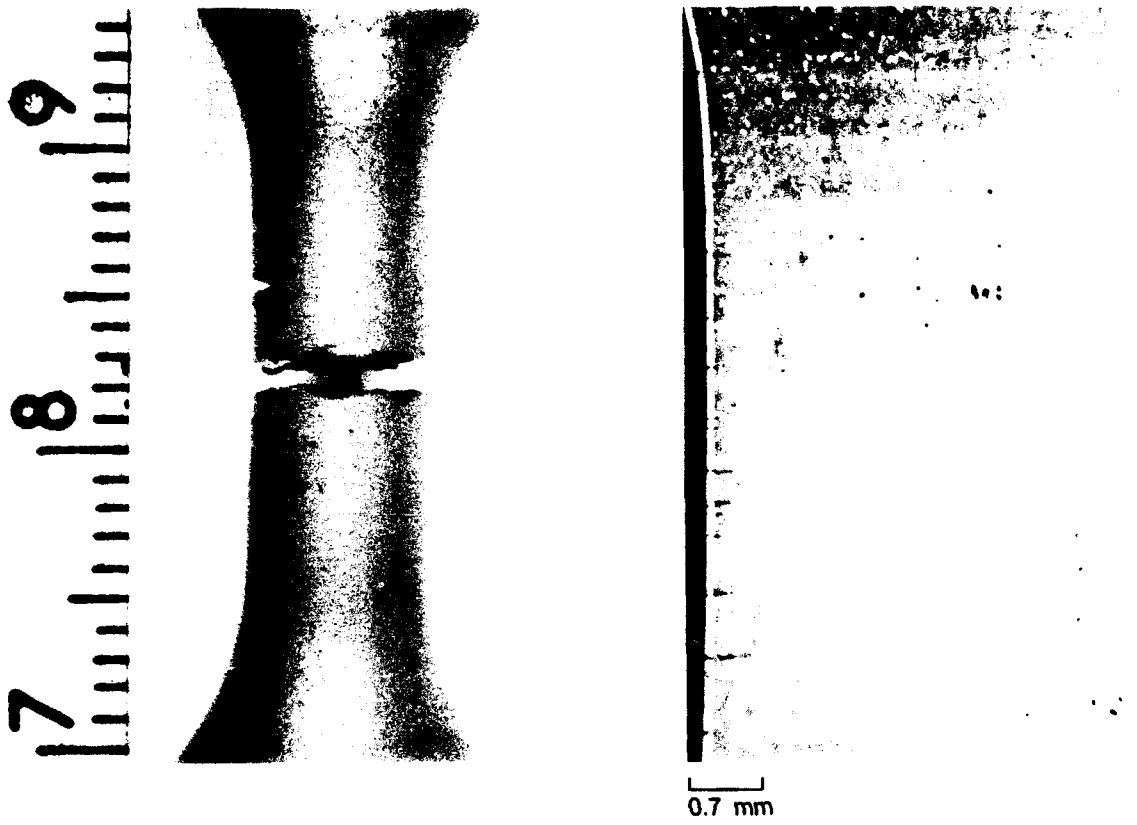

Figure 16. Surface Condition and Longitudinal Cross Section of PWA 1480/LPPS NiCoCrAlY TMF Sample (Δε = 0.6%, Cycles to Failure = 5445)

A secondary crack near the radius, i.e., in the cooler area less affected by time-at-temperature exposure, was also examined on the scanning microscope. Again the crack showed a tendency to lie within areas of γ phase (Figure 19).

The effect of strain range on post-test microstructure of the coating is a tendency for more cracks at higher strain range (as shown by a low magnification survey of the gage section) as well as the center gage microstructural coarsening illustrated in Figure 20. Lower volume fraction of β-NiAl and elongation of the β phase parallel to the direction of deformation are particularly evident at 0.4 percent strain, although the microstructural alteration is still not drastic. Further, coating oxidation and coating/substrate interdiffusion are still minimal, even after 16,000 cycles. Hence it appears highly unlikely — possibly excepting the relatively long time to crack initiation at Δε = 0.40 — that oxidation or interdiffusion processes significantly affected the fatigue behavior of 1480/NiCoCrAlY for the range of cyclic variables investigated.

Lastly in this series of experiments, a Type 1 test was run at Δε = 0.35 percent and terminated at 5445 cycles to duplicate the time-at-temperature history of a sample which failed in the same exposure time at Δε = 0.6 percent. Visual inspection with a binocular microscope revealed 37 small cracks distributed randomly over the gage section. The cracks counted were obvious and unequivocal; typical length was of the order of 1 mm, and initiation could usually be associated with surface imperfections (Figure 21).

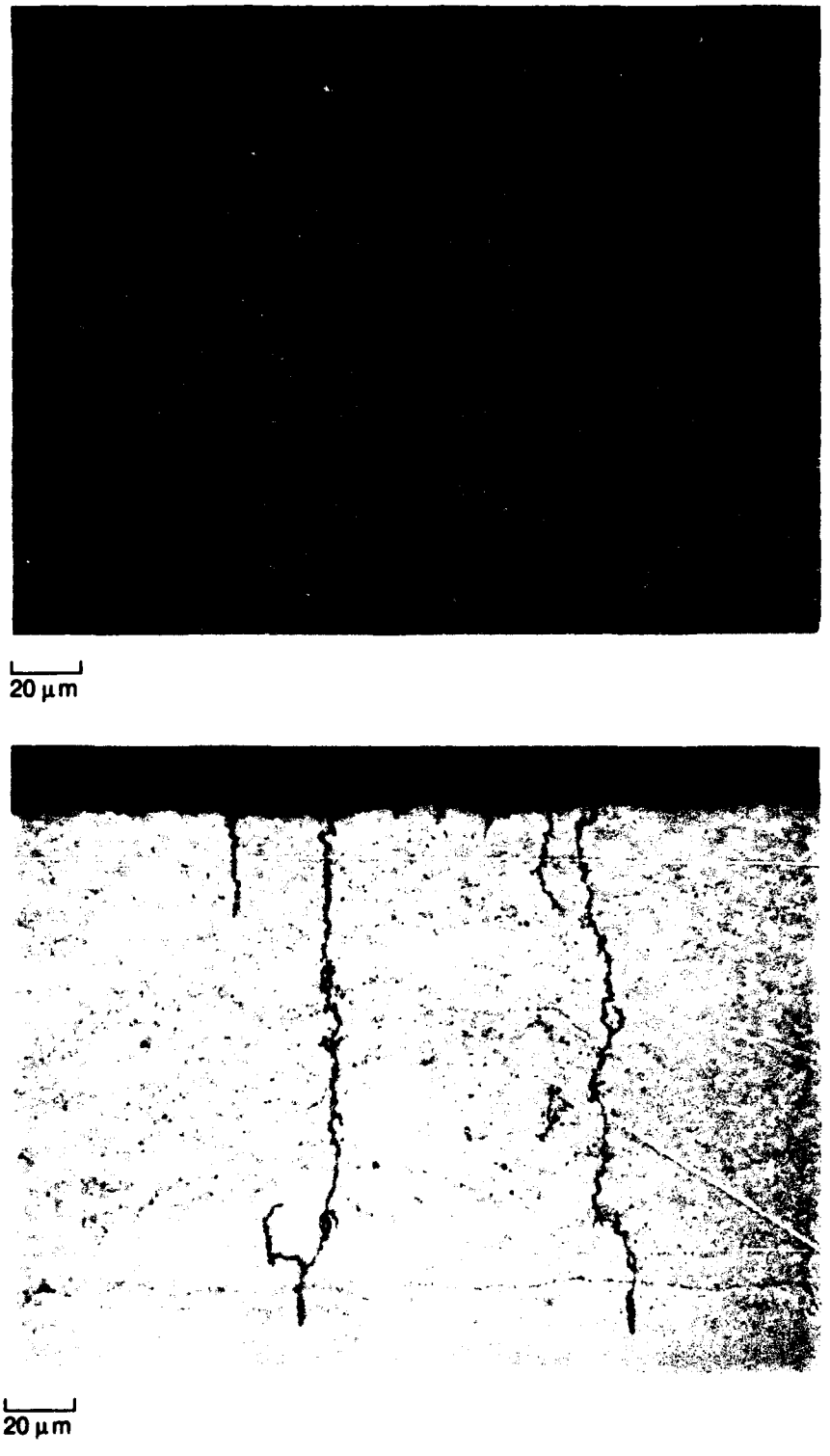

Figure 17. Variation in Microstructure and Crack Morphology Due to Temperature Gradient Between Radius and Center Gage

6.6 µm

a. Crack Length and Surface Depression at Initiation Site

1 µm

b. Crack Tip

FD 357892

Figure 18. SEM Characterization of Secondary Crack in Gage Section

3.3 μm a. Crack Length and Phase Morphology

1 μm b. Crack Tip

FD 357893

Figure 19. SEM Characterization of Fine Secondary Crack Near Radius

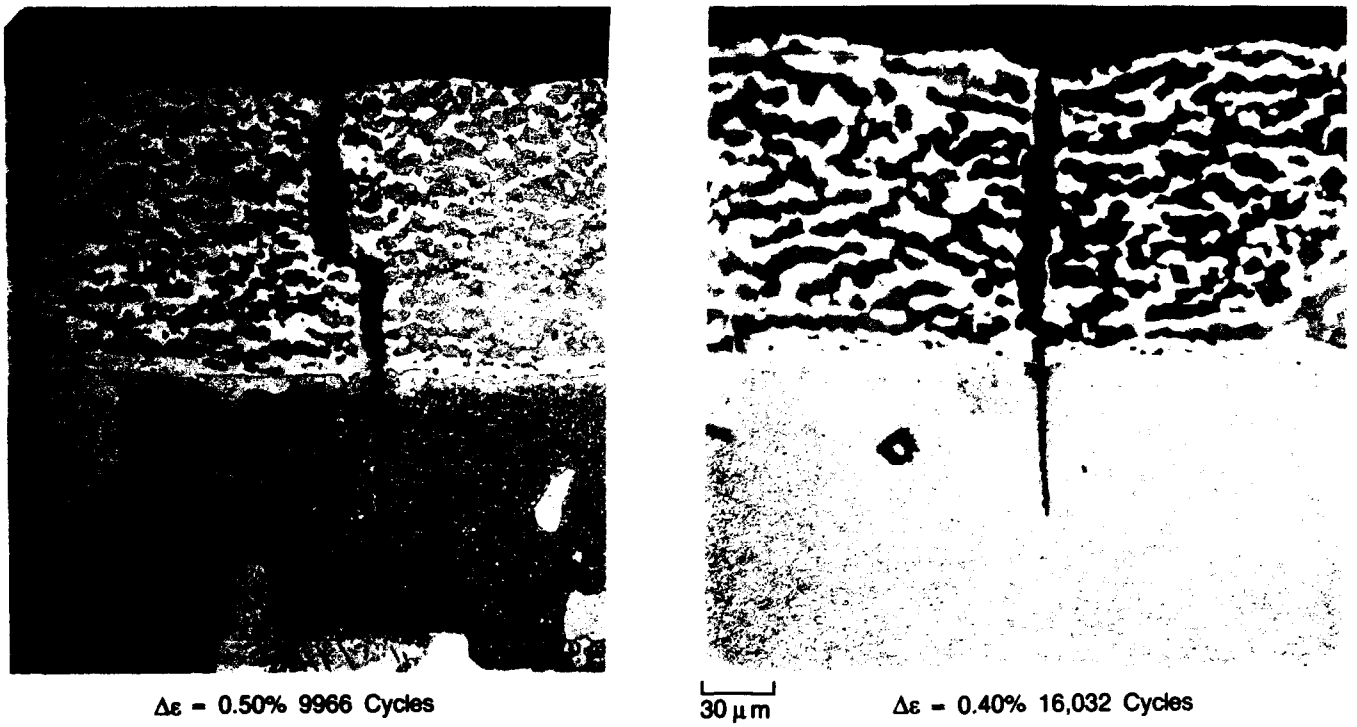

Figure 20. Typical Center Gage Microstructure of LPPS NiCoCrAly on PWA 1480 TMF Samples (Type 1 Cycles, T_{min} = 800°F, T_{max} = 1900°F)

Low magnification metallography showing rumpling and Ostwald ripening at the gage section in comparison with the unaffected areas near the radius is presented in Figure 22. Comparison with a specimen tested at the same temperature limits but higher strain range showed comparable phase coarsening, diffusion zone thickness, and surface oxidation (Figure 23). A tendency of the higher strain range to increase interdiffusion and surface oxidation would be expected (straining of the lattice would facilitate atom movement, and oxide would tend to crack and spall more profusely at higher strain), but the effect apparently is not sufficiently pronounced to be detected at these conditions.

A second sample at the same conditions was intended to be run to failure to observe the microstructural effects of much longer exposure time. Cycles to crack initiation were consistent with previous observations, but the specimen unexpectedly failed at slightly over 10,000 cycles. Post-test metallography showed the failure was due to a short but very severe overtemperature.

4.2.2.2 Type 1 Cycles at T_{max} = 2100°F, $\bar{\varepsilon}$ = 0

As expected, experiments at this temperature proved much more difficult than at T_{max} = 1900°F. Oxidation and surface rumpling were more noticeable, and the resultant changes in surface emissivity interfered with temperature control. Difficulties in temperature control in turn led to excessive deformation because the material weakens rapidly above the desired T_{max}.

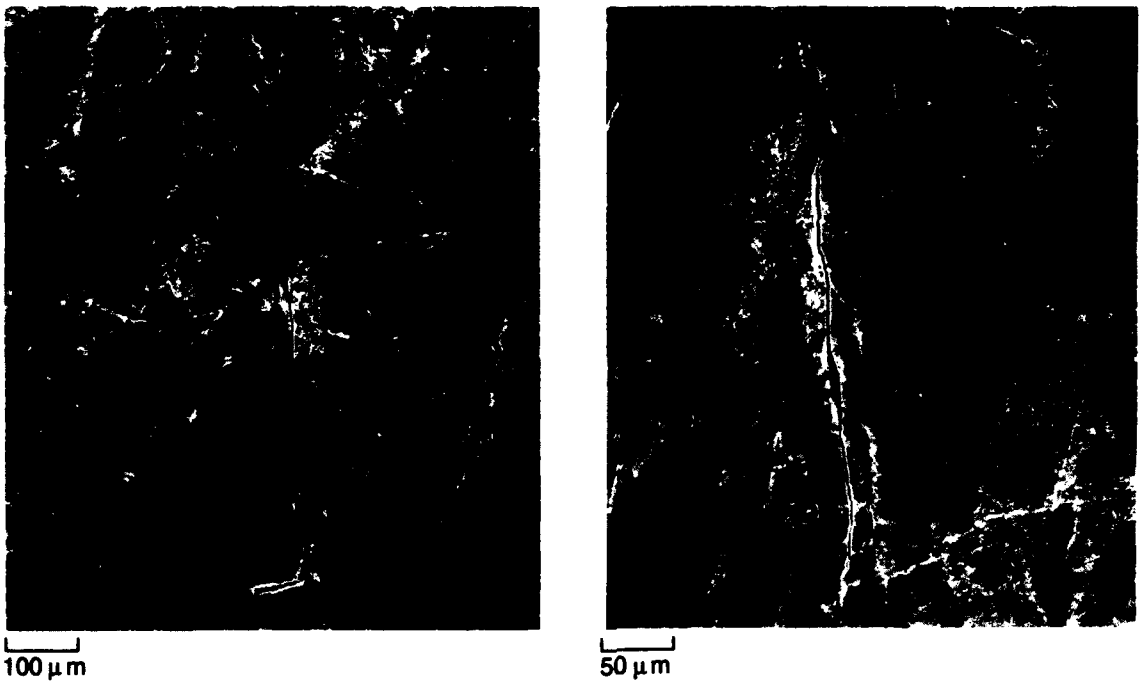

Figure 21. TMF Cracks in LPPS NiCoCrAlY Coasting (Type 1 Cycle, T_{min} = 800°F, T_{max} = 1900°F, Δε = 0.35%, Exposure Time = 5445 Cycles; Tensile Axis Horizontal)

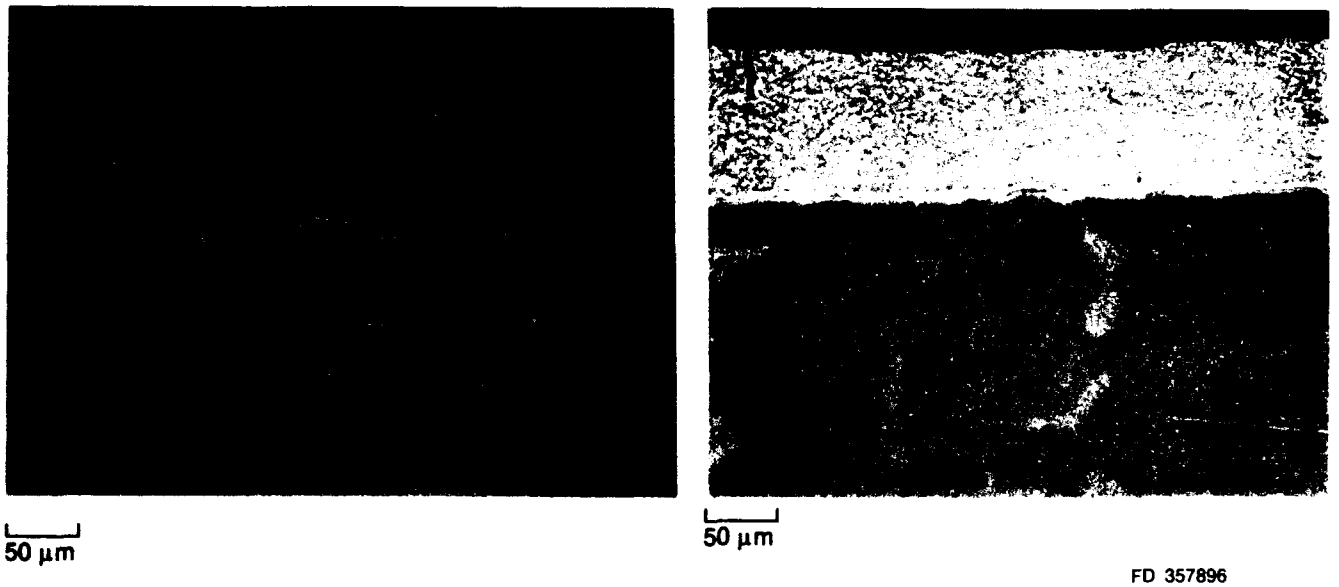

Figure 22. Microstructure and Surface Rumpling in Gage Section Versus Radius Area of 0.35% TMF Sample

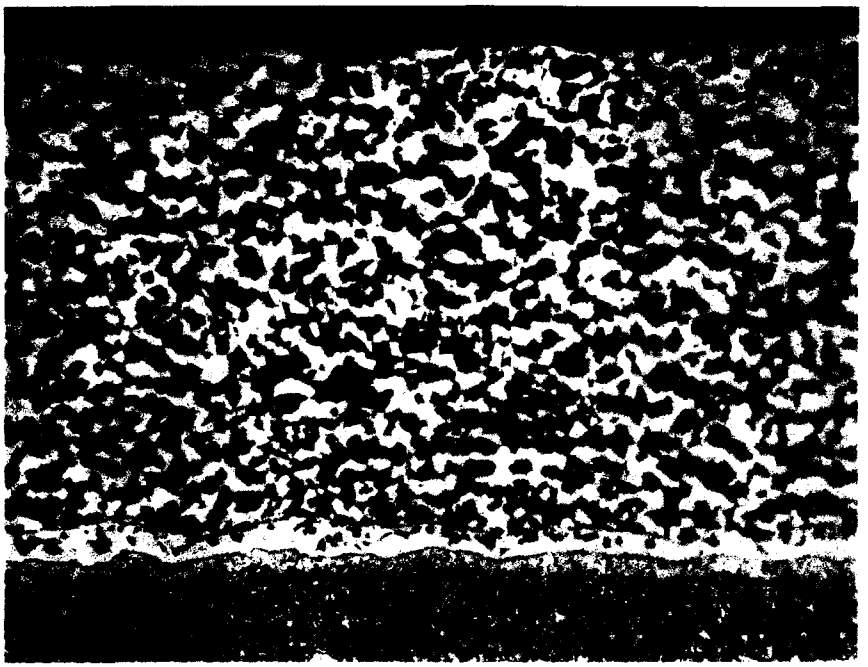

20μ m a. Specimen Failed at $\Delta\varepsilon$ = 0.6%

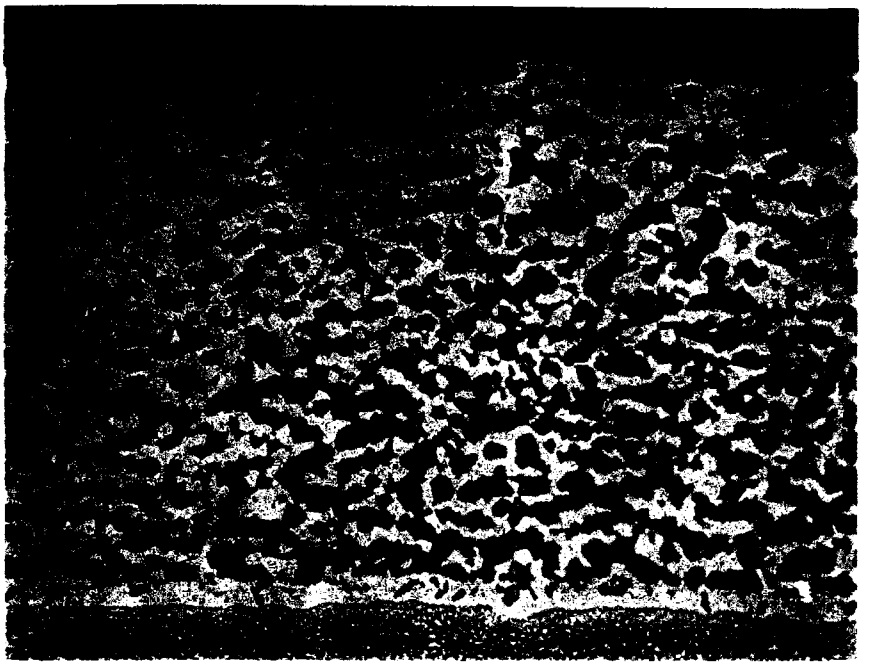

20μ m b. Test Termiated at Same Exposure Time; $\Delta\varepsilon$ = 0.35%.

FD 357897

Figure 23. Gage Section Microstructures of LPPS NiCoCrAlY Coating After 5445 Type 1 TMF Cycles at 800-1900°F

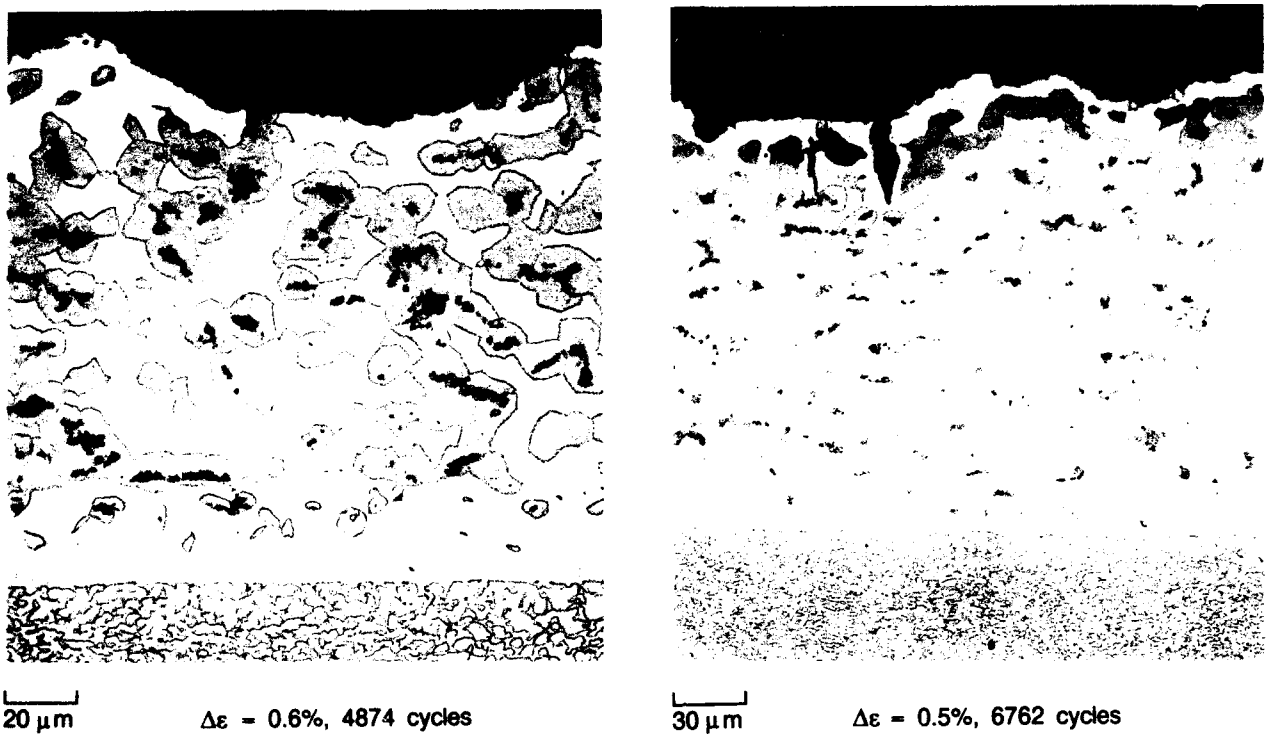

Figure 24. Typical Center Gage Microstructure of LPPS NiCoCrAlY on PWA 1480 TMF Samples (Type 1 Cycle, T_{max} = 2100°F)

In spite of these problems, cycles to failure data for the samples successfully run to breakage of the material were consistently dependent on strain range (Table 1, Figure 15), and center gage microstructures — in comparison with those of 1900°F samples — showed the expected increase in β dissolution and phase coarsening due to the higher test temperature (Figure 24).

The 0.4 percent sample exhibited unusual surface features with irregular longitudinal grooves forming a grain-like network with the circumferential cracks and ridges. This condition and the corresponding microstructure are illustrated in Figure 25.

The three samples just discussed do not exhibit a systematic dependence of phase coarsening and β dissolution on exposure time as in the case of the 1900°F samples. Scatter in microstructural features is perhaps inherently greater in the 2100°F test due to the more substantial rumpling and greater alteration of coating chemistry. The substrate interdiffusion zone is correspondingly larger than in the 1900°F tests, although an effect on TMF behavior via reduction in the load-carrying cross section is still unlikely.

A test at 0.3 percent strain range was attempted to continue the cycles to failure data and perhaps produce sufficient oxidation/interdiffusion to affect durability of the system. Cracking was again observed after approximately 1000 cycles, however, probably too soon for the structure and properties of the coating to have been significantly affected.

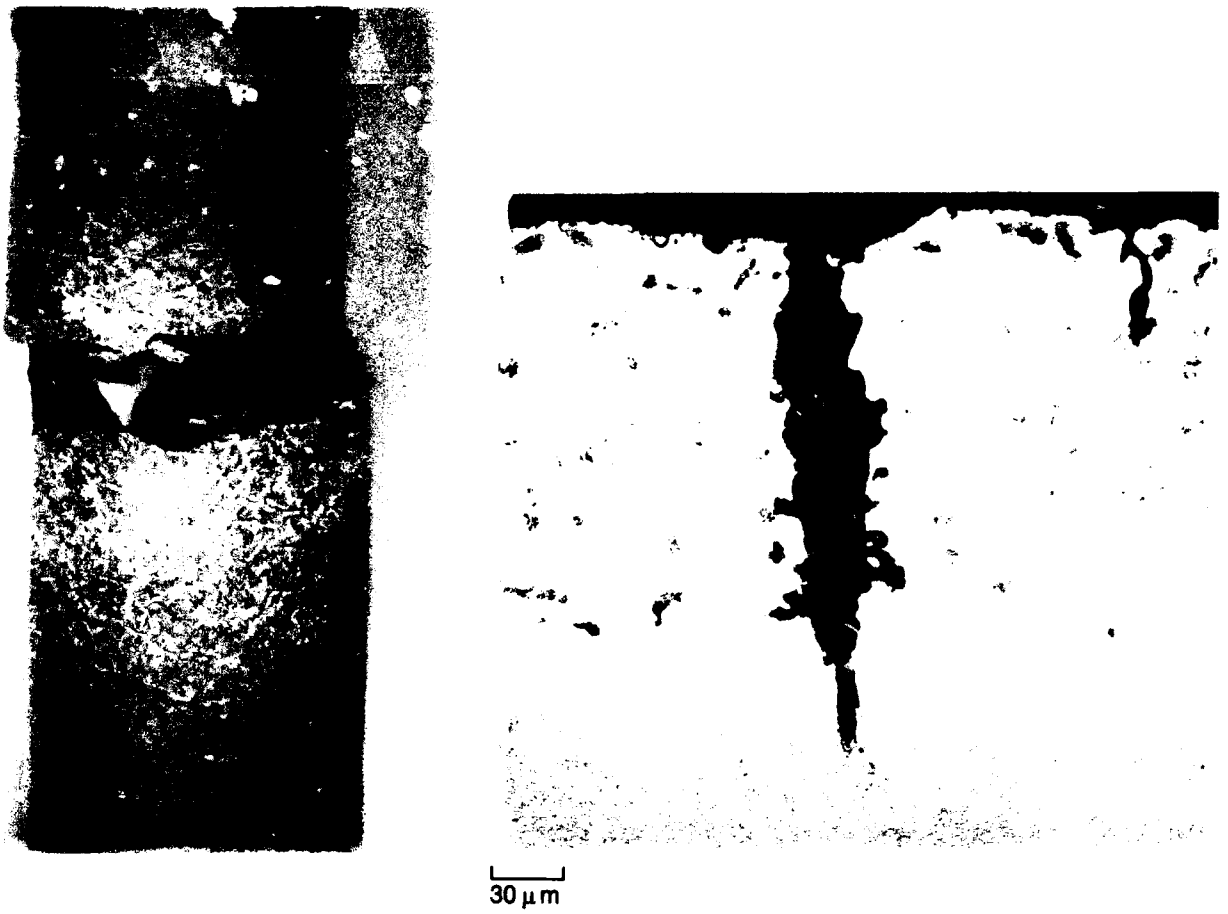

Figure 25. Type 1 TMF Sample of LPPS NiCoCrAlY on PWA 1480 (T_{max} = 2100°F, Δε = 0.4 %, Cycles to Failure = 10,831)

The test was terminated at 9106 cycles because the gage section was noticeably bulged. Surface condition and corresponding microstructures — including a transverse section through center gage to examine the span-wise cracking inferred from visual inspection — are illustrated in Figure 26. Indeed the metallographic examination indicated the lengthwise cracks, i.e., those revealed in the transverse cross section, were generally deeper and more heavily oxidized than the circumferential cracks.

In spite of the difficulties and wide scatter usually encountered in judging initiation of fatigue cracks, the tests listed in Table 1 clearly indicate that cycles to initiation are less at 2100°F than at 1900°F. The reason for this is shown in the schematic diagram (Figure 27), which compares stress-strain behavior at fixed strain range but maximum temperatures of 1900 and 2100°F respectively. Most obvious and straightforward in comparing the two curves is that maximum compressive stress is less for T_{max} = 2100°F because the material is weaker at the higher temperature. (Hence, it requires less load to compress the specimen to the fixed strain limit.) Also, as shown in Figure 27, the stress range is lower in the 2100°F test because the average elastic modulus is lower. On cool-down from T_{max} = 2100°F, however, an increased tensile component must be applied to reverse the significant inelastic deformation which

occurred on the initial cycle. This causes the peak tensile stress to be slightly higher in the high-temperature test, even though the strain range and minimum temperature are the same.

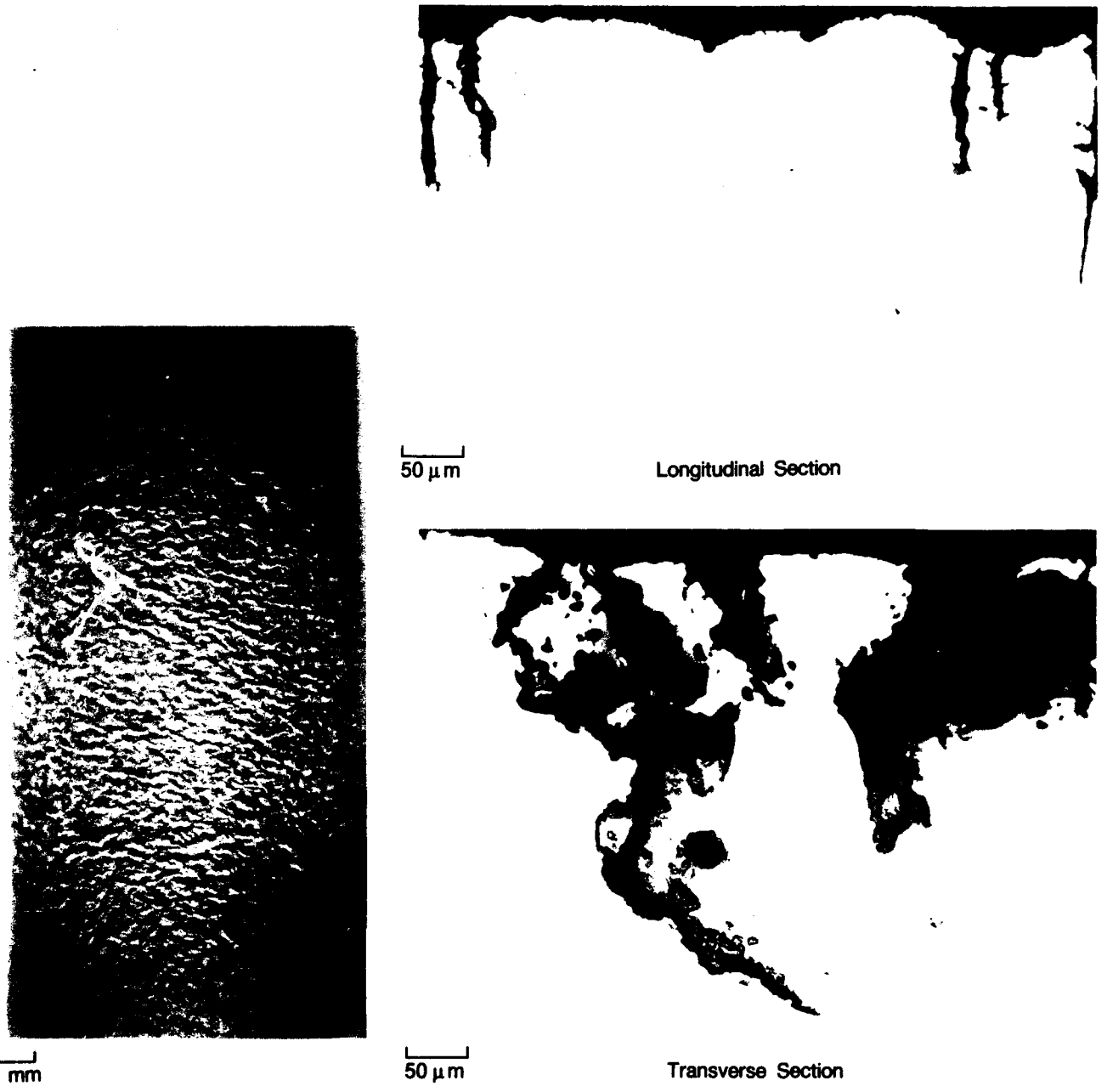

Figure 26. Surface Condition and Gage Section Microstructures of LPPS NiCoCrAlY Coating on Type 1 TMF Sample (T_{max} = 2100°F, Δε = 0.30%, Exposure Time = −106 cycles)

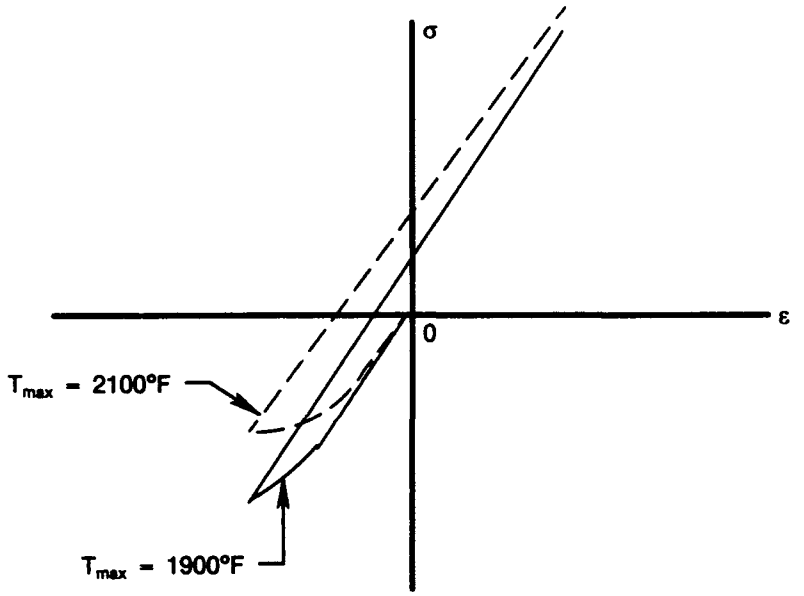

Figure 27. Schematic Diagram Showing Stress-Strain Relationships for Initial Cycle of Load-Adjusted TMF Test at T_{max} = 1900 and 2100°F

Subsequent cyclic stress relaxation continues more rapidly for the test at T_{max} = 2100°F, which sustains the peak tensile stress at a higher level throughout the cyclic exposure than for the 1900°F test. Since coating ductility is at a minimum while the sample is under maximum tensile load, the 2100°F cycle would be expected to initiate coating cracks earlier. Also, the cycle having the larger temperature difference between T_{max} and T_{min} would induce more pronounced effects of thermal expansion mismatch between the coating and substrate, further contributing to the tendency for earlier crack initiation and propagation of coating cracks into the substrate alloy.

These data are not sufficient to establish conclusively whether the shorter thermal fatigue life at 2100°F is due primarily to earlier initiation or faster crack growth. Earlier initiation at T_{max} = 2100°F appears to be conclusively established and rationalized, and the results in Table 1 and Figure 15 could be attributed entirely to initiation effects. However, the argument for earlier crack initiation — namely the higher tensile stress component due to the higher maximum temperature — would also tend to promote faster crack growth, so it is likely that both initiation and growth rates are involved in the T_{max} effect.

4.2.2.3 *Type 1 Cycles With Mean Compressive Strain*

Type 1 TMF tests were run at previously used temperature limits and strain ranges but a mean compressive strain of −0.2 percent. These conditions retain the testing convenience and interpretability of the straight-line cycle but simulate the mean compressive strain typical of engine conditions.

The initial experiment at T_{max} = 2100°F was terminated after 1037 cycles because of an accidental overtemperature (to approximately 2230°F between 800 and 1000 cycles). Surface condition was characterized by slight bulging (due to inelastic compressive deformation at the higher than intended T_{max}) and consequent rumpling of the coating; corresponding microstruc-

tures showed phase coarsening in the hot section but minimal interdiffusion (Figure 28). The plane of polish examined did not exhibit cracks.

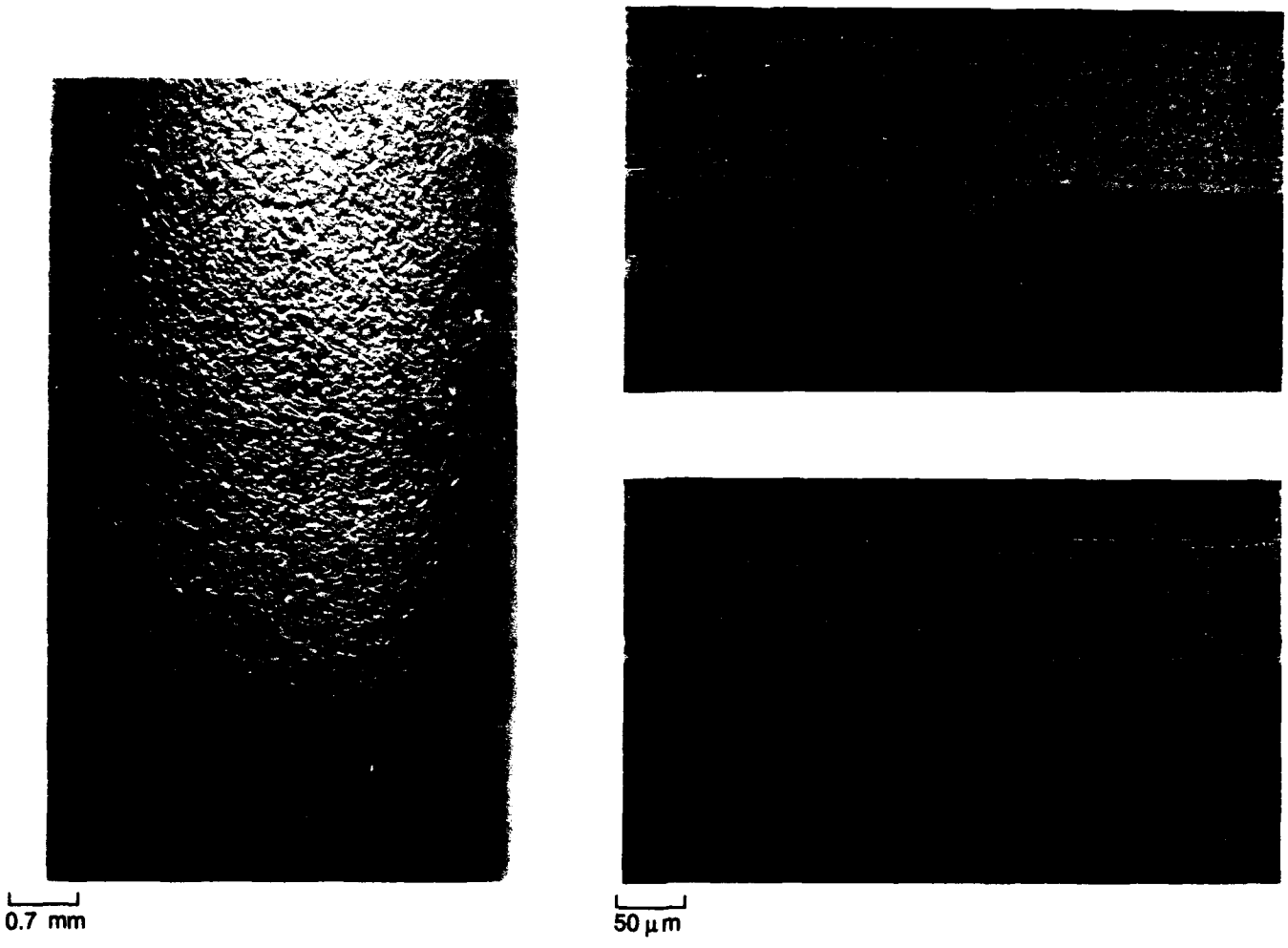

Figure 28. Load-Adjusted Type 1 TMF Sample of LPPS NiCoCrAlY on PWA 1480 Showing Differences in Surface Appearance and Microstructure Between Gage Section and Cooler Area Near Radius ($\bar{\varepsilon}$ = −0.2%, $\Delta\varepsilon$ = 0.6%, T_{min} = 800°F, T_{max} = 2100°F, Exposure Time = 1037 cycles)

A second test was run at the same strain range but T_{max} = 1900°F to minimize the effect of compressive creep and the risk of an overtemperature (due to change in emissivity with surface oxidation). Cracks were observed at 410 cycles (sooner than encountered at $\bar{\varepsilon}$ = 0), but cycles to failure were the same. The surface was much smoother than that of the high-temperature specimen just described, although there were numerous and deep secondary cracks (Figure 29).

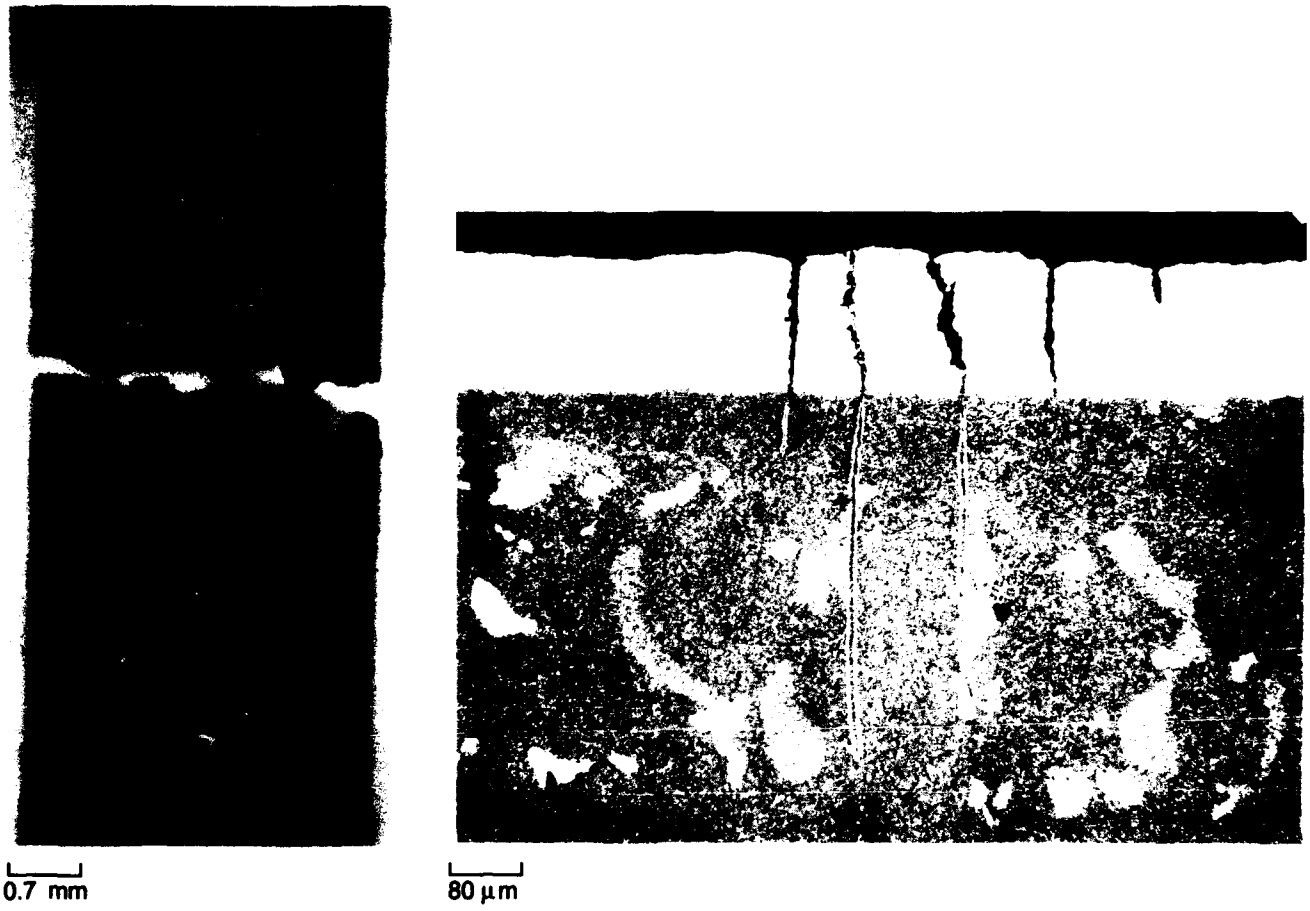

Figure 29. Load-Adjusted Type 1 TMF Sample of LPPS NiCoCrAlY on PWA 1480 ($\bar{\varepsilon}$ = −0.2%, $\Delta\varepsilon$ = 0.6%, T_{min} = 800°F, T_{max} = 1900°F, Cycles to Failure = 5445)

Although the reproducibility of these limited data has not been established, earlier cracking in the test with mean compressive stress is consistent with the same type of argument advanced to rationalize the T_{max} effect. The higher compressive strain at T_{max} (0.5 percent versus 0.3 percent for testing at mean strain of zero) induces a greater inelastic component as well as a greater tendency for rumpling under high-temperature compression. On reversal of the load, the inelastic component must be overcome by tensile stress, and cracks probably tend to develop at the base of the rumples because the rumples act as stress raisers.

4.2.3 Type 1 Tests at 2 Cycles Per Minute

For the coating/substrate combination being evaluated, the primary incentive for a faster Type 1 cycle is economy of testing time. Such an incentive is extremely powerful, however, particularly considering that the most realistic strain ranges in terms of engine conditions result in undesirably long testing times.

The magnitude and direction of a small change, i.e., factor of two rather than order of magnitude, in testing rate is difficult to predict. The role of oxidation and interdiffusion would be

reduced, since time-at-temperature per cycle is less. However, these processes do not appear to be major effects in Type 1 TMF of LPPS NiCoCrAlY, at least in the case of a maximum temperature of 1900°F. Inelastic deformation would also tend to be less, since there is less time for the thermally induced dislocation movement involved in high temperature deformation.

To investigate the cyclic rate effect, Type 1 tests were run at a speed of 2 cycles per minute and strain range of 0.4 percent. The 1900°F sample broke at 14,814 cycles (versus 16,032 at 1 cpm); the 2100°F, in 9296 cycles (versus 10,831 at 1 cpm). Surface condition, as characterized by rumpling, scale spallation, and reformation of alumina, appeared comparable at the two cyclic speeds.

Surface condition and gage section microstructure of the 1900°F specimen are illustrated in Figure 30. Compared with the equivalent test at 1 cpm (Figure 20), the center gage microstructure is less altered by the cyclic exposure. Phase coarsening is clearly noticeable, however, and the major cracks are completely surrounded by γ phase. Hence it appears unlikely that the minor difference in microstructure had a significant effect on TMF behavior.

A similar characterization of the 2100°F specimen is presented in Figure 31. Comparison with Figure 30 shows the effect of higher T_{max} on both surface appearance and gage section microstructure, while comparison with Figure 26 shows the effect of the faster cycle (less severe interdiffusion and phase coarsening due to the shorter time at temperature). As in the case of the 1900°F sample just discussed, however, the crack path in the 1 cpm and 2 cpm samples is the same, i.e., through the matrix γ phase, so the slightly less severe microstructural coarsening is unlikely to have affected the cycles to failure value.

These results suggest that testing speeds of 1 versus 2 cycles per minute have no significant effect on number of cycles-to-crack initiation or specimen failure.

4.2.4 Quad Cycles

In addition to the engine-related reasons discussed in the Introduction, it was hoped that the response of a material to a different strain-temperature history would help in defining fatigue mechanisms. Probably the most significant metallurgical effect with respect to cycle shape is that compressive strain peaks prior to maximum temperature in the realistic cycles, and maximum strain relaxes at T_{max}. It is thus of major interest to determine if an effect on cycles to failure or degradation microstructure could be related to the open versus straight-line cycles.

4.2.4.1 Strain-Controlled Calibration Tests

Strain-controlled tests were carried out with uncoated PWA 1480, using the hollow tube sample shown in Figure 6. Due to limitations in the heating and cooling rate of the larger sample, maximum feasible testing speed was 0.5 cycles per minute.

The first sample experienced 50 percent load drop (the usual failure criterion in strain-controlled testing) in 6983 cycles. The gage section was heavily oxidized, and circumferential cracking was evident. Longitudinal cross sections were characterized by the oxidation and crack morphology shown in Figure 32.

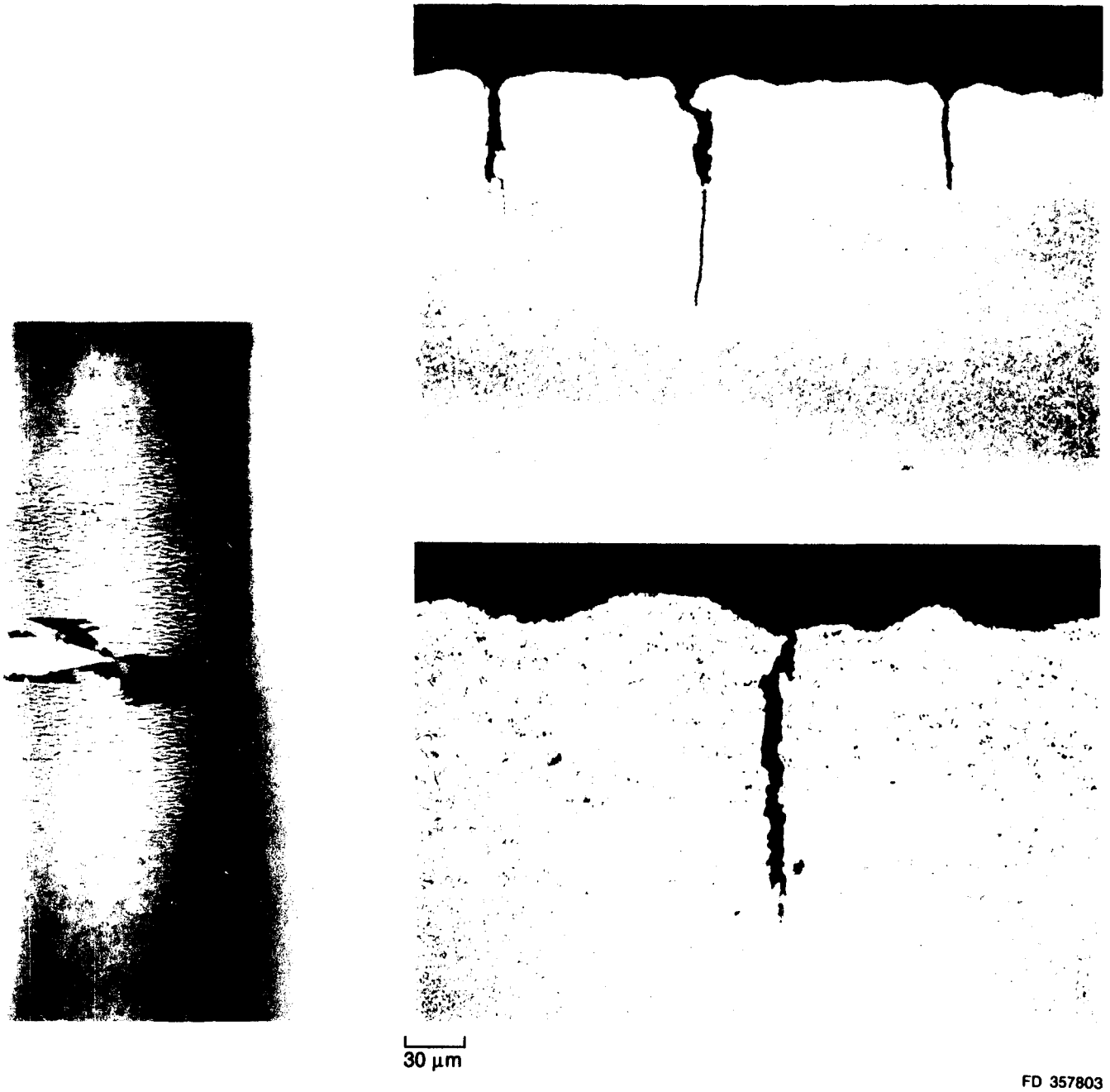

Figure 30. Surface Features and Gage Section Microstructure of 2-cpm TMF Specimen (Type 1 Cycle, T_{min} = 800°F, T_{max} = 1900°F, $\Delta\varepsilon$ = 0.4%, Cycles to Failure = 14,814)

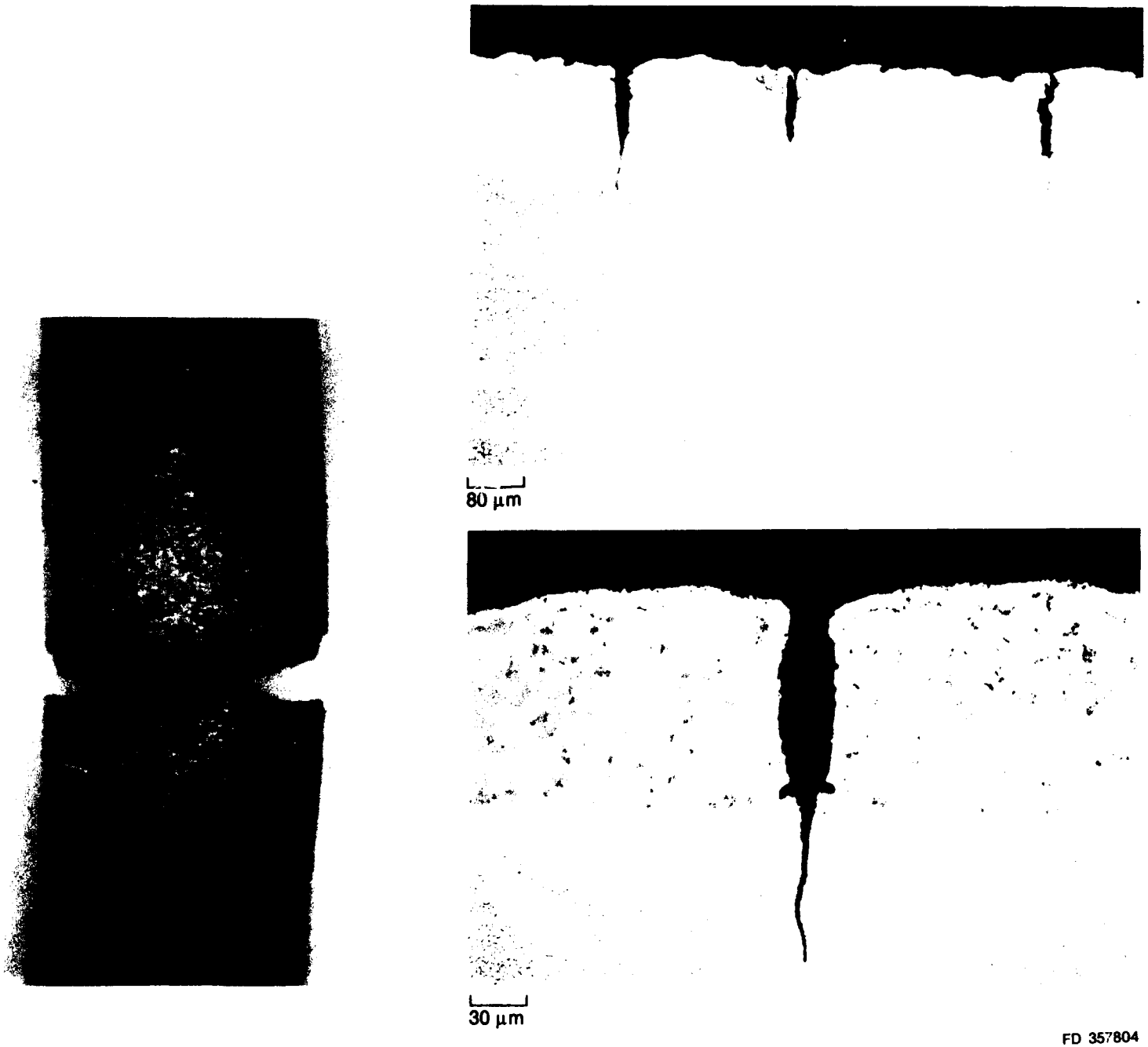

Figure 31. Surface Features and Gage Section Microstructure of 2-cpm TMF Specimen (Type 1 cycle, T min = 800°F, T'_{max} = 2100°F, Δε = 0.4%, Cycles to Failure = 9296)

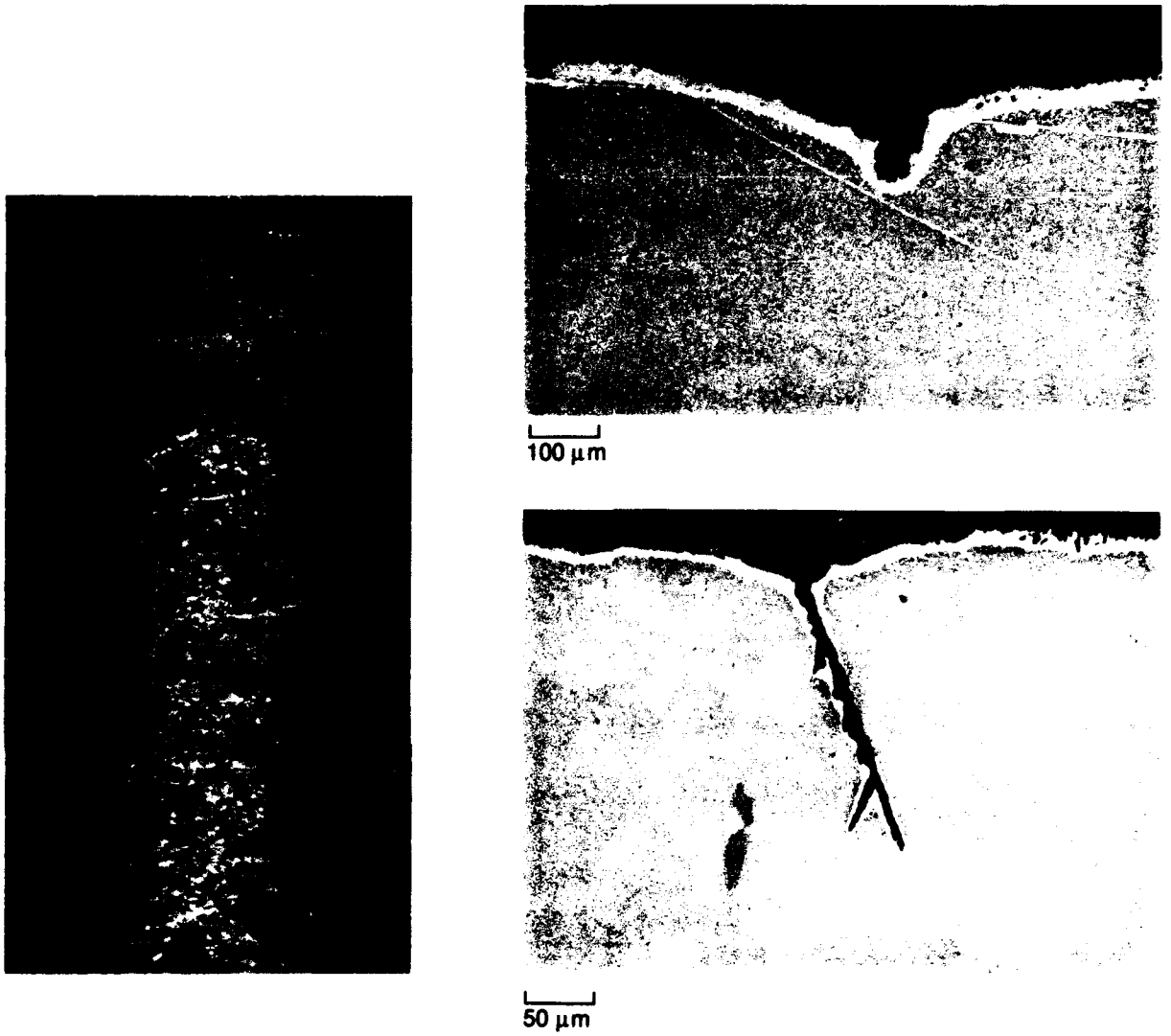

Figure 32. Uncoated PWA 1480 Quad Cycle TMF Specimen (Strain/Temperature Endpoints of Cycle: −0.1%/800°F, −0.6%/1800°F, −0.3%/2000°F, +0.1%/1280°F)

The duplicate specimen failed in 6100 cycles. Post-test metallography also reproduced the type and severity of surface oxidation and fatigue damage, including circumferential cracking as well as a tendency for massive {111} slip (Figure 33).

Stress-temperature data from the first quad cycle test are plotted in Figure 34, where the magnitude of the shake-down effect is indicated by a comparison of initial and stabilized waveforms. Equivalent data from the second test were averaged with those of the first and replotted in the form of a closed loop in Figure 35. The stabilized stress/temperature endpoints in this diagram were used for running the quad cycle on the load-adjusted rigs.

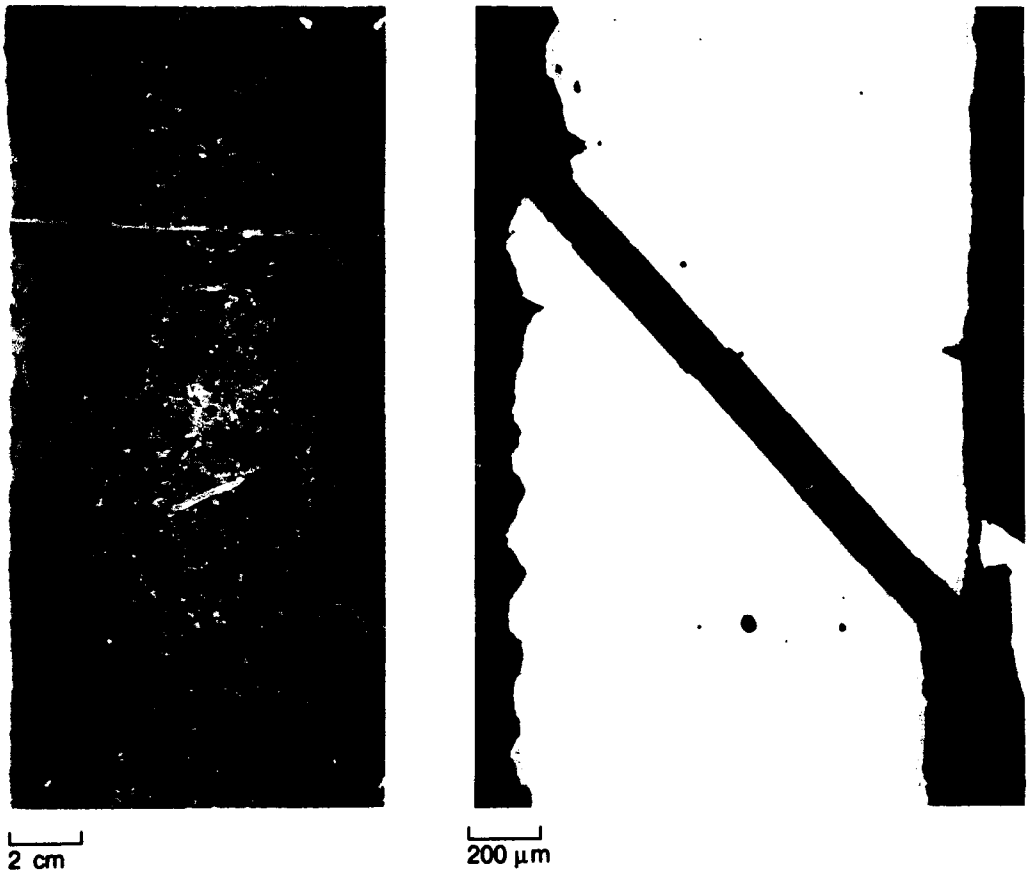

Figure 33. Surface Condition and Cross Section of Uncoated PWA 1480 TMF Sample (Cycle as Described in Figure 32, Cycles to Failure = 6100)

It is interesting to note from the stress-temperature plots that the specimen is under tensile load for most of the cycle, even though the corresponding strain is compressive (i.e., the sample is shorter than its original length). This circumstance results from the need to apply a tensile load to overcome the high temperature inelastic deformation which occurred in compressing the material to its minimum length.

4.2.4.2 Load Adjusted Test Results

The quad cycle was run in load control on uncoated PWA 1480. The gage section turned noticeably green by about 1300 cycles, and oxide mounds developed by 4200 cycles. Small cracks were probably observed by 4200 cycles, although their identification at this point still involves subjective judgment. The pits expanded into uniform coverage of the center gage section by about 9000 cycles. The test was terminated at 15,770 cycles when oxidation was becoming increasingly severe. A prominent circumferential crack was observed on visual inspection, although load was stable and failure did not appear imminent.

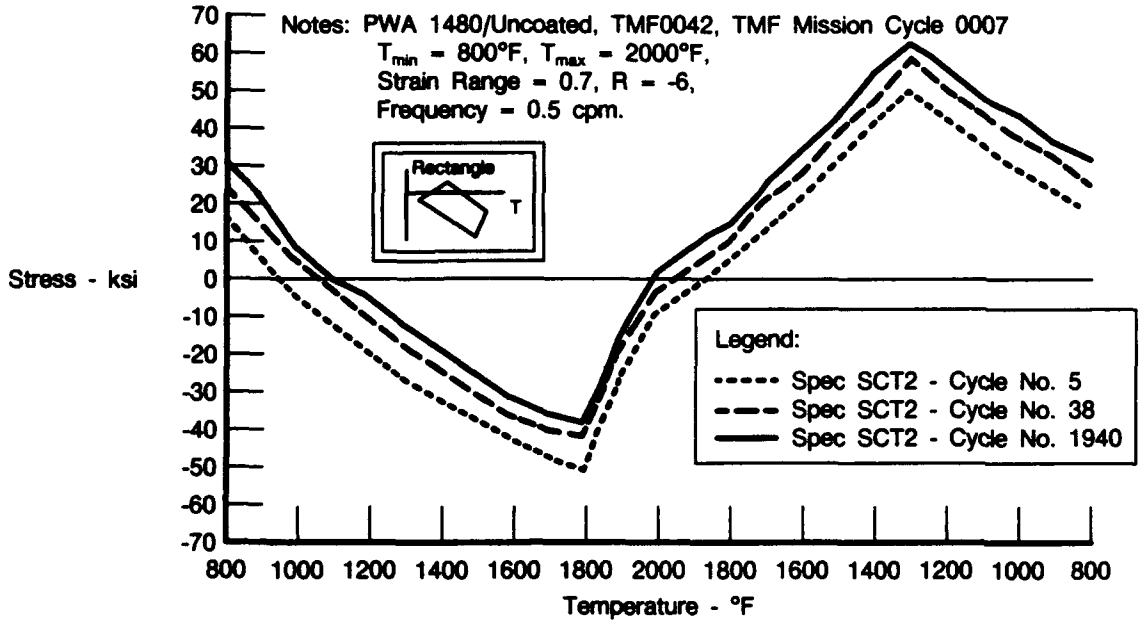

Figure 34. Stress Versus Temperature Data From Strain-Controlled Quad Cycle TMF Test

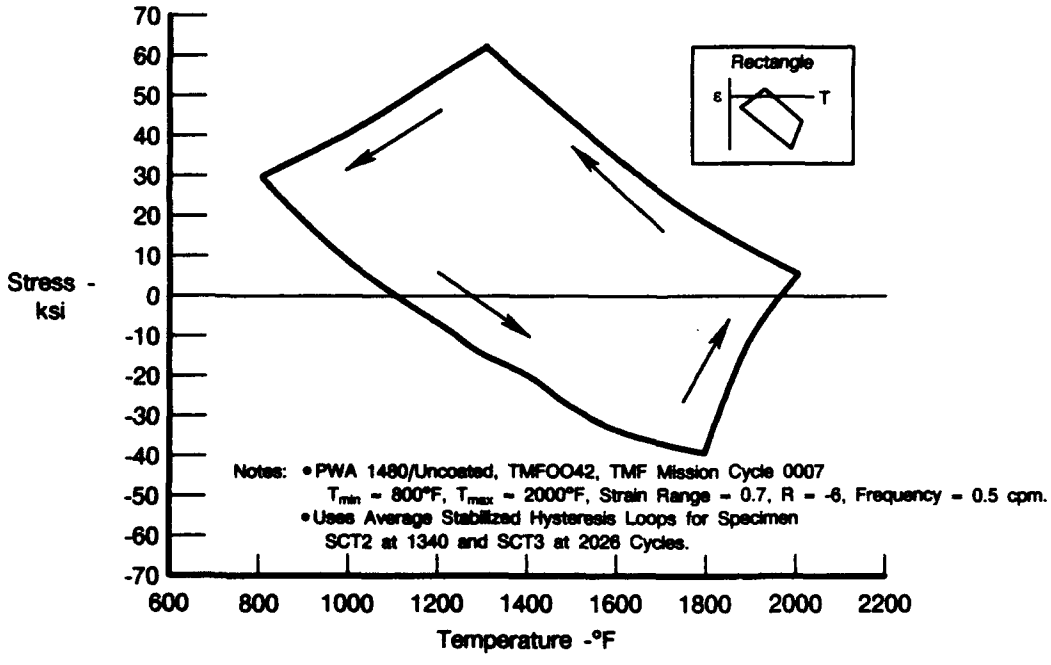

Figure 35. Stabilized Stress/Temperature Quad

Surface condition and a corresponding longitudinal cross section including the major crack are shown in Figure 36. Both show good correlation with the the nature and severity of surface oxidation as well as the depth, frequency, and morphology of secondary cracking encountered in the strain-controlled tests.

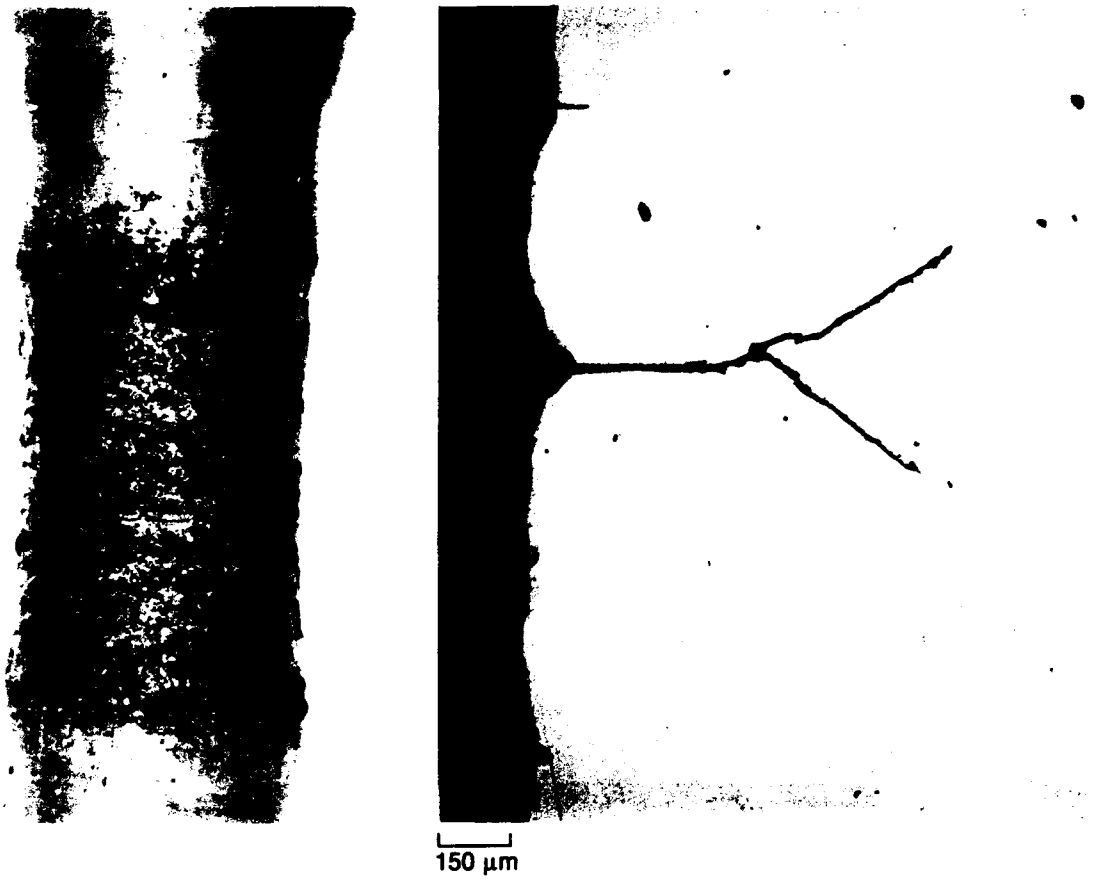

Figure 36. Load-Adjusted Quad Cycle TMF Sample of Uncoated PWA 1480 Single Crystal (Strain/Temperature Endpoints of Cycle: −0.1%/800°F, −0.6%/ 1800°F, −0.3%/2000°F, +0.1%/1280°F)

In the initial test of coated material with the quad cycle, the surface became noticeably rumpled by approximately 1400 cycles. Cracks had probably developed at the base of some of the rumples by 3000 cycles. The crack which ultimately led to failure was first observed at about 6000 cycles. The specimen broke at 12,842 cycles, a substantially longer life than characteristic of Type 1 cycles at the same temperature limits and strain range (0.7 percent between maximum tension and maximum compression).

Surface condition and a corresponding low magnification cross section are illustrated in Figure 37. The nature of the rumpling varies from center gage toward the radius, but is generally finer than that characteristic of Type 1 TMF. The fracture surface is highly crystallographic, although the secondary cracks initiate normal to the coating surface.

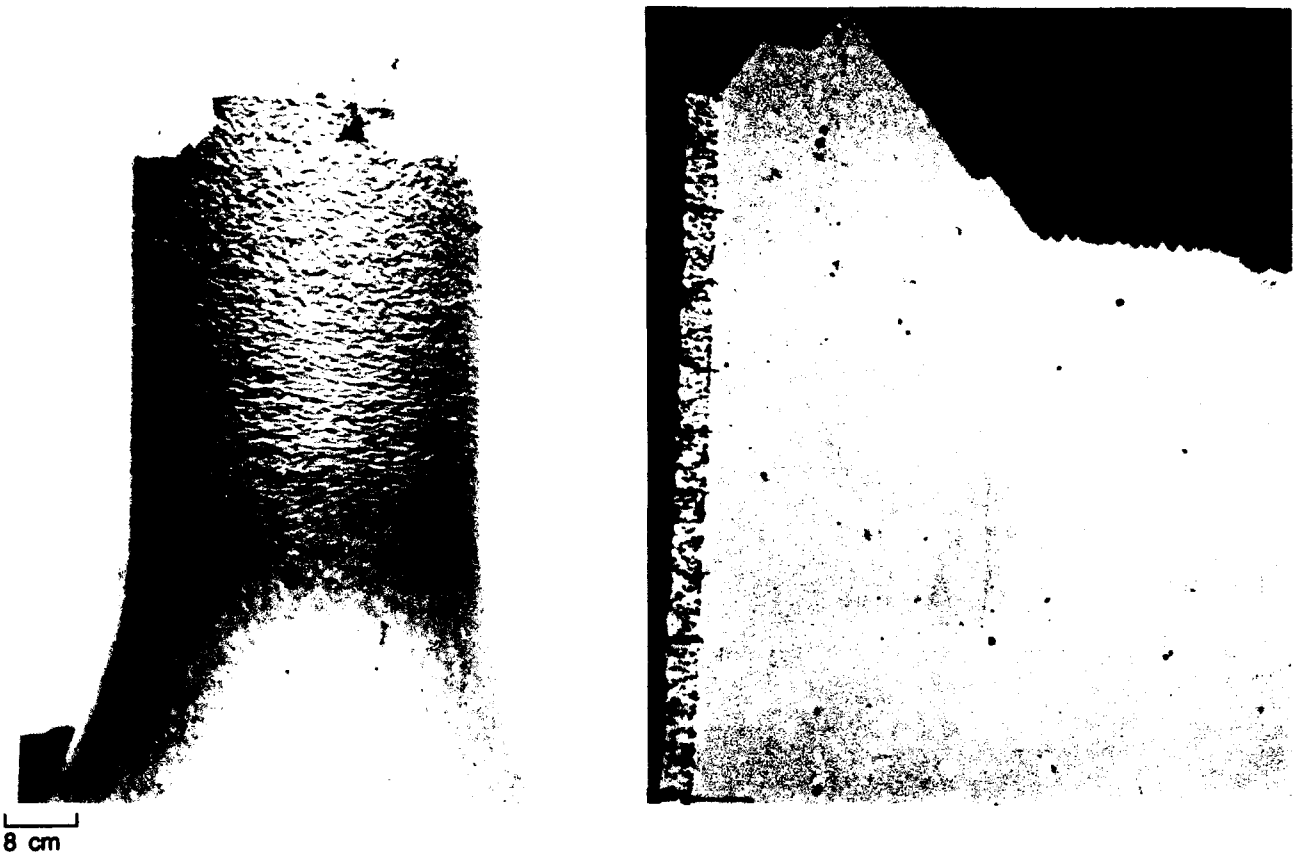

Figure 37. Surface Condition and Longitudinal Section of Load-Adjusted Quad Cycle TMF Sample of PWA 1480/LPPS NiCoCrAlY (Cycle as Described in Figure 36, Cycles to Failure = 12,842)

Figure 38 includes degradation microstructures near center gage (a, b, c) and in the less affected areas toward the radius. The β-NiAl phase is almost completely dissolved and/or preferentially oxidized at center gage. However, the substrate interdiffusion zone is very thin (about 10 μm), indicating that the microstructural changes are primarily due to loss of aluminum to the surface. Also, in spite of the selective β consumption and aluminum depletion, bulk oxidation of the degraded coating material is minimal.

The oxidation morphology observed in this test is not typical of unstressed exposure, e.g., furnace cyclic or burner rig oxidation, or of isothermal oxidation under load (as in a creep or stress rupture test). Similar features had been observed, however, in β-NiCrAlY and diffusion aluminide coatings exposed to triangle- and dipper-shaped cycles in a previous program (ref. 10). Since the degradation microstructure of these high-aluminum coatings had been found particularly sensitive to the change from type 1 to open cycles, it was decided to run the quad on an hourglass sample of aluminized 1480 for comparison with the unexpected oxidation mechanism of the NiCoCrAlY.

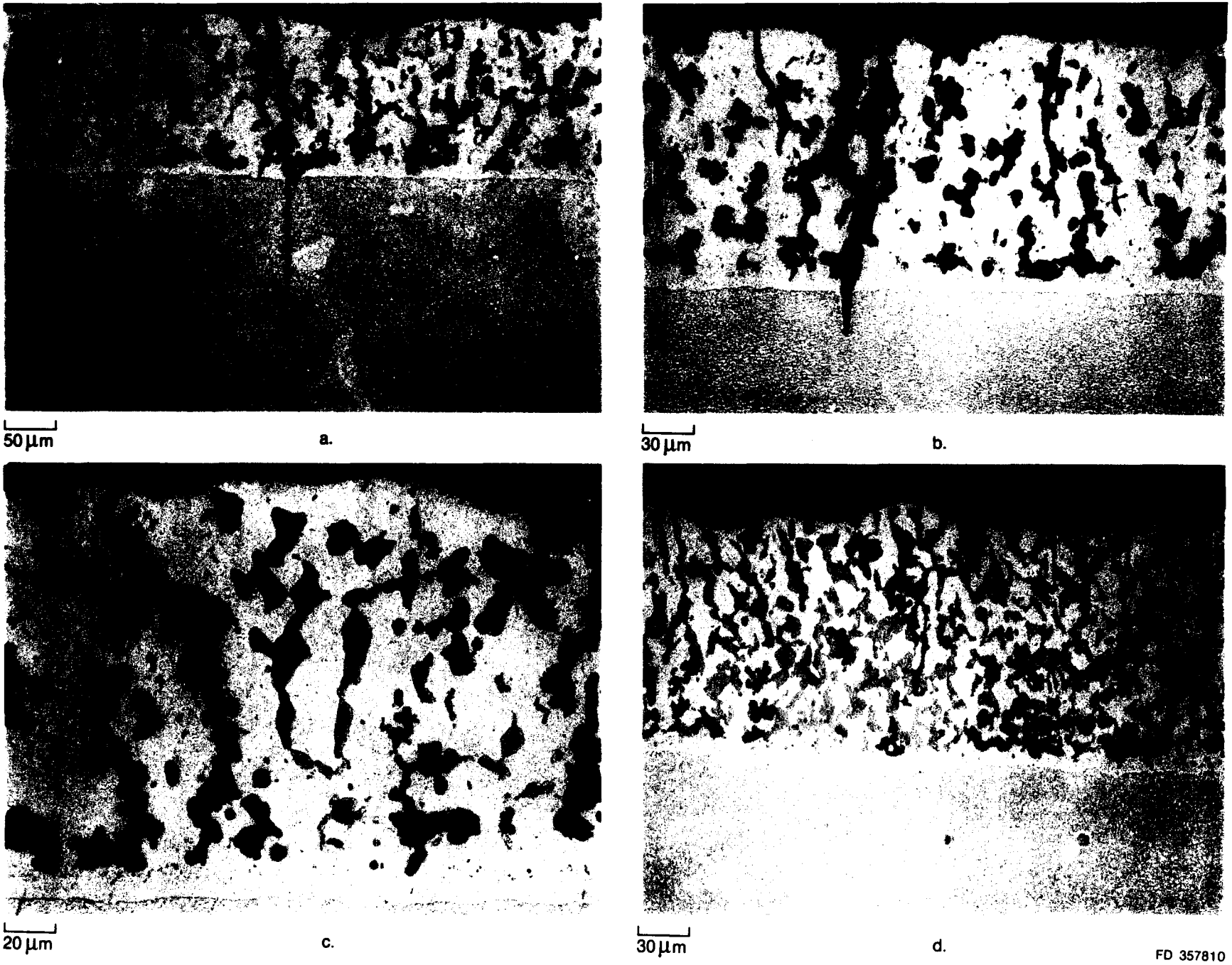

Figure 38. Microstructures of LPPS NiCoCrAlY After 12,842 Quad TMF Cycles

Paralleling the severe degradation of the high aluminum coatings documented in the earlier work, the aluminized surface was observed to be green in color by 6300 cycles. The test was terminated at 7455 cycles because of the coating delamination illustrated in Figure 39. Post-test metallography confirmed the substantial substrate oxidation inferred from visual inspection, suggesting that coating cracks allowed penetration of oxygen relatively early in the test. The adjacent coating was recognizable but severely oxidized, and morpholpgy appeared similar to the deep selective attack of the β-NiAl phase as found in the LPPS NiCoCrAlY.

Since the coating microstructures in Figures 36 through 39 are not typical of isothermal or unstressed cyclic exposure, they appear to be a direct consequence of the nature of the strain/temperature/time parameters of the TMF cycle. The tendency for deep but highly localized attack — selectively of the β-NiAl phase in NiCoCrAlY and at grain boundaries of the originally single phase aluminide — suggests a strain-induced process involving cyclic damage to the oxide scale and tensile separation along γ — β interfaces and/or grain boundaries of β, thus allowing oxygen to penetrate more deeply into the microstructure.

Oxide morphologies produced by such a mechanism would be unique to thermal mechanical fatigue rather than unstressed cyclic oxidation because of the critical role of the mechanical load in pulling apart the grain boundaries of the coating. Also, the degradation microstructure would be unique to TMF rather than isothermal creep because of the role of the thermal mechanical cycling in causing mechanical damage to the oxide, thus allowing the ingress of oxygen into the strained coating.

These speculations appear to rationalize the existence of aggravated environmental attack and unusual oxidation morphologies in thermal mechanical fatigue. More difficult to explain is why the observed microstructures are produced by the open cycles, i.e., triangle-, dipper-, or quad-shaped, but not by straight-line Type 1 or Type 2 cycles of similar temperature limits and strain ranges.

Three arbitrary cycles were designed to seek information in this area:

(1) A Type 1 test was run between strain/temperature limits of +0.1 percent/1280°F and −0.3 percent/2000°F (the upper right boundary of the quad cycle), thus exposing the material to the high temperature, tensile loading portion of the cycle which might be expected to have produced the oxidation damage.

(2) The speed of the quad cycle was increased to two cpm, thus reducing by a factor of two the time-at-temperature exposure per cycle.

(3) The maximum compressive strain of the quad cycle was arbitrarily changed from −0.6 percent to -0.45 percent, thus reducing the tensile load required to offset the high temperature compression.

The Type 1 sample failed in 18,428 cycles. Failure was near the limit of the temperature-affected area (Figure 40), and a large secondary crack was observed in a similar location near the opposite radius. The gage section microstructure exhibited phase coarsening and dissolution consistent with the long testing time. However, there was no evidence of the strain-induced oxidation characteristic of the quad cycle, in spite of the longer exposure time and higher average temperature.

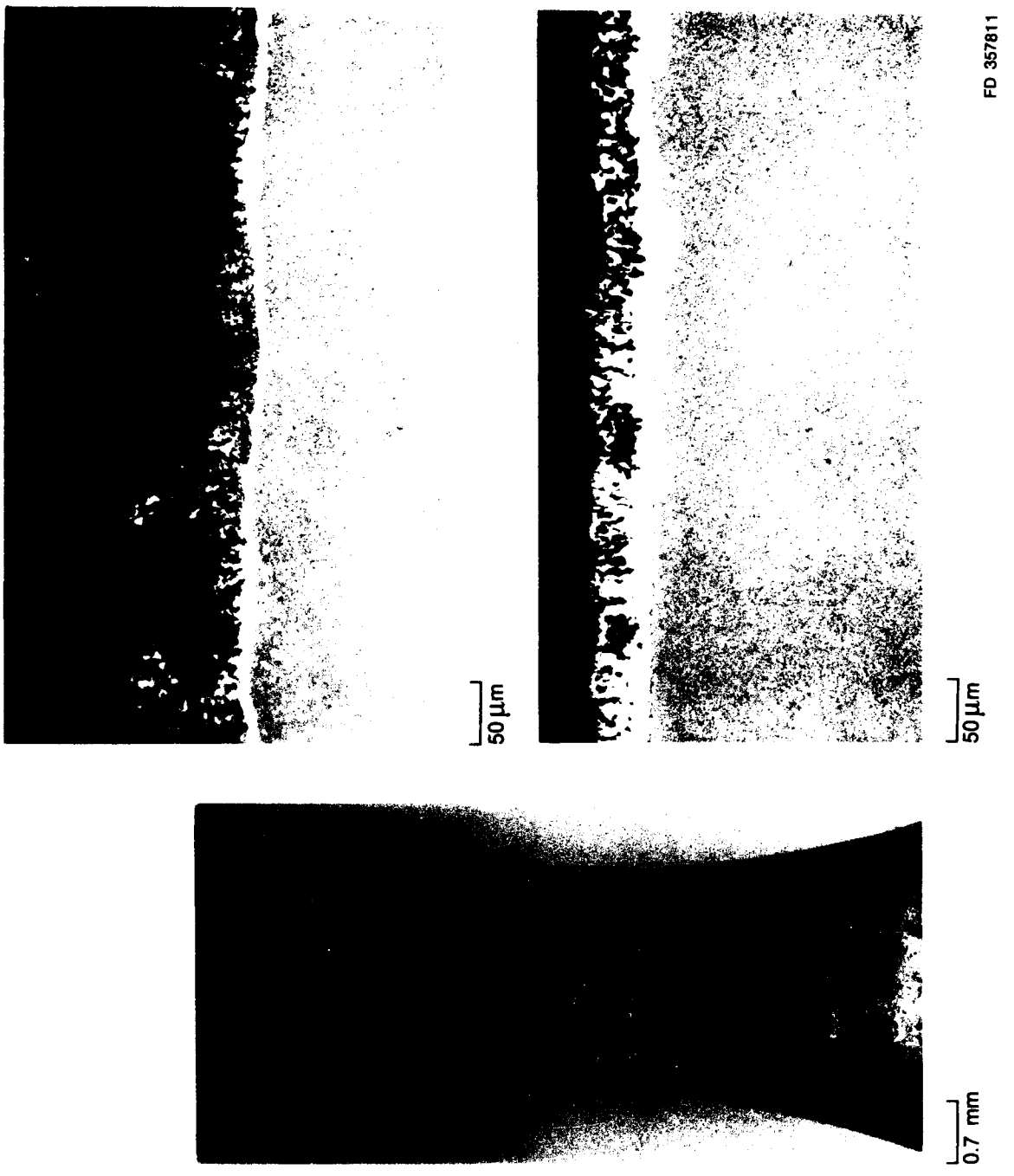

Figure 39. Quad Cycle TMF Sample of PWA 275 Gas Phase Aluminide on PWA 1480 (Cycle as in Figures 36 and 37, Exposure Time = 7455 Cycles)

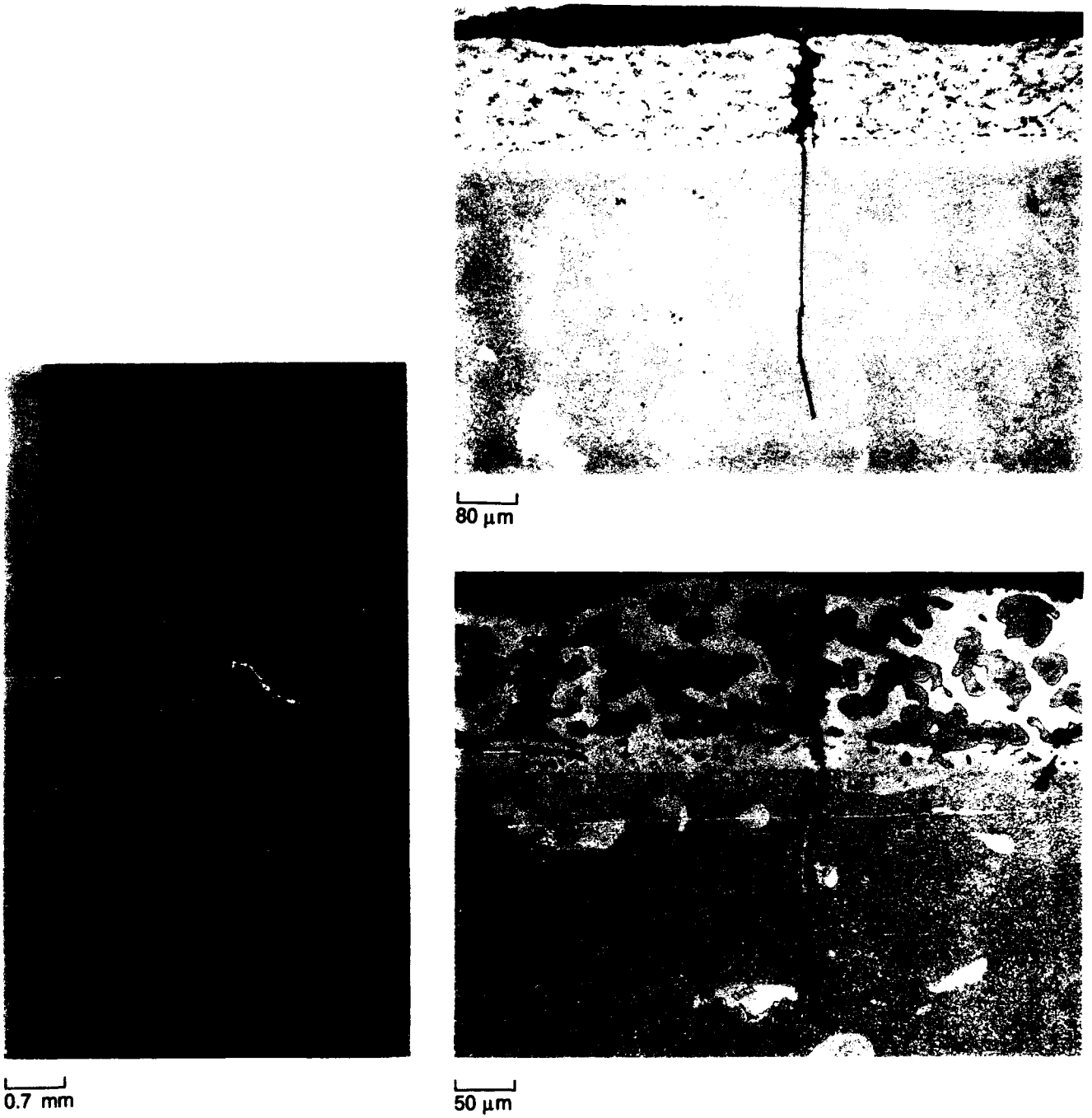

Figure 40. Surface Condition and Center Gage Microstructure of Type 1 TMF Sample of PWA 1480/LPPS NiCoCrAlY (Strain/Temperature Endpoints of Cycle: +0.1%/1280°F, −0.3%/1280°F; Cycles to Failure = 18,428)

The 2-cpm quad cycle specimen failed in 12,321 cycles, essentially the same as in the equivalent test at 1 cpm. Surface condition and gage section microstructure are illustrated in Figure 41. As in the case of the sample just discussed, there is metallographic evidence of the strain-induced oxidation morphology encountered in the initial quad cycle experiment, but the extent of beta consumption appears too slight to have contributed significantly to initiation or propagation of TMF cracks.

The low strain range quad failed in 14,285 cycles (versus 12,842 for the same temperature cycle but higher strain range); surface condition and microstructure at this point are shown in Figure 42. The type of selective oxidation observed in the high strain range quad cycle test of NiCoCrAlY is evident but not nearly as severe (cf. Figure 42 with the complete beta consumption in Figures 37 and 38).

4.2.4.3 Surface Features of NiCoCrAlY Coatings Exposed to Type 1 Versus Quad Cycles

Supplementing the metallographic documentation presented in the preceding sections, surface features of selected samples were examined by in-test scanning microscopy. The most significant results are probably the comparison of Type 1 (T_{max} = 2100F) versus the low strain range quad cycle specimen as summarized in Figures 43 and 44.

The Type 1 sample (Figure 43) is noticeably affected, although a complex, irregular pattern of rumples, cracks, and oxidized areas is not easily described. Obvious and significant, however, is that the coating is cracked in both the circumferential and lengthwise direction. Comparisons with Type 1 samples at T_{max} = 1900°F suggest the tendency for spanwise cracking, i.e., parallel to the axis of loading, is accentuated by the higher temperature.

Post-test metallography of this sample was presented in Figure 26. Although the comparision is somewhat compromised by the compressive overstraining of the sample shortly before termination of the test, it is clear that some of the lengthwise cracks have developed into areas of severe coating consumption and penetration of the fatigue cracks into the substrate.

A similar characterization of an LPPS NiCoCrAlY coating after approximately the same number of quad cycles is presented in Figure 44. Again the surface is noticeably oxidized and rumpled. Typical features include numerous short cracks, both circumferential and lengthwise, as well as small areas of localized but apparently deep oxidation attack (arrows in Figure 44; these features are not observed in Type 1 samples). The cracks and oxidized areas were usually associated with each other, although it is not clear whether one is primarily the cause and the other primarily an effect.

Post-test metallography of the quad cycle sample was presented in Figure 42, where the localized attack seen in the SEM photos seems to correlate with a tendency for selective oxidation of the β-NiAl phase observed in the longitudinal cross sections.

4.2.4.4 Comparison With Service Hardware

Undoubtedly the most difficult part of basic or applied research into TMF is use of the results to predict and understand relative TMF resistance and ultimate failure mechanisms of various coating/substrate combinations in the engine environment.

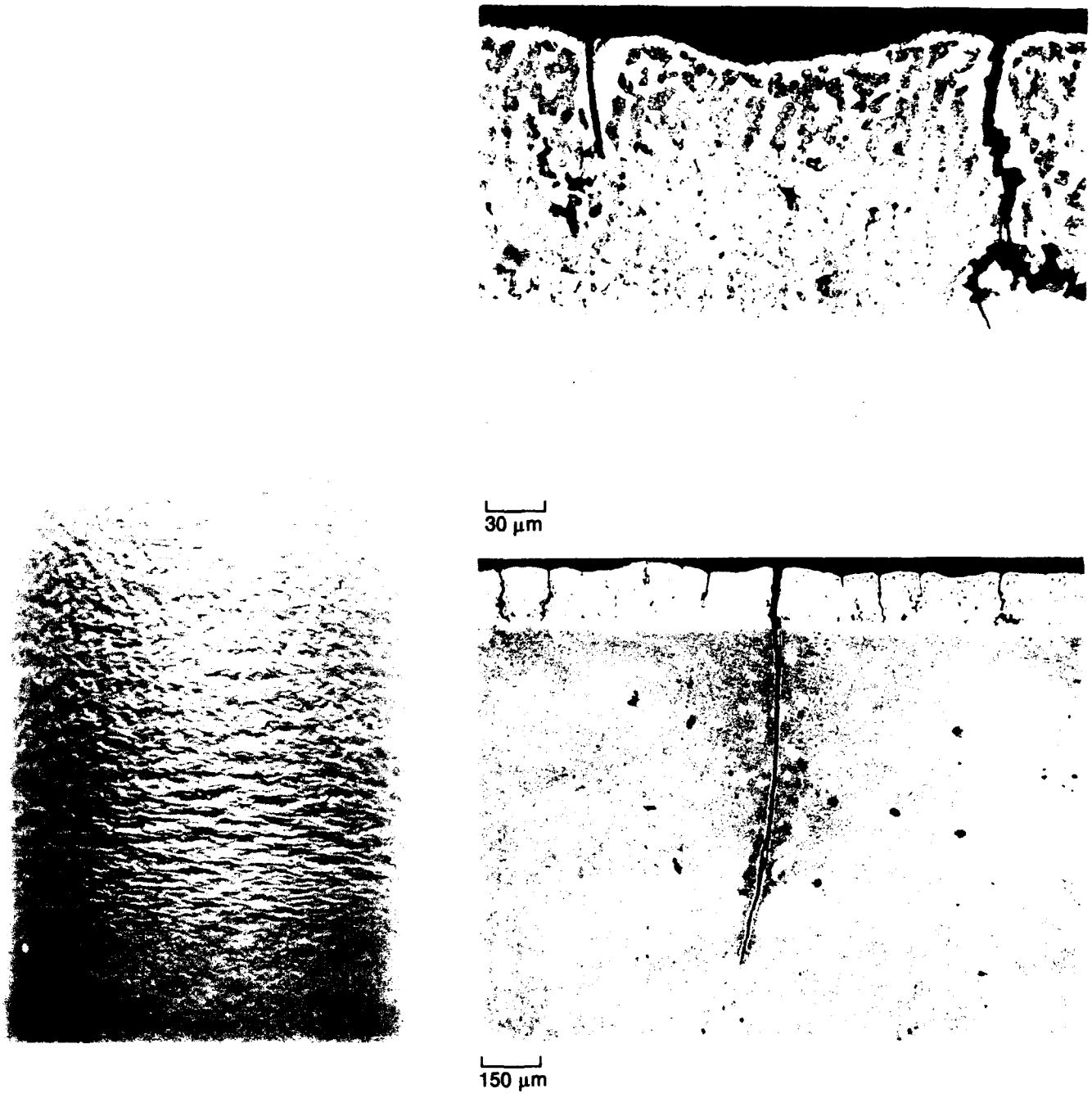

Figure 41. Surface Condition and Typical Microstructure of PWA 1480/LPPS NiCoCrAlY Quad Cycle TMF Specimen (Strain/Temperature Endpoints of Cycle: −0.1%/800°F, −0.6%/1800°F, −0.3%/2000°F, +0.1%/1280°F; Testing Speed = 2 cpm; Cycles to Failure = 12,321)

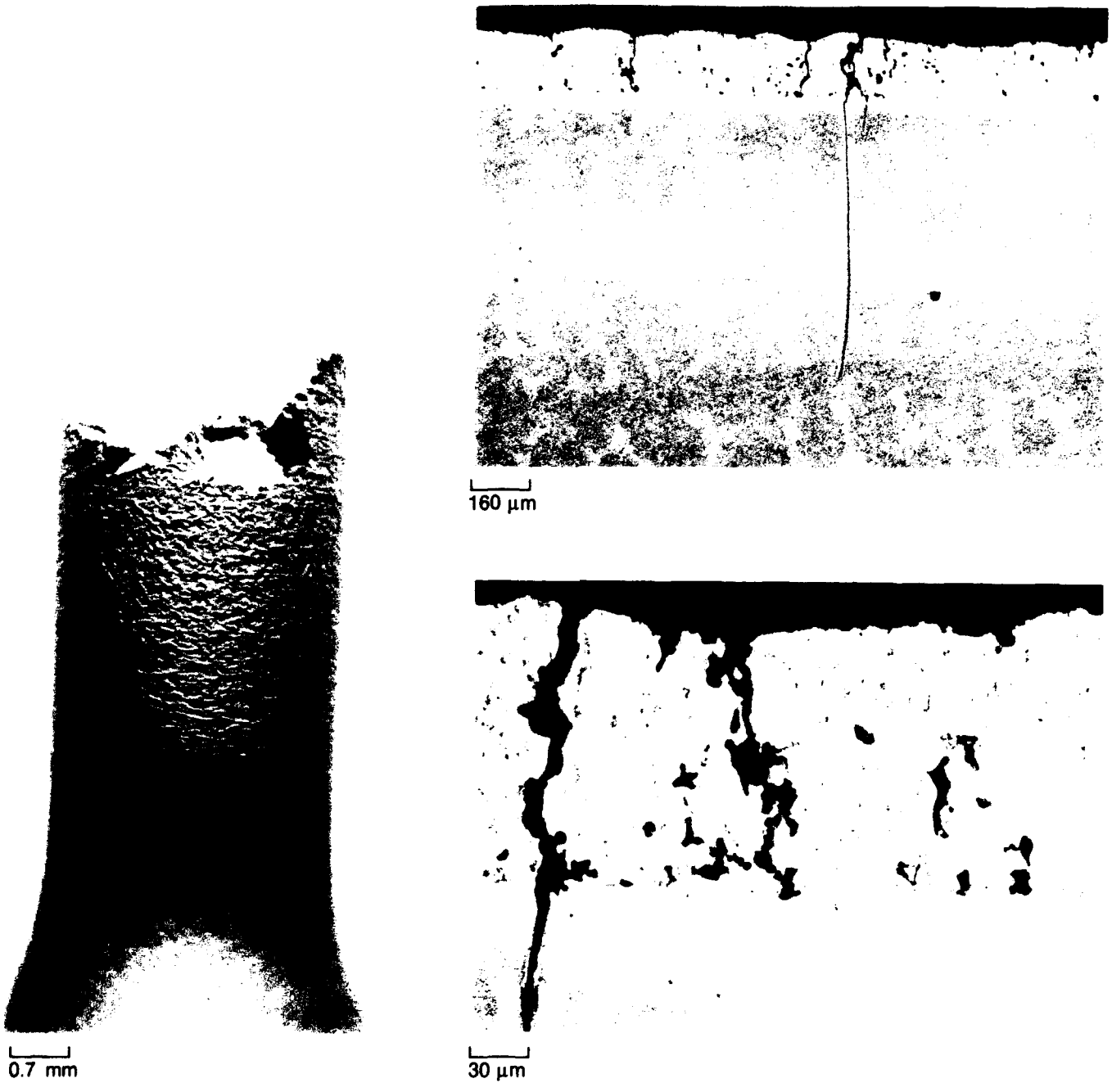

Figure 42. Surface Condition and Corresponding Microstructure of PWA 1480/LPPS NiCoCrAlY Quad Cycle TMF Specimen (Strain/Temperature Endpoints of Cycle: −0.1%/800°F, −0.45%/1800°F, −0.3%/2000°F, +0.1%/1280°F; Testing Speed = 1 cpm; Cycles to Failure = 14,285)

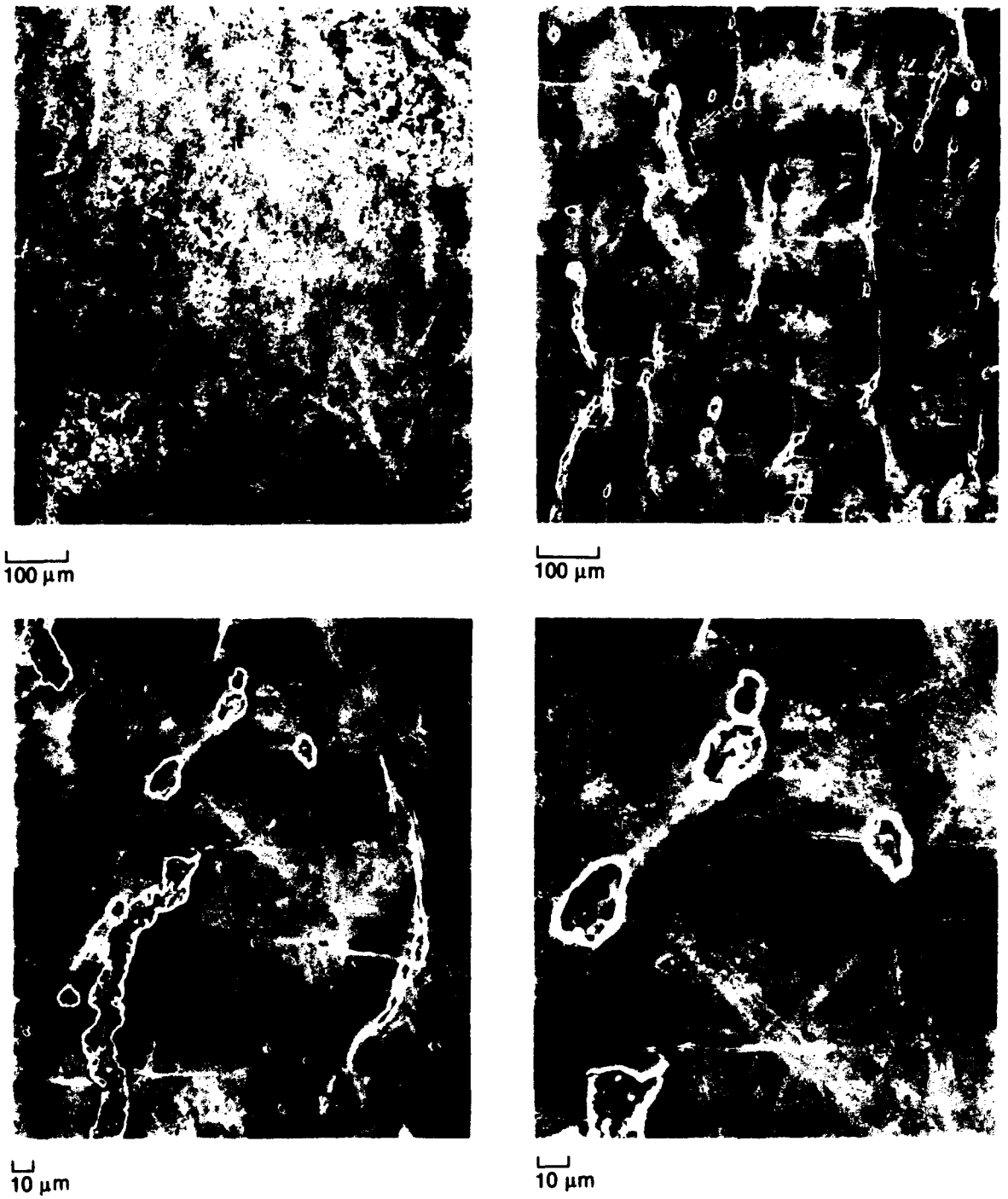

Figure 43. Surface Condition of LPPS NiCoCrAlY Coating on Type 1 TMF Sample After 4814 Cycles (T_{max} = 2100°F, Δε = 0.30%)

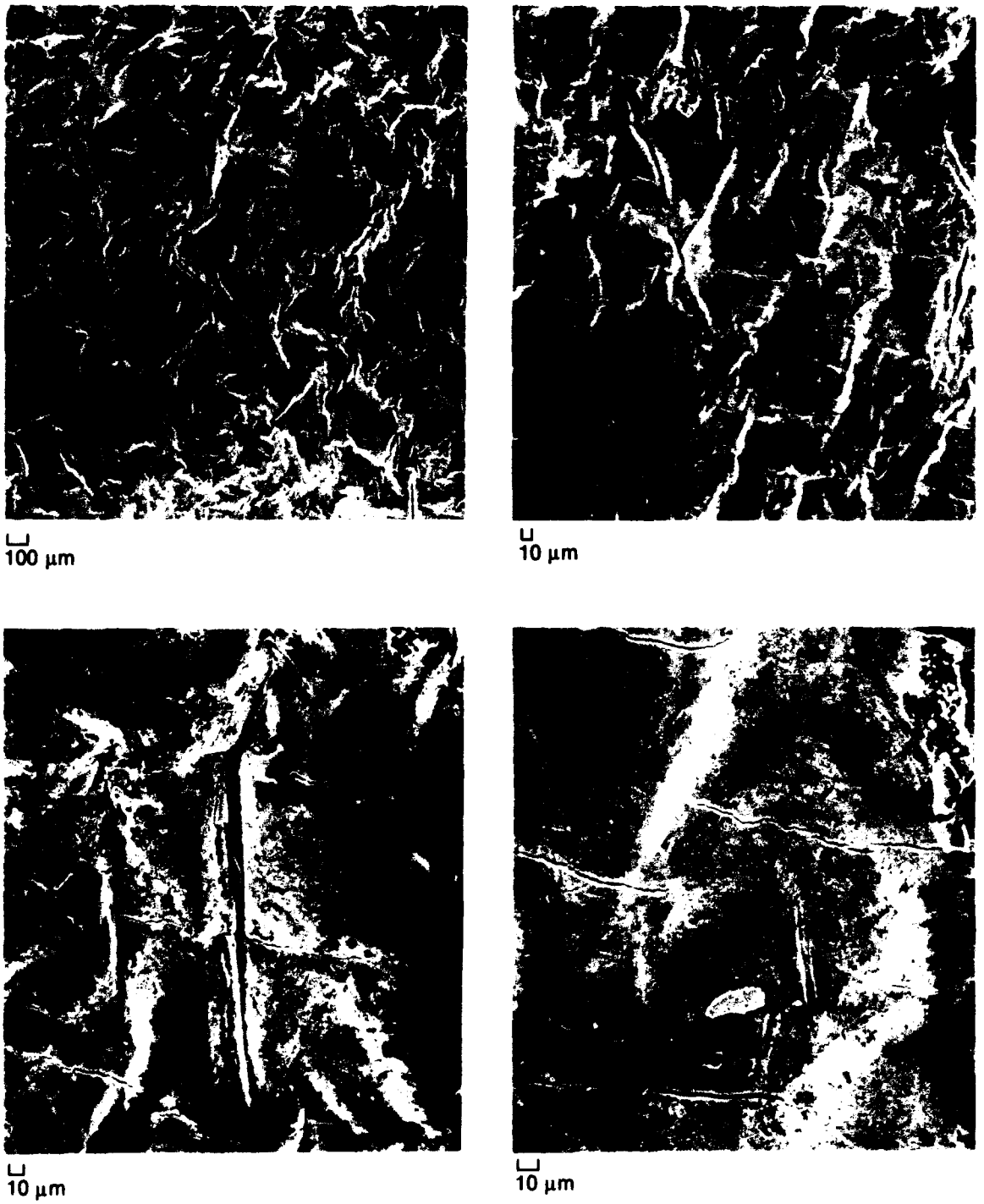

Figure 44. Surface Condition of LPPS NiCoCrAlY Coating on Quad Cycle TMF Specimen After 4515 Cycles, Including Unaffected Area Toward Radius (Top Left) and Typical Features in Gage Section

Analysis of TMF degradation in service hardware is formidably complicated by the complex geometry of airfoil shapes, the lack of accurate knowledge and control of metal temperatures and temperature gradients, and the difficulty of isolating the contribution of "normal" operating conditions from short but potentially very damaging excursions from the usual operating parameters of the engine. Hence it is virtually impossible to define a "typical" example of engine-induced thermal mechanical fatigue damage or degradation microstructure.

Nevertheless certain observations are frequent, if not universal; and it is possible to compare them with laboratory testing. Figure 45, for example, characterizes leading edge damage of a NiCoCrAlY-coated turbine blade from an advanced fighter engine after approximately 600 TAC cycles. The position of the leading edge (approximately at mid span) is established by the top left photo, and the blade was held in the same orientation for the rest of the examination.

In the area studied, the major degradation mode is spanwise cracking, and cracks which penetrated into the substrate are apparent on the exposed leading edge. The tendency of cracks to develop at the base of rumples — as shown by virtually all of the metallography in this report — is particularly well documented. Also evident in the same photos are chordwise markings which appear to be either cracks or incipient cracks. Although the similarity is not striking, the comparision with the lengthwise and circumferential features in the quad cycle TMF sample of Figure 45 suggests a similarity of the degradation mechanism. Lastly, in the area close to the exposed leading edge, Figure 45 shows the very irregular, multidirectional ridges and valleys similar to features produced by Type 1 testing at T_{max} of 2100°F (e.g., Figures 24, 25, and 43).

Deductions from microstructural observations of engine hardware are also not straightforward. Virtually any combination of mechanical and environmental damage can be found by looking at enough engine parts. The two extremes relevant to this discussion are illustrated in Figures 46 and 47. TMF cracks, for example, are frequently observed in engine hardware in the complete absence of significant oxidation or interdiffusion (Figure 46). Obviously the strain-induced oxidation discussed in connection with the quad cycle was not a factor in this type of damage. Neither is it likely that compositional or microstructural alteration by coating/substrate interdiffusion was a factor in this case.

In the opposite direction, the microstructures of Figure 47 appear to resemble the quad cycle oxidation morphology (cf. Figure 38), and bond coat oxidation of this type has apparently led to spallation of the thermal barrier coating. The coating in this case is not cracked, and failure was not premature. However, if the oxidation morphology is indeed strain-induced, this example does suggest that engine features can sometimes be related to definable cycle shape effects.

4.2.4.5 Hold Time and Cycle Shape Effects

Additional changes in cycle shape, testing time, and strain-temperature end-points were arbitrarily introduced into both quad and Type 1 cycles to look for rational trends in microstructure and/or cycles to failure data.

Hold time in the test cycle simulates isothermal exposure between thrust change transients. The effect of such exposures is probably an interaction between increased oxidation/interdiffusion and thermally activated stress relaxation processes which are promoted by the prolonged high temperature portion of the TMF cycle.

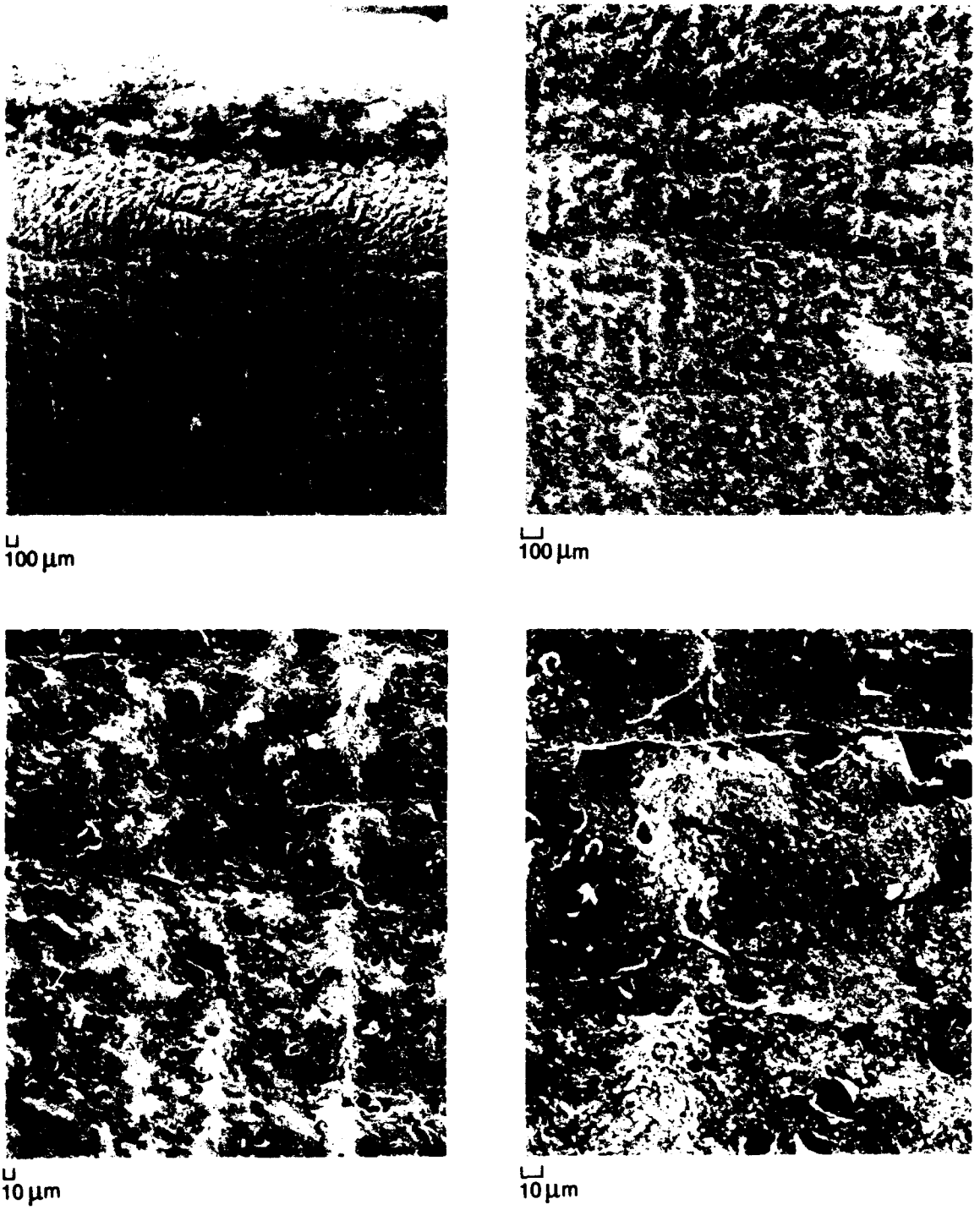

Figure 45. Surface Condition of NiCoCrAlY-Coated Turbine Blade From Tactical Fighter Engine

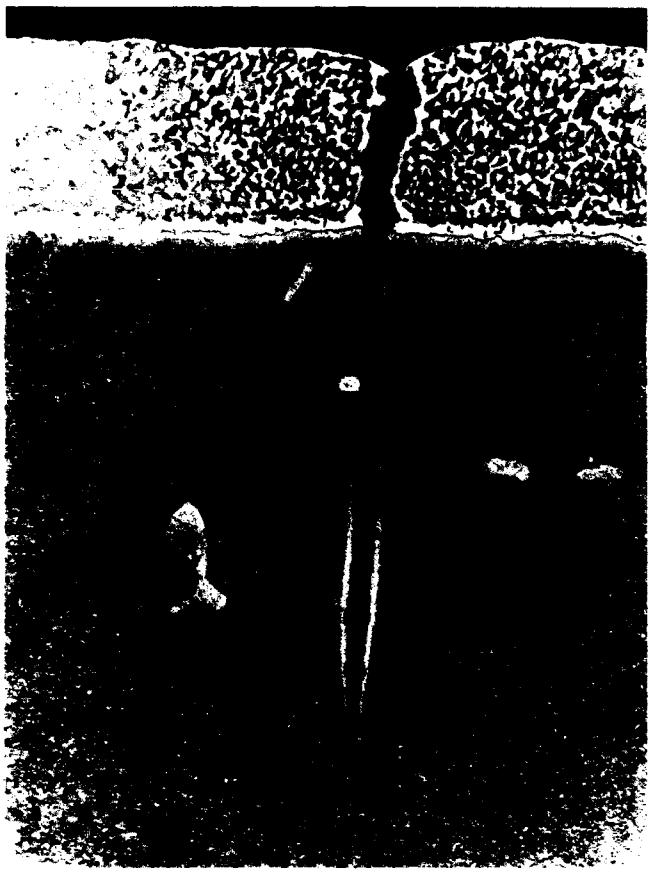

Figure 46. TMF Crack in Test Engine 1st-Stage Blade of PWA 1480/PWA 270 NiCoCrAlY After 1350 TAC's

Hold time data from quad cycle TMF tests of PWA 276 NiCoCrAlY are presented in Table 2. The initiation data are not readily interpretable, probably due in part to the difficulty of precisely determining the appearance of the initial cracks, while the trend for fewer cycles to specimen failure with increasing hold time seems well established.

As expected, metallographic examination showed increased β dissolution in the center gage microstructure of the hold time specimens (Figure 48). Even in the 2-minute hold sample, however, there was no evidence of bulk coating oxidation from diffusion-induced depletion. Also, the substrate interdiffusion zone was only 15 μm, so the decrease in cyclic life is not attributable to reduction in the load-carrying cross section.

Considering both the cycles to failure data and the metallographic observations, these results appear to relate the hold time effect to crack propagation in the substrate rather than a coating or interdiffusion effect. The trend in cycles to failure data seems clear, but there is no evidence of earlier crack initiation due to the hold time. Hence, assuming the consistency and reproducibility of the data, the decrease in cycles to failure must reflect crack growth in the substrate during the isothermal hold or a higher value of da/dn in the substrate alloy for the cycles separated by a hold time at T_{max}.

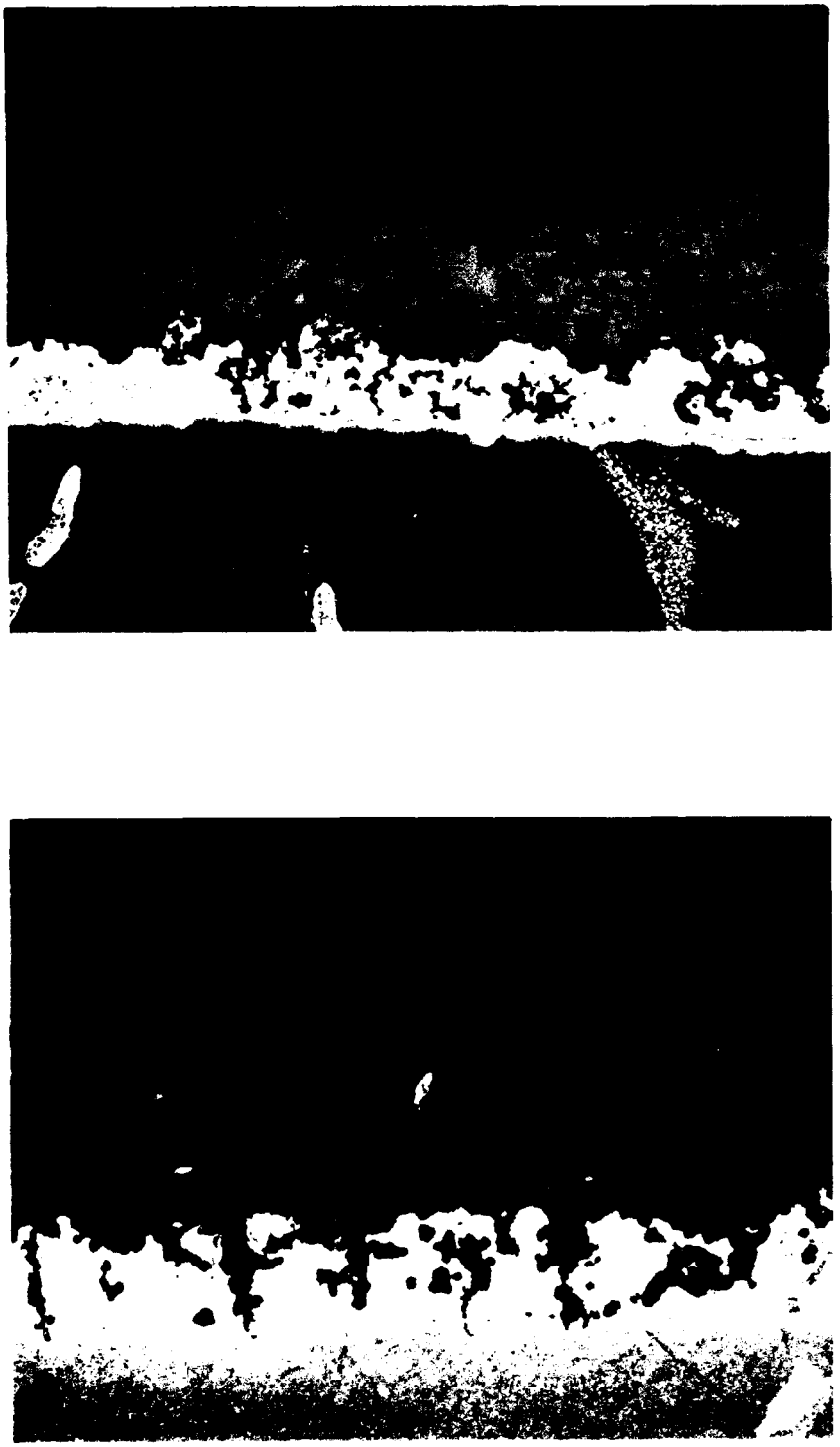

Figure 47. Bond Coat Oxidation in JTDE 2nd-Stage Vane After 4235 TAC's

Table 2. *Cycles to Initiation/Failure vs Hold Time (at Tmax) for Quad Cycle (0.55 Percent Strain Range) TMF Testing of LPPS NiCoCrAlY on PWA 1480*

Hold Time	*Cycles to Initiation*	*Cycles to Failure*
0	1,397	14,285
15 sec	4,569	10,338
60 sec	3,708	8,214
120 sec	3,093	6,980

R19528/10

One or both of these possibilities may be related to the stress-strain-temperature interactions of the quad-shaped TMF cycle. As discussed in connection with Figure 35, the quad cycle involves tensile load under T_{max}, even though the specimen is still shorter than its original length. The tensile load is small but perhaps sufficient to pull the cracks apart and allow access of oxygen to the crack tip. Oxidation-assisted crack growth could thus occur either at T_{max} or under the tensile loading which continues the cycle after the isothermal hold.

The final contributions to the cycle shape and strain range data base were Type 1 and quad cycle tests between the following strain/temperature limits:

(a) +0.1%/800°F, −0.45%/2000°F
(b) −0.1%/800°F, −0.45%/1800°F, −0.3%/2000°F, +0.1%/1280°F

Note that the strain range and mean strain are the same, so that the two tests differ only in the straight line versus the open cycle. Because temperature is ramped on a sine wave between T_{min} and T_{max} in both tests, the time-at-temperature history is also identical. However, the instantaneous value of strain at a given temperature differs substantially in the two cycles

The Type 1 test was interrupted for inspection of the sample at 1015 cycles. Coating degradation was not evident to optical examination, although SEM characterization showed the surface was superficially oxidized and unequivocally cracked. The cracks appeared to be initiating at media finishing grooves oriented near-normal to the stress axis. The groove orientation effect is strikingly demonstrated in Figure 49, where the center groove has developed into a crack while adjacent grooves of comparable depth but different orientation are not affected by the cyclic exposure.

Based on the SEM photos, the sample was cut for metallography. Cracks were readily detectable (the deepest on the plane of polish was over half of the coating thickness) and similar in morphology to those previously observed in short time tests.

The corresponding quad cycle test was stopped at the same exposure time. Again, no cracking was detected visually, although side-by-side comparison indicated the quad sample was more heavily oxidized than the Type 1 (as judged by a slightly darker blue color). SEM examination confirmed the generally greater surface oxidation (Figure 50 versus Figure 49), but it was not apparent that the cracks extended into the metallic material.

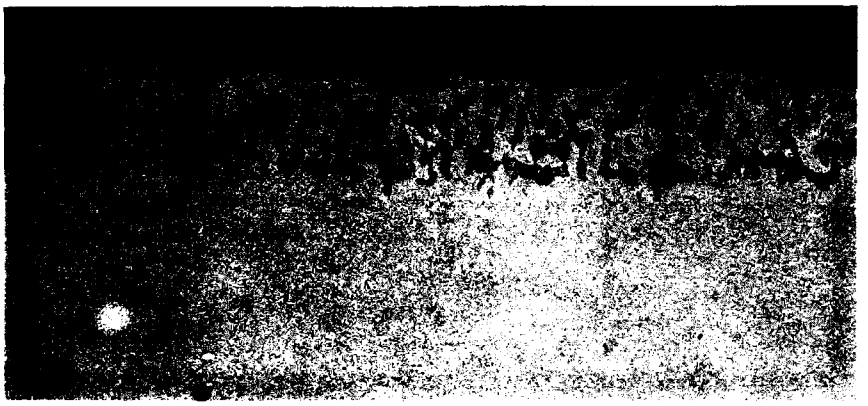

100 μ m

No Hold Time

100 μ m

1-Minute Hold

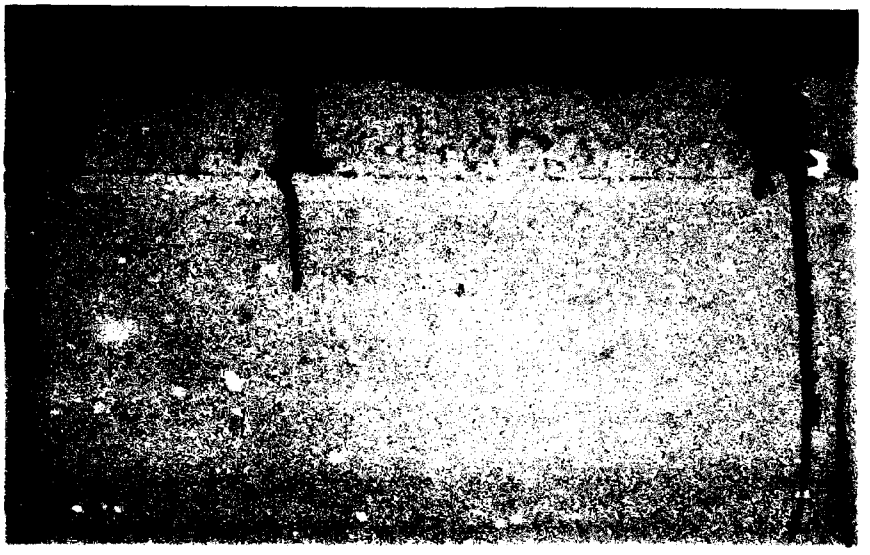

100 μ m

2-Minute Hold

FD 357818

Figure 48. Typical Dissolution and Diffusion Zone Thickness in TMF Samples

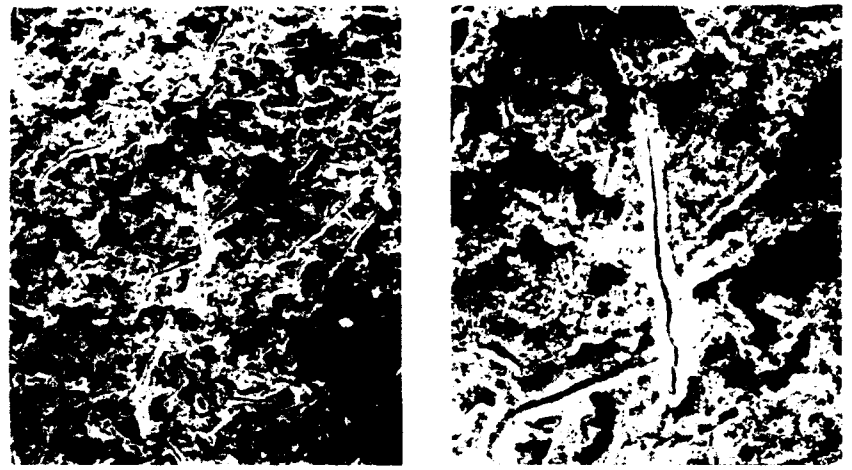

FD 357819

Figure 49. Typical Surface Morphology of Type 1 TMF Sample (T_{max} = 2000°F, GDε = 0.55%, Exposure Time = 1015 Cycles)

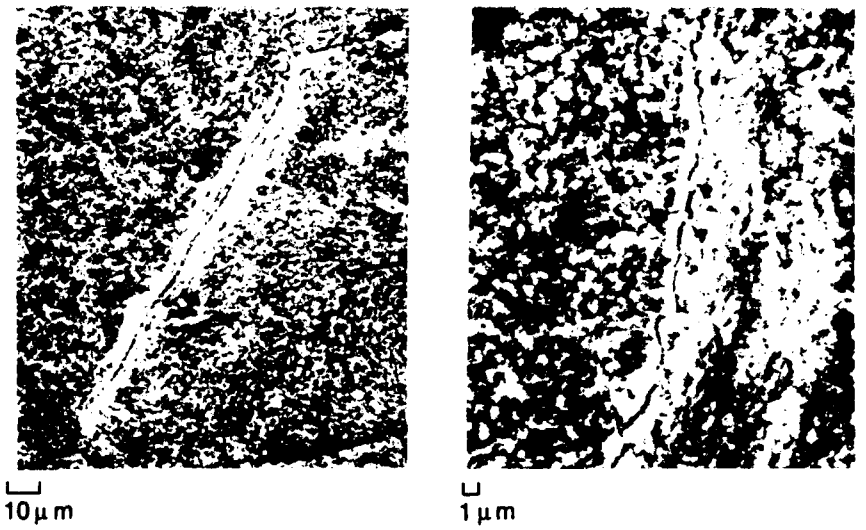

FD 357820

Figure 50. Typical Surface Morphology of Quad Cycle TMF Sample (T_{max} = 2000°F, Δε = 0.55%, Exposure Time = 1006 Cycles

Sectioning of the sample revealed surface profiles, as shown in Figure 51. The coating is rumpled, and sites where cracks will eventually develop are evident. A meaningful definition of whether or not the sample is "cracked" is still not straightforward, however.

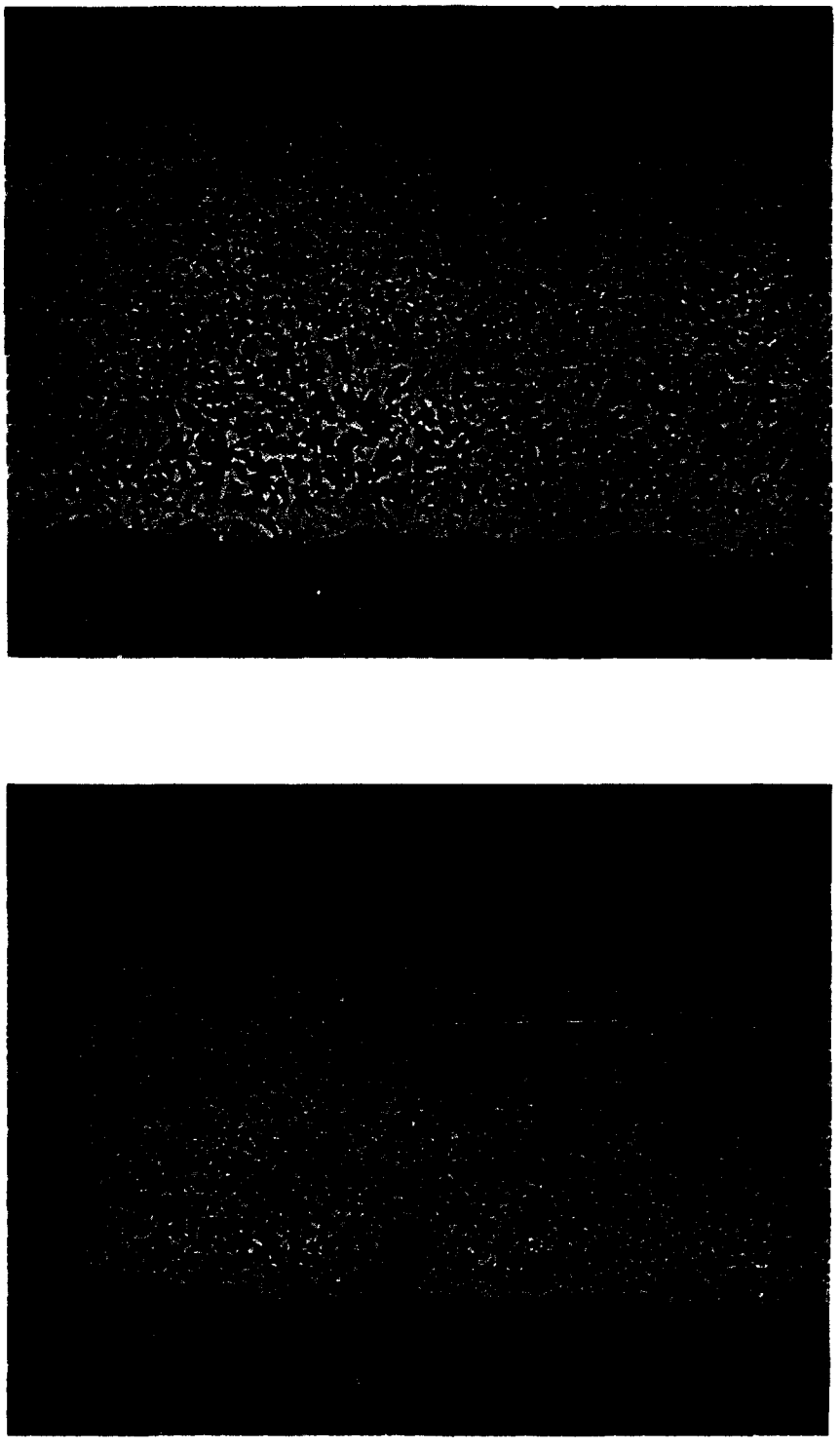

Figure 51. Cross Section of the Quad Cycle TMF Specimen Shown in Figure 50

A new specimen was run to 2000 cycles. Cracks in the oxide scale were more pronounced as a result of the longer exposure time, although they still did not appear as deep as in the Type 1 sample after only 1000 cycles.

These results, i.e., that the Type 1 sample was clearly cracked after 1000 cycles, while crack initiation was doubtful in quad samples, indicate that cycles-to-crack initiation are longer for the quad cycle than for Type 1 with the same strain range and temperature limits.

4.2.4.6 Surface Finish Effects

The observation of cracks initiating in media finishing grooves suggested a need for further information on surface finish effects. A sample was therefore lathe polished with 1 μm diamond polishing compound and exposed to the 0.55 percent strain range quad cycle.

A visual comparison of the polished and as-tumbled coatings after 4000 cycles is presented in Figure 52, where the difference in pre-test condition is evident in the unaffected area near the radius. The originally polished sample still appears slightly smoother, although both are distinctly rumpled and both are cracked.

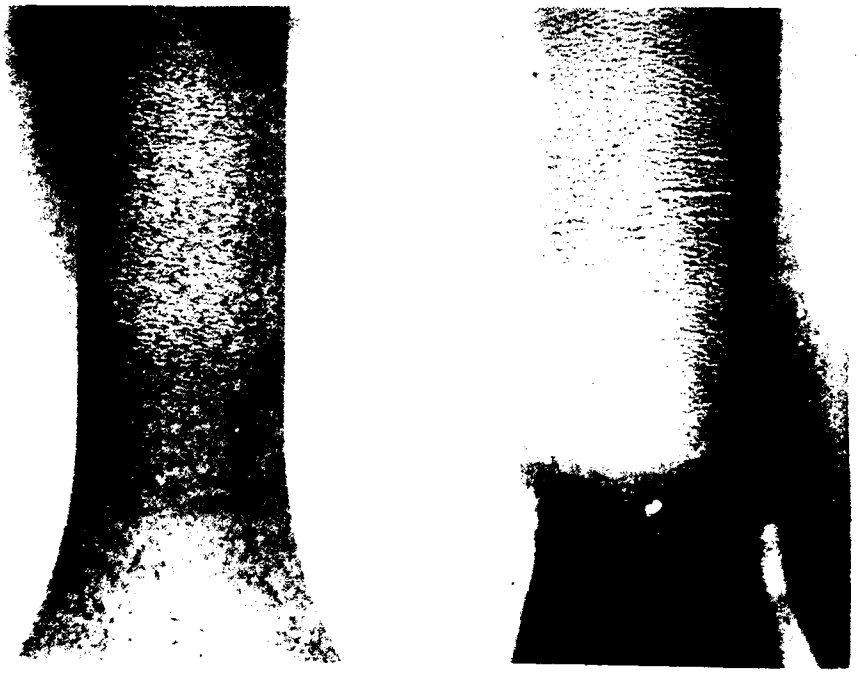

Figure 52. Surface Appearance of As-Tumbled Versus Lathe-Polished TMF Specimens After 4000 Quad Cycles

SEM examination of the same specimens after 8000 cycles showed primarily circumferential features on the polished specimen (undoubtedly paralleling the lathe polishing groves). Circumferential cracks were prominently visible to binocular microscope and SEM inspection. Conversely, surface features of the as-tumbled sample were multidirectional, reflecting the random angle of impact of the media finishing stones.

Center gage microstructures are illustrated in Figure 53. Neither sample is extensively cracked on the plane of polish, although there are numerous sites on the as-tumbled specimen where cracks are about to develop. The depth of rumpling and the spacing between peaks of the rumples appears comparable on both samples.

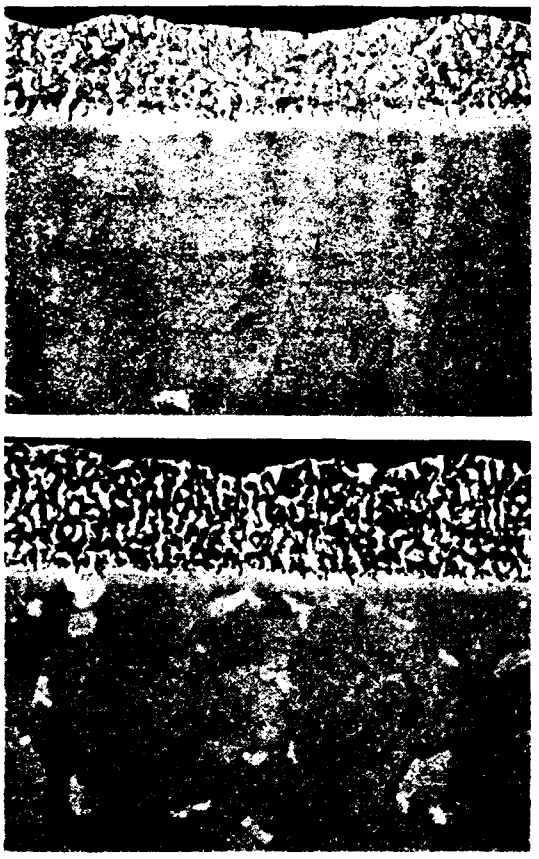

FD 357821

Figure 53. Longitudinal Section of the Lathe-Polished and As-Tumbled TMF Samples shown in Figure 52

From previous results on as-sprayed rather than tumble-finished surfaces, it is still believed that major differences in surface finish can affect TMF life in the cycles being used for these tests. The observations just presented, however, appear to indicate limited benefit of polishing below 30 microinches; even the highly polished surface soon becomes rumpled, and cracks initiate in the valleys of the rumples.

4.2.4.7 Type 1 and Quad Cycle Testing of LPPS NiCrAlTaHfY

A series of tests was run to compare behavior of an experimental coating (Ni-9.6Cr-11.7Al-6.1Ta-0.22Hf-0.50Y) with that of PWA 276 NiCoCrAlY in type 1 and quad-shaped cycles. The experimental coating was formulated for increased strength and lower thermal expansion mismatch with the PWA 1480 substrate; the coated samples were processed and heat treated in the same manner as previous specimens of NiCoCrAlY.

Coating cracks in a Type 1 sample tested at $\Delta\varepsilon = 0.7$ percent were observed after 700 cycles, and the sample failed at the radius after 2364 cycles. Evident from binocular microscope inspection is that failure occurred at a circumferential crack outside of the uniformly rumpled gage section, and equivalent cracks developed at the opposite radius. (Figure 54).

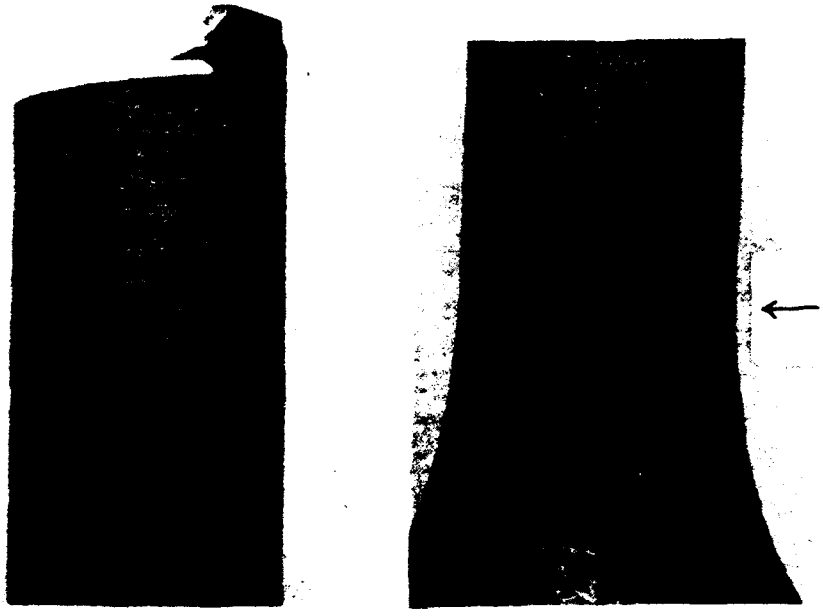

Figure 54. Surface Condition of Type 1 TMF Specimen of LPPS NiCrAlTaHfY on PWA 1480 (T_{min} = 800°F, T_{max} = 2000°F, Δε = 0.7%, Cycles to Failure = 2364

A specimen tested at Δε = 0.55 percent (to match the strain range of the quad cycle) failed in the gage section at 8062 cycles (versus an expected life of 7000 cycles for NiCoCrAlY at the same conditions). Post-test inspection revealed numerous short cracks in the gage section and a fine circumferential crack at one of the radii (Figure 55).

Quad cycle tests were next run at the same strain range as those used in Type 1. The sample exposed to the high strain range (0.70 percent) quad failed in center gage at 13,589 cycles*, in spite of the observation of a radius crack early in the test. This result compares with an average of 12,586 cycles for two specimens of LPPS NiCoCrAlY under the same conditions and with failure of the Ta-strengthened coating at 2364 Type 1 cycles. On post-test inspection, the radius crack was found to extend only part way (about 90 deg) around the circumference, and there were no other radius cracks. The gage section was rumpled, but many of the rumples had not cracked (Figure 56). The unusual oxidation morphology previously attributed to the time-temperature relationships of the quad cycle was detectable but probably not of an extent which influenced crack initiation or propagation.

* In the load-adjusted TMF test, specimen strain as monitored by machine deflection changes rapidly in the last 100 cycles prior to failure. To avoid introducing additional distortion from the rapidly increasing strain and facilitate metallography of the symmetrical specimen shape, the test was terminated when deflection increased sharply and the life-limiting crack was obvious to visual inspection. The reported cycles to failure are within 100 or so cycles of those which would have broken the specimen.

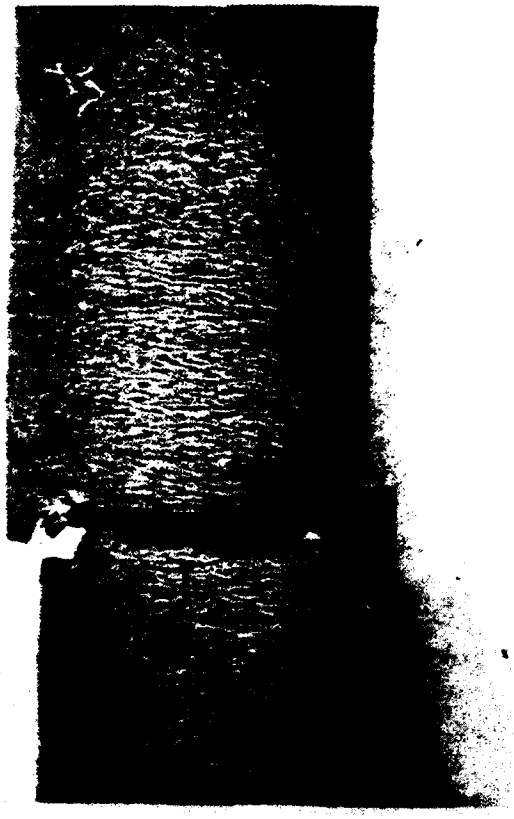

Figure 55. Surface Condition of Type 1 TMF Specimen of LPPS NiCrAlTaHfY on PWA 1480 (T_{min} = 800°F, T_{max} = 2000°F, $\Delta\varepsilon$ = 0.55%, Cycles to Failure = 8062)

A specimen tested at lower strain range (0.55 percent) failed in 17,859 cycles (versus 14,285 for NICoCrAlY under the same conditions and 8062 for this coating in Type 1 at the same strain range); cycles-to-crack initiation as judged by in-test inspection were approximately 9000. Post-test metallography again showed the expected extent of rumpling, but numerous rumples had not developed into cracks.

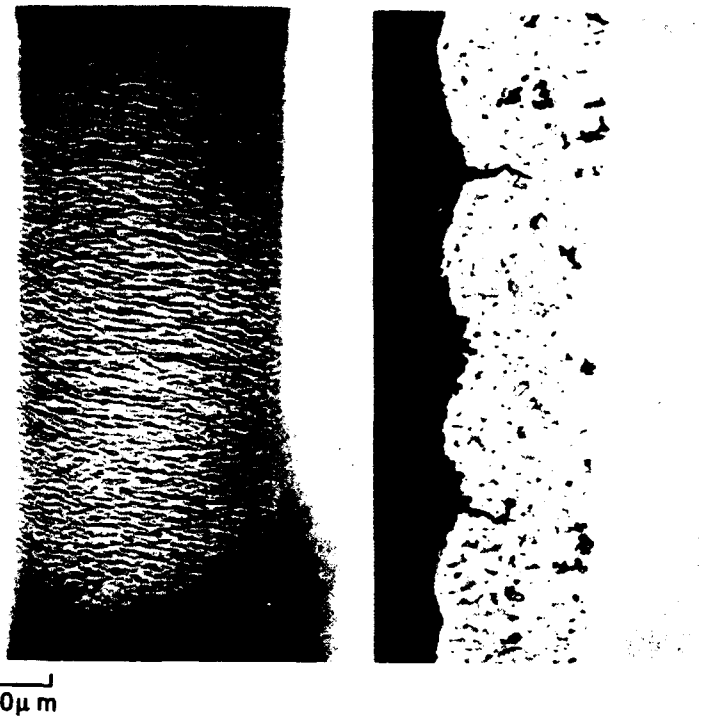

FD 357822

Figure 56. Surface Condition and Longitudinal Microstructure of Quad Cycle TMF Specimen of NiCrAlTaHfY on PWA 1480 (Cycles to Failure = 13,589)

SECTION 5.0
TASKS II AND III — EFFECTS OF TMF EXPOSURE ON MICROSTRUCTURE AND PROPERTIES

5.1 OBJECTIVE

A distinction between two tasks was made for cost accounting purposes; interpretation of the technical results is facilitated by combining the data.

The intent of this work was to expose coated specimens to various percentages of the cycles to crack initiation as determined in Task I and to document the effect of these exposures on ductility, composition, and microstructure of the coating. The technical approach was tensile ductility testing, including determination of strain to crack by acoustic emission, and post test metallography to correlate diffusion-affected grain structure and composition with mechanical properties and crack morphology.

5.2 RESULTS AND DISCUSSION

The original test plan for these tasks was based on observations in Advanced Coating Research that cycle shape strongly impacts TMF behavior and that major changes in composition and microstructure of overlay coatings result from time-at-temperature interdiffusion. It was hypothesized that such changes in coating composition (and, consequently, in mechanical properties and thermal expansion of the coating material) might be a factor in determining TMF durability of the coating/substrate system. Hence the experimental approach was to study cycles to initiation/failure versus cycle shape in Task I for the purpose of selecting an optimum cycle and material. In the remianing Tasks of the program, coated samples were to be exposed to various percentages of expected cyclic lifetime to determine if fatigue behavior could be related to degradation of composition and microstructure of the coating during TMF exposure.

Of the cycles examined, the choice of quad-shape over type 1 for these experiments was obvious. The longer cyclic lifetime and the tendency for straininduced oxidation maximized the possibility of producing observable oxidation or interdiffusion effects prior to onset of TMF cracking.

The same reasoning — plus the desire to test a different coating than the extensively investigated PWA 276 NiCoCrAlY — suggested use of the Ta-strengthened NiCrAlTaHfY coating.

Acoustic emission tensile ductility tests were run at 800°F (T_{min} of the TMF cycle) on as-processed samples of the LPPS NiCrAlTaHfY coating. Both exhibited strong acoustic signals at approximately 1 percent strain. The samples were pulled another 0.1 percent, and the test terminated for fluorescent penetrant inspection and metallography. Both showed a uniformly spaced series of circumferential cracks as illustrated in Figure 57.

A specimen for ductility testing was exposed to 3030 quad cycles. The TMF exposure resulted in surface rumpling as illustrated in Figure 58. Numerous fine cracks in the oxide scale were evident on binocular microscope inspection, but none appeared to extend into the bulk coating material.

Figure 57. Black Light Surface Photo and Crack Morphology in 800°F Tensile Specimen of As-Processed NiCrAlTaHfY on PWA 1480 (Strain to Crack = Approximately 1%)

Figure 58. Surface Condition of Quad Cycle TMF Specimen for Acoustic Emission Ductility Testing (Exposure Time = 3030 Cycles)

On tensile ductility testing of the TMF-exposed specimen, acoustic emissions were encountered at approximately the same strain as observed for the as-processed material. and those in the gage scction were more widely spaced than those near the radius. Rumpling of the coating was evident in a longitudinal cross section, but the tensile cracks did not form in the valleys of the rumples.

Another sample was exposed to 6000 TMF cycles. As judged by binocular microscope examination, some of the rumples appeared to have developed into cracks. The sample was acoustically noisier than those previously tested, although the initial major emission was again at about 1 percent. On post-test inspection the sample was so severely rumpled that fluorescent penetrant adhered uniformly to the gage section. No gage section cracks were detected by either visual inspection or metallography; a large crack near one of the radii was apparently responsible for the acoustic signal.

SECTION 6.0
TASK IV — QUAD CYCLE SHAPE EFFECTS

6.1 OBJECTIVE

This work continues and expands the quad cycle studies initiated in Task I. As in Task I, its purpose was to generate basic thermal mechanical fatigue data versus systematic changes in shape and speed of the quad cycle.

6.2 BACKGROUND AND APPROACH

This task began a major redirection of the program formulated when Task II/III data were indicating that coating oxidation and interdiffusion effects — at least in the type of cycles so far studied — were not of major importance because coating cracks initiated and propagated into the substrate long before the composition and microstructure of the coating were significantly altered. Hence the concept of attempting to relate TMF exposure to time dependent changes in chemistry and properties of the coating was not yet tenable.

Considered necessary in place of the original work statement was a more detailed evaluation of quad cycle shape effects. Although still believed to incorporate a key factor in behavior of the system, i.e., that compressive strain peaks before maximum temperature, the quad cycle was producing failure modes not typial of service exposure, and no advantage of the quad cycle (over the faster and less complicated type 1) in predicting relative engine performance and failure mode was yet discernable.

The test plan diagrammed in Figure 59 was devised to build on previous results by comparing the modified cycles with data already available from Task I to define the effect of the isolated variable. Also included in the new task was a comparison of aluminide versus overlay coatings for the purpose of defining the response of a coating of significantly different microstructure and mechanical properties to a given cycle shape effect.

6.3 RESULTS AND DISCUSSION

6.3.1 Cycle Speed

Higher cyclic speeds are of major importance in simulating the fast transients of the engine and for the very practical advantages of reduced testing time. Also, from the point of view of the underlying fundamentals of TMF behavior, the existence or absence of a frequency effect may suggest the relative importance of elastic versus creep processes in the overall thermal fatigue damage mechanism. (Elastic processes would be frequency independent, since they do not involve thermally activated dislocation movement, while plastic deformation and creep would depend on time-at-temperature per cycle.)

Limited data in Task I had suggested that 1 versus 2 cpm were not a factor in Type 1 data. The quad cycle showed a metallographically discernable effect due to differences in the extent of strain-induced coating oxidation, but the fundamental nature of the oxidation morphology or cycles to initiation/failure data were not affected.

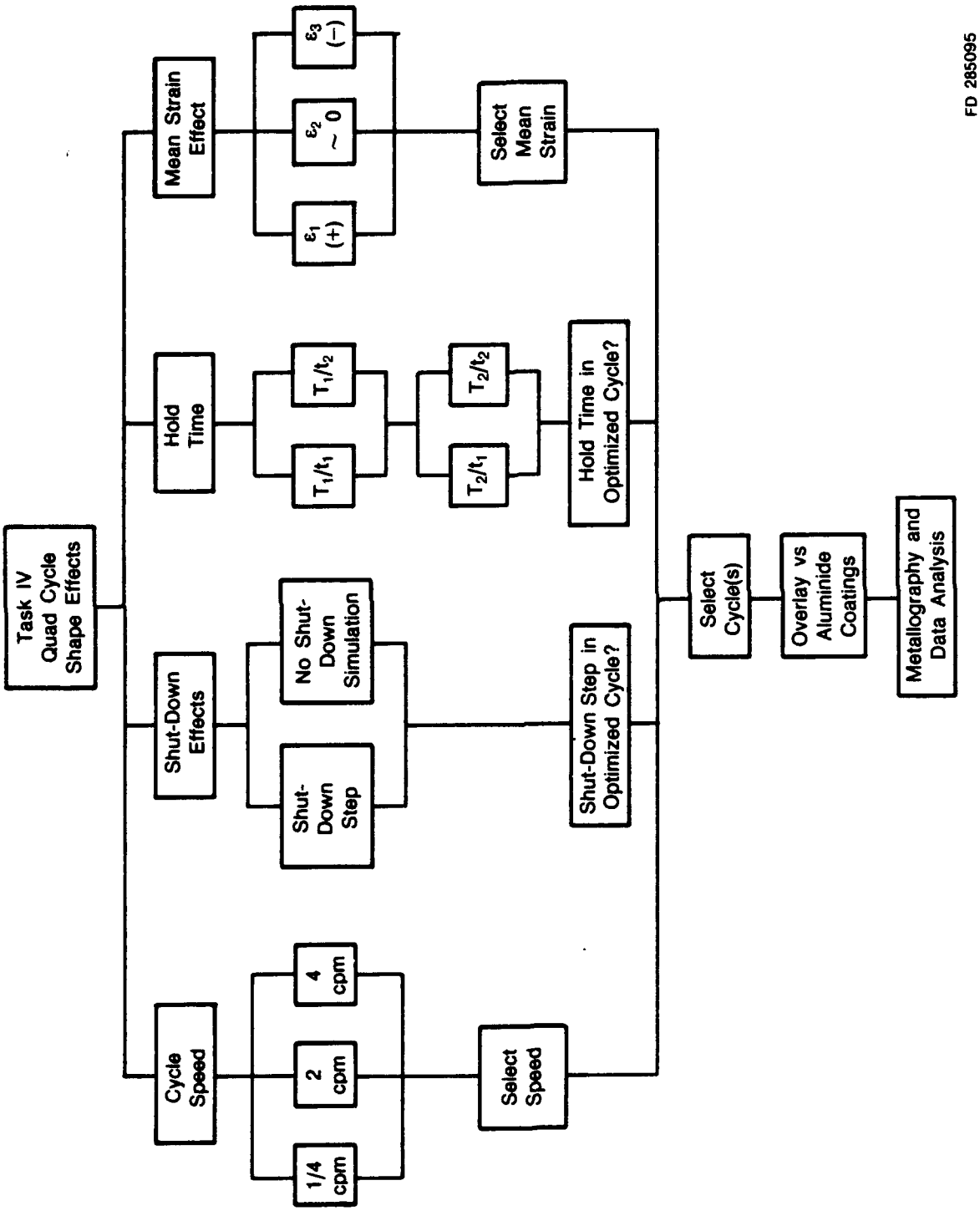

Figure 59. Flow Diagram of Task IV

Initial work in this task was documentation of cycle speed effect over a wider temperature range. Tests at 1/4 cpm, i.e., 4 minutes to traverse the quad, and 1/2 cpm failed in 10,579 and 11,473 cycles, respectively (versus 12,842 at 1 cpm).

The surface condition and center gage microstructure of the 1/4 cpm sample are shown in Figure 60. The coating is heavily rumpled, and the microstructure of the hot zone is almost completely devoid of β-NiAl. As in the previously studied quad cycle specimens, however, the interdiffusion zone is thin, indicating that most of the β phase was consumed by surface connected oxidation rather than coating/substrate interdiffusion. The extent of β loss is slightly greater than at faster testing speeds, although there is no evidence that the microstructural effect significantly influenced mechanism of crack initiation/propagation in the coating.

Figure 60. Surface Condition and Longitudinal Microstructure of Quad Cycle (−0.1%/800°F, −0.6%/1800°F, −0.3%/2000°F, +0.1%/1280°F) TMF Specimen (1/4 Cycle per Minute, Cycles to Failure = 10,579)

Tests at greater than 2 cpm required the hollow tube sample diagrammed in Figure 61. It was recognized that a change in specimen design would preclude some of the cyclic variable comparisons being attempted in this Task, but results of other work (primarily the comparison of load-adjusted versus strain controlled data) were dictating use of hollow samples on the load-adjusted rig, and the advantages of the hollow specimen were beleived to outweigh the problems of changing specimens in the midst of a program.

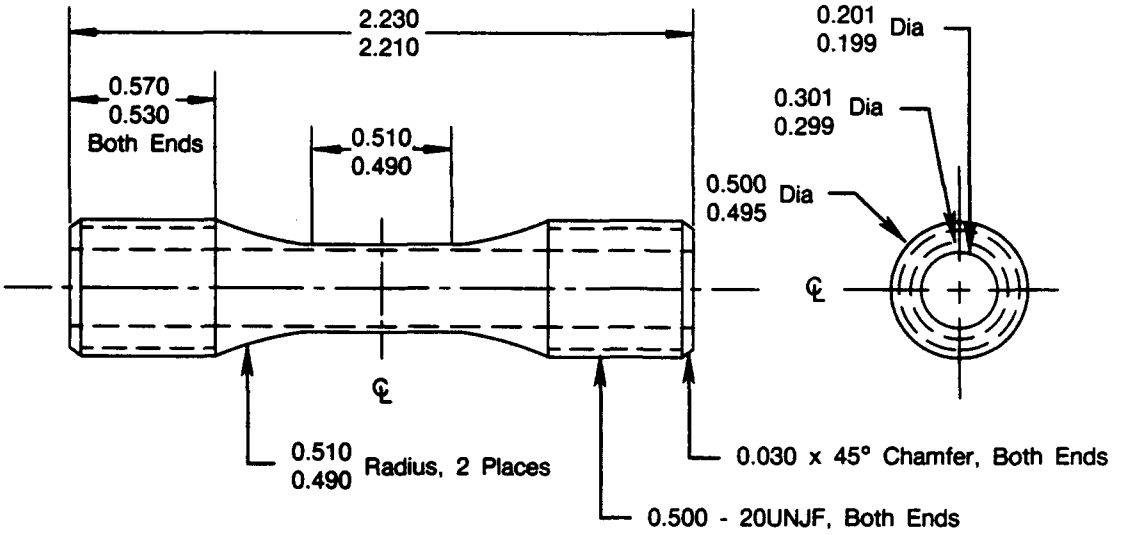

Note: All Dimensions in Inches.

FDA 356248

Figure 61. Hollow Load-Adjusted TMF/Coating Ductility Specimen for High-Speed Testing

The high speed effect was studied in 2 versus 4 cycles per minute tests of PWA 275 diffusion aluminide. This coating was known to be especially susceptible to strain-induced oxidation in the quad cycle, and it was reasoned that effects of shorter testing times would be most readily observable in the all-surface layer of the PWA 275 microstructure.

The behavior of PWA 275 in the quad cycle at 2 cpm is illustrated in Figure 62. The test was terminated after 9881 cycles due to coating spallation in center gage (Figure 62a). The exposed substrate was dark blue-green, i.e., a mixture of chromia and spinels, and the adjacent coating was heavily oxidized (Figure 62b, c). The limit of the affected area (Figure 62d) indicates the degradation process began with oxidation of grain boundaries in the β-NiAl layer; there was no significant interdiffusion or surface depletion prior to grain boundary oxidation.

The next test under the same conditions was terminated after 2517 cycles to characterize the initial stages of coating oxidation. Figure 63 shows a well- defined zone of blueish-white oxide in center gage and the corresponding microstructure of the affected area. It is clear that the degradation process involves grain boundary oxidation of the outer β-NiAl layer of the coating. Oxidation then proceeds laterally through the γ and along the interface with the diffusion zone, leading eventually to complete loss or consumption of the coating.

The 4 cpm test to determine if the faster testing speed, i.e., less time-at-temperature per cycle, would reduce the extent of coating oxidation is shown in Figure 64. Comparison with Figure 62 indicates the effect of the faster speed is not significant, since surface oxidation, coating spallation, and severe microstructural degradation were encountered in approximately the same number of cycles as in the test at 2 cpm.

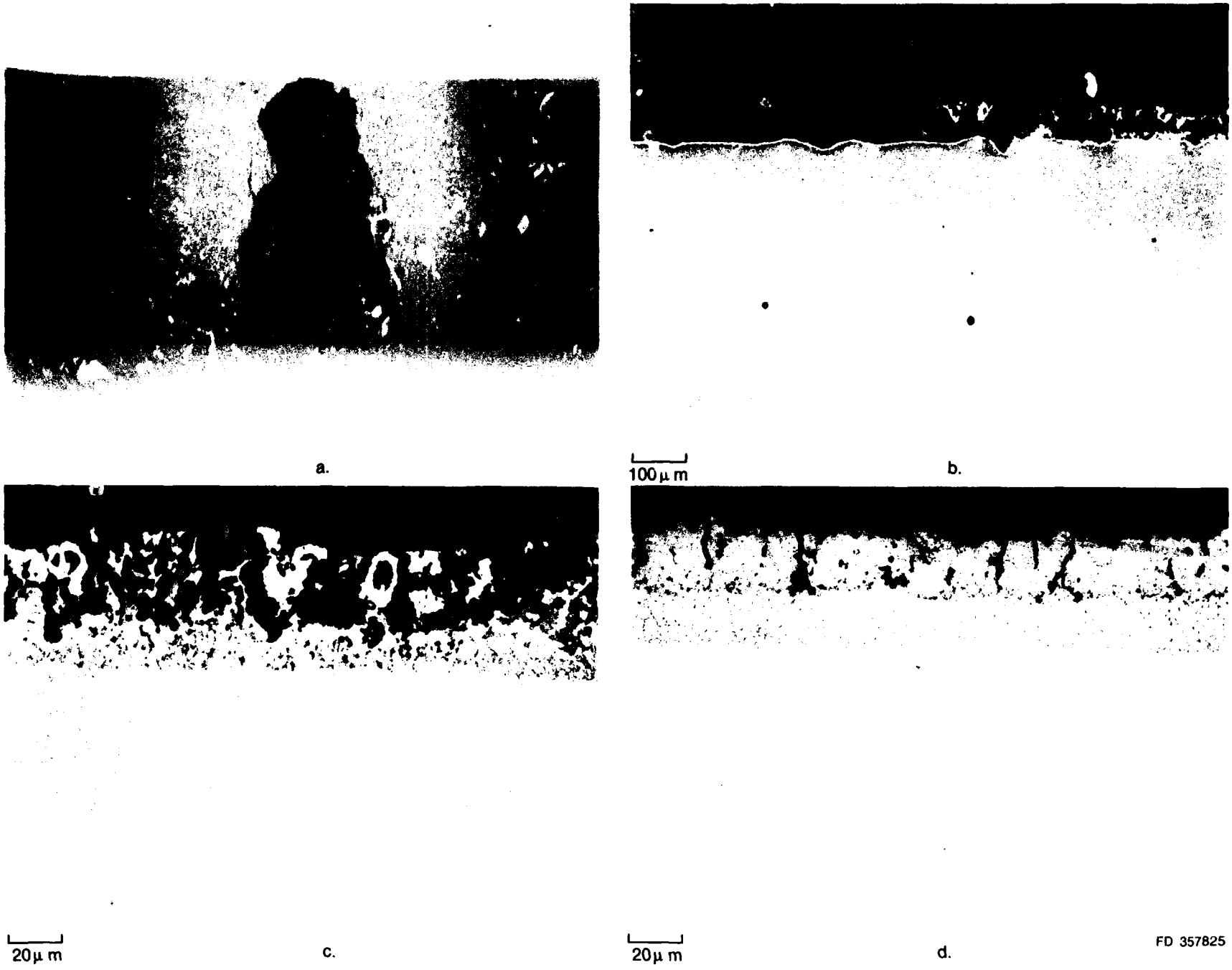

Figure 62. Surface Condition and Gage Section Microstructures of Quad Cycle (-0.1%/800°F, −0.6%/1800°F, −0.3%/2000°F, +0.1%/1280°F) TMF Specimen of Gas Phase Aluminized PWA 1480 (Exposure Time = 9881 Cycles)

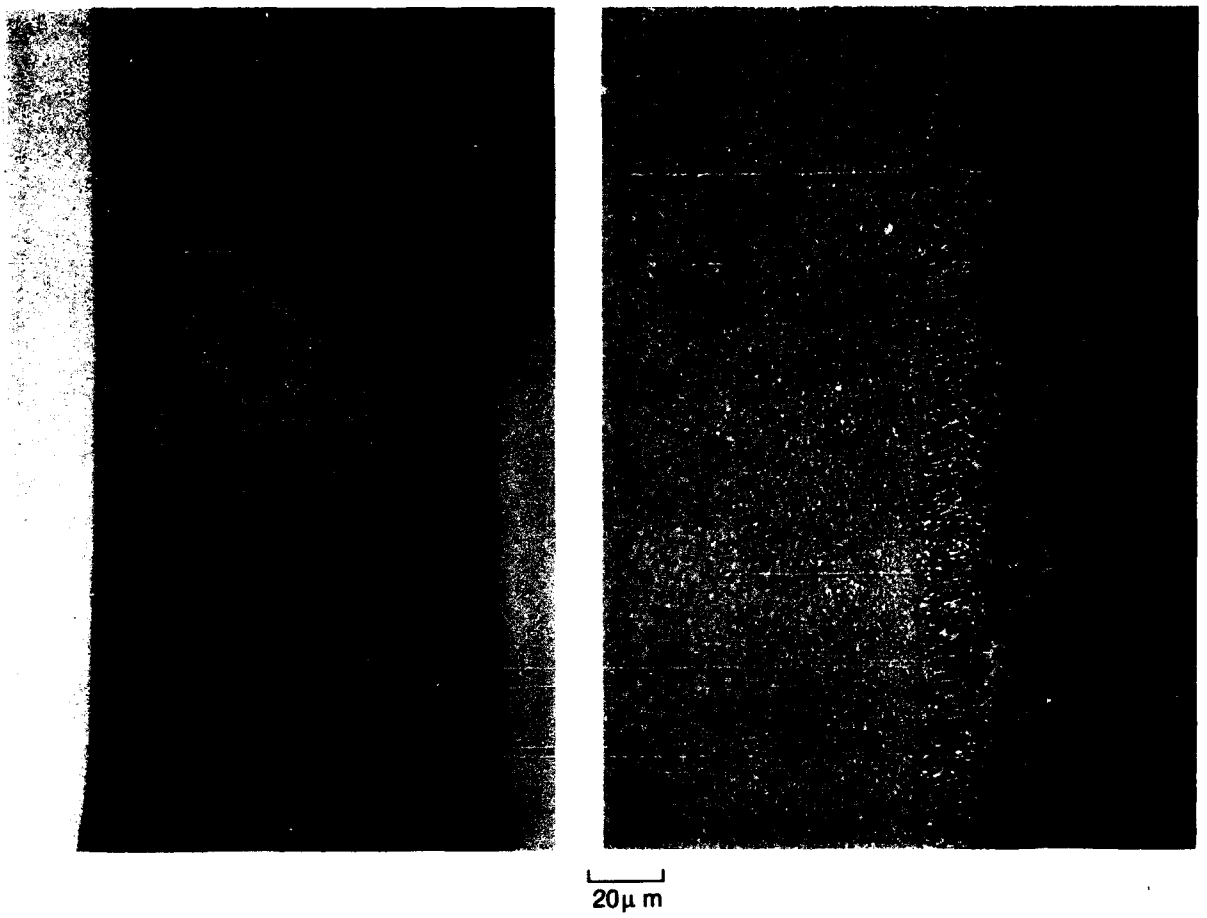

Figure 63. Surface Condition and Gage Section Microstructure of Quad Cycle (−0.1%/800°F, −0.6%/1800°F, −0.3%/2000°F, +0.1%/1280°F) TMF Specimen of PWA 1480/PWA 275 (Exposure Time = 2517 Cycles at 2 cycles/minute)

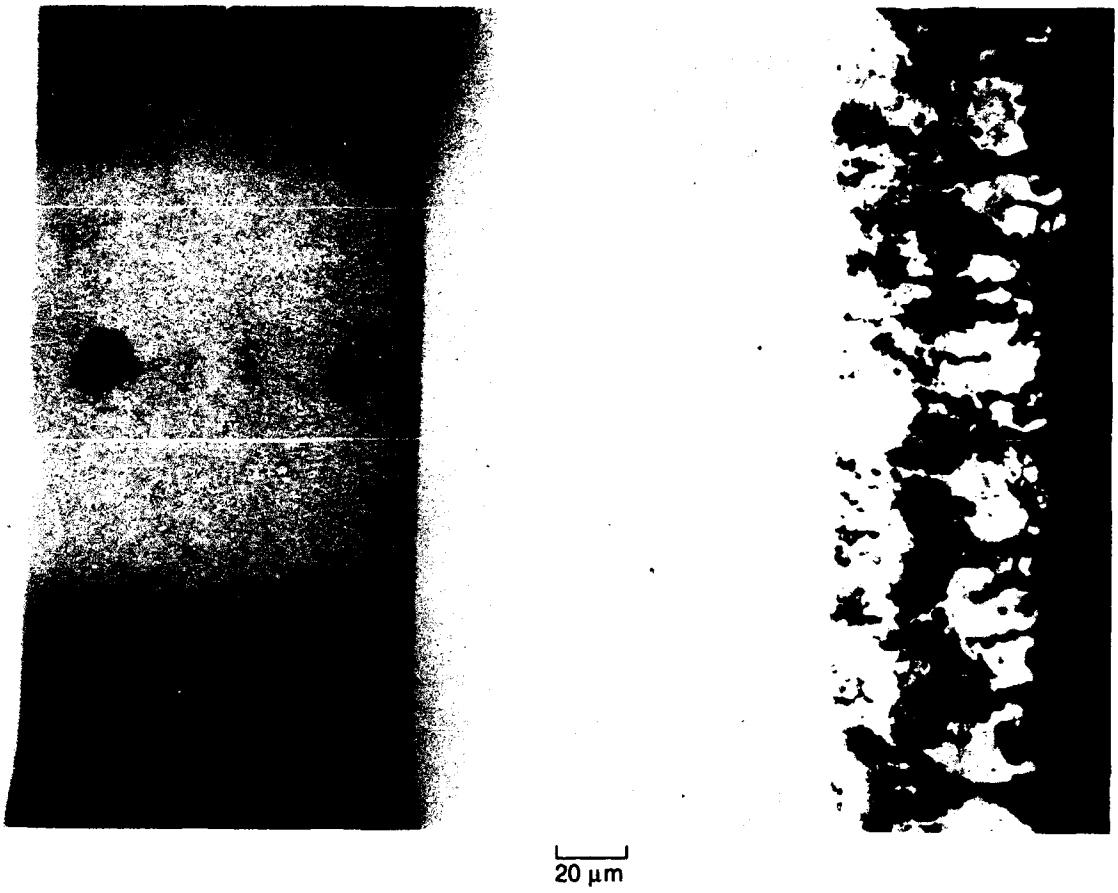

Figure 64. Quad Cycle (−0.1%/800°F, −0.6%/1800°F, −0.3%/2000°F, +0.1%/1280°F) TMF Specimen of PWA 1480/PWA 275 (Exposure Time = 7882 Cycles at 4 Cycles per Minute)

Lastly in this series of experiments, it was considered desirable to demonstrate dramatically the effect of cycle shape on coating oxidation and TMF behavior. A 2-cpm Type 1 test was therefore run at a strain range of 0.7 percent and temperature limits of 800 to 2000°F. The sample broke in 3594 cycles; secondary cracks were observed near the fracture, but no coating oxidation was discernable by visual inspection or metallography, even though the sample had seen greater time-at-temperature than an oxidized quad cycle specimen exposed to the same temperature limits and strain range (cf. Figure 65 versus Figure 63).

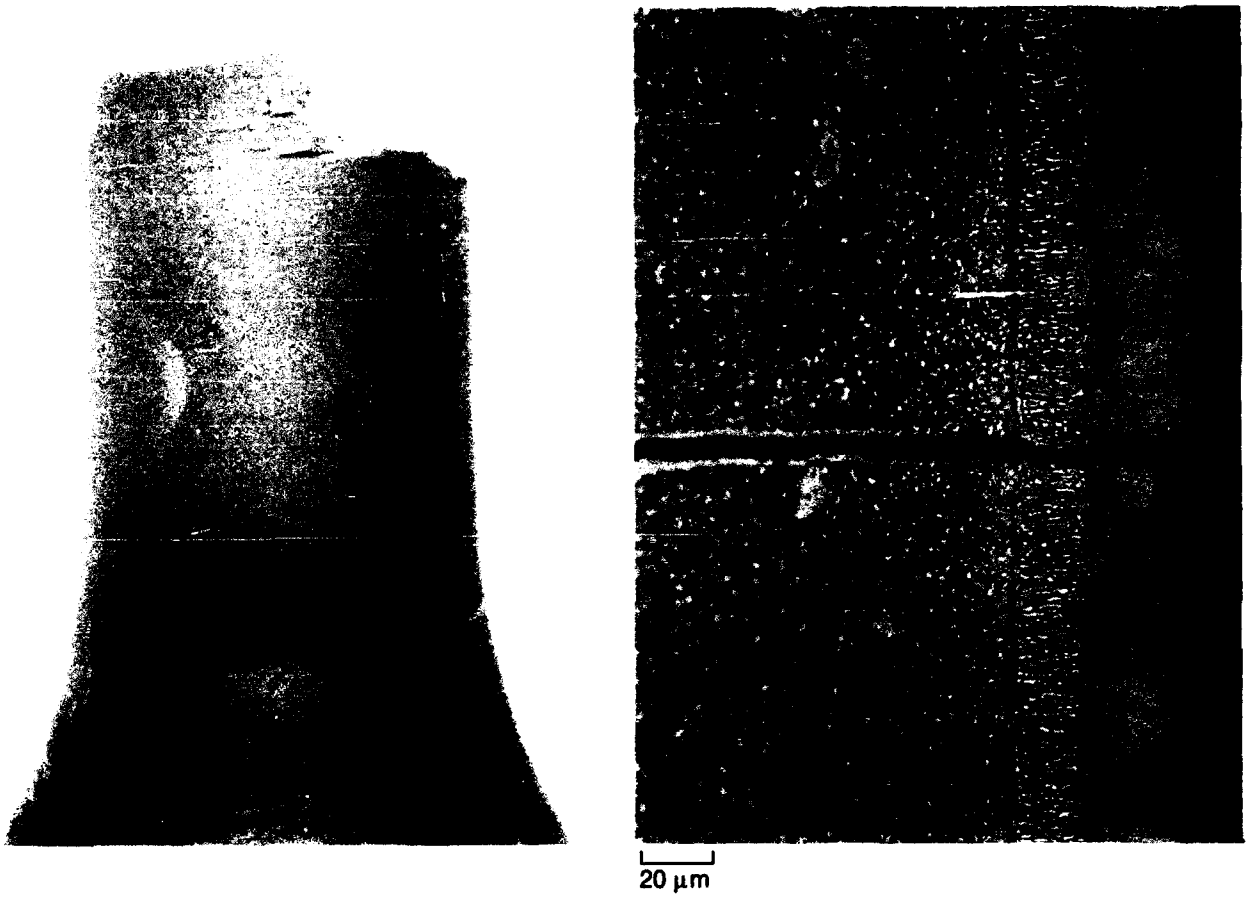

Figure 65. Surface Condition and Gage Section Microstructure of Type 1 TMF Specimen of PWA 1480/PWA 275 (T_{min} = 800°F, T_{max} = 2000°F, Δε = 0.7%, Cycles to Failure = 3594 at 2 Cycles per Minute)

6.3.2 Shutdown Effects

In spite of its more realistic simulation (in comparison with Type 1 cycles) of strain-temperature history in turbine airfoils, the quad cycles so far used in this program have neglected a potentially significant effect of engine shutdown. Basically, the shutdown effect would be an increase in tensile stress as elements of the airfoil are cooled to room temperature but still constrained by the surrounding material. The increased tensile load is obviously a driving force for crack initiation and propagation, but the effect might be mitigated because it occurs at low tempertures where thermal gradients would be smaller and oxidation at the crack tip would not be a factor.

The reason for neglecting shutdown effects is primarily experimental convenience. Since cooling rate is proportional to temperture differences, the cool-down from a T_{min} of 800°F to ambient temperature adds significantly to rig time and consequently the cost of the test. The following experiments were therefore carried out to determine if additional information gained from a shutdown step would justify the increased expense and complexity of the test.

A simulated shutdown step was incorporated into the quad cycle as sketched in Figure 66. The cool-down and reheating from 800°F took approximately 30 seconds, and the rest of the

quad was traversed in 16 seconds. Hence the time per cycle at high temperature is essentially the same as for the 4-cpm quad cycle tests just discussed. The primary effects of the shutdown step, therefore, are that the wider temperature range increases thermal strain on the coating, and, during cool-down from from 800 to 100°F, tensile stress was increased from approximately 30 to 33 KSI to maintain constant mechanical strain as elastic modulus increases with decreasing temperature. It was anticipated that greater tensile loads might contribute to both earlier crack initiation and faster crack growth.

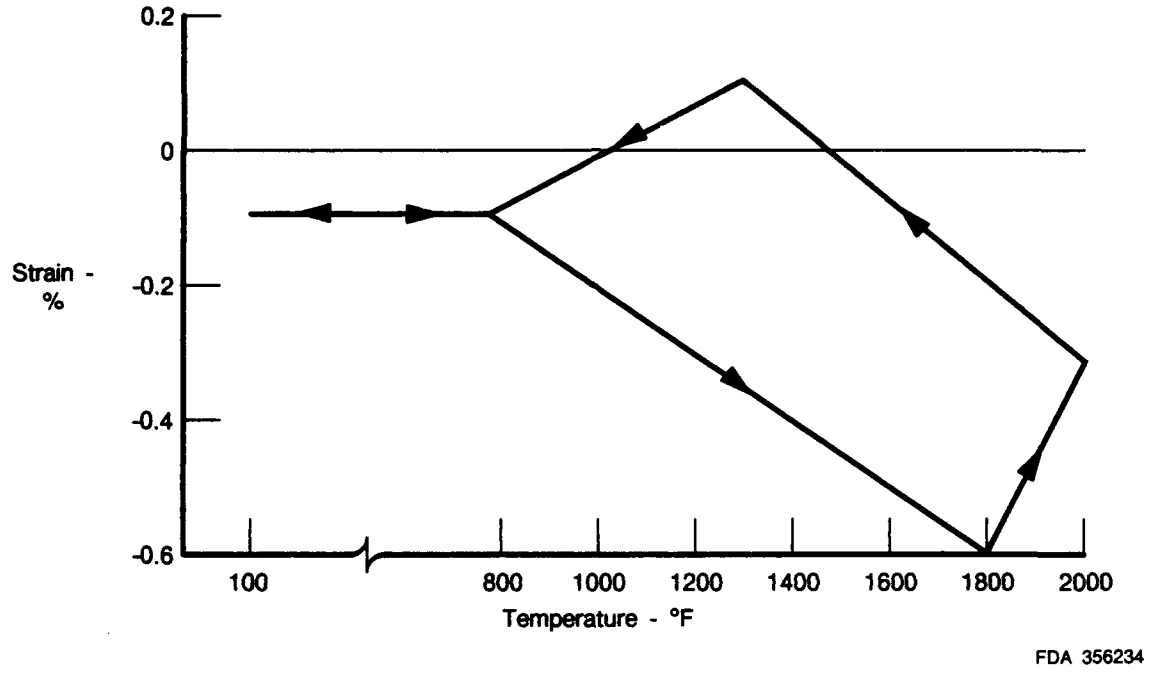

Figure 66. Quad Cycle with Simulated Shutdown Step, i.e., Cooling of the Material to Ambient Temperature

The specimen was run for 11,600 cycles and terminated because of the short but prominent coating cracks illustrated in the surface photo and corresponding longitudinal microstructure of Figure 67. The surface cracks appear to be more pronounced than encountered with the baseline quad cycle, but the fundamental nature of quad cycle behavior, i.e. severe grain boundary cracking, but the cracks do not propagate into the substrate, was not altered by the shutdown step.

The shutdown step was next imposed from 1280°F (to increase the average stress by cooling under maximum tensile load), and a sample of PWA 1480/PWA 275 was again exposed to 11,600 cycles. The effect was essentialy the same as in the previous experiment; virtually all of the β-NiAl grain boundaries were pulled apart, and the interdiffusion zone was heavily oxidized. Again, however, no TMF cracks extended into the substrate, in spite of the fact that Type 1 specimens at this temperature and strain range fail in approximately 3000 cycles.

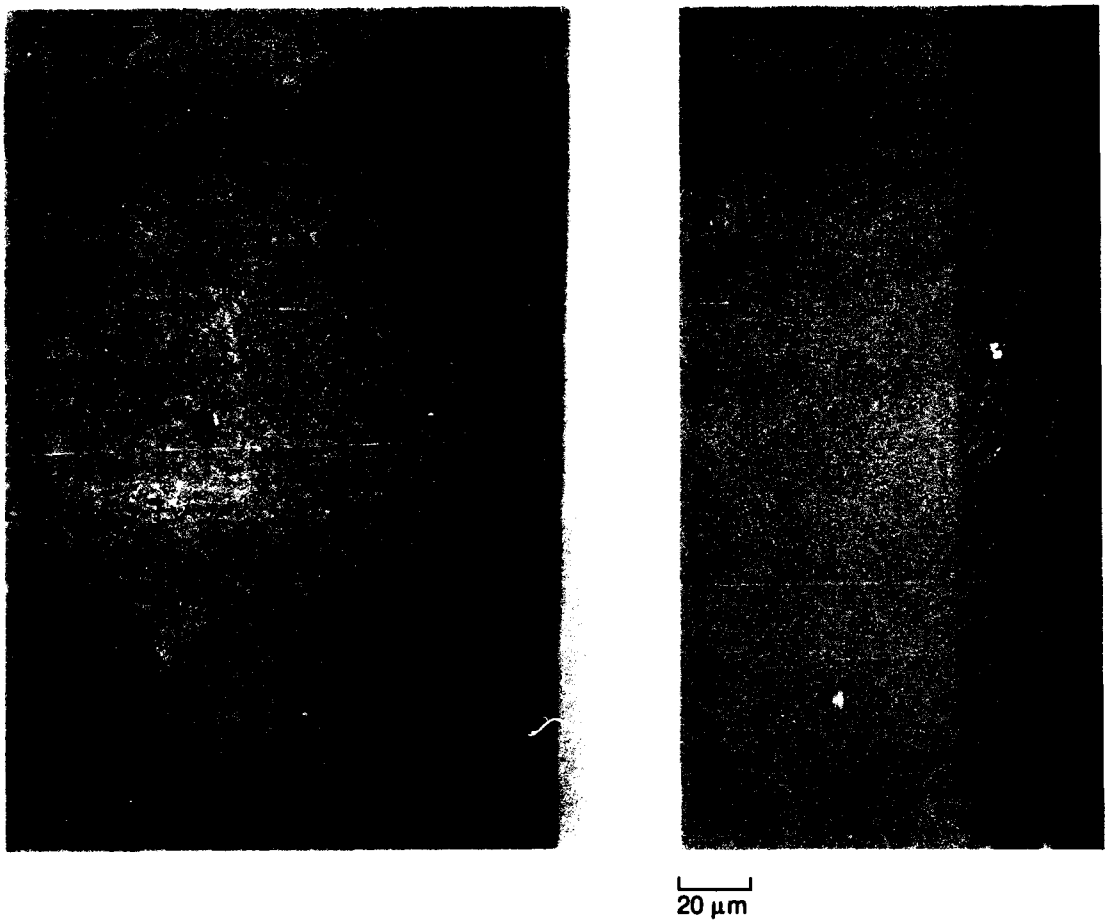

Figure 67. Surface Condition and Typical Microstructure of Quad Cycle/Shutdown TMF Specimen (Exposure Time = 11,600 Cycles)

A sample of PWA 1480/PWA 276 NiCoCrAlY exposed to the quad/shutdown (from 800°F) cycle failed in 8,967 cycles. Heavy rumpling, initiation of secondary cracks at the valley of the rumples, and preferential β-phase oxidation in the vicinity of the cracks were discernable in the microstructure (Figure 68). Microstructural degradation of the two-phase NiCoCrAlY was considerably less than that of PWA 275 in the same cycle, although oxidation effects may have influenced coating durability in that the fracture surface of the coating and some of the secondary cracks appeared to follow the γ-β interface, (i.e., the path of preferential oxidation).

Lastly, to examine the initial stages of microstructural degradation, a shutdown sample was run for 4000 cycles on both PWA 275 aluminide and PWA 276 NiCoCrAlY coatings. No cracks were detected on visual inspection of the aluminide, although substantial grain boundary oxidation was evident in the cross section, and the initial stages of eventual undercutting and spallation of the β-NiAl layer were obvious (Figure 69). The PWA 276 sample was heavily rumpled, and TMF cracks were initiating at some of the rumples (Figure 70).

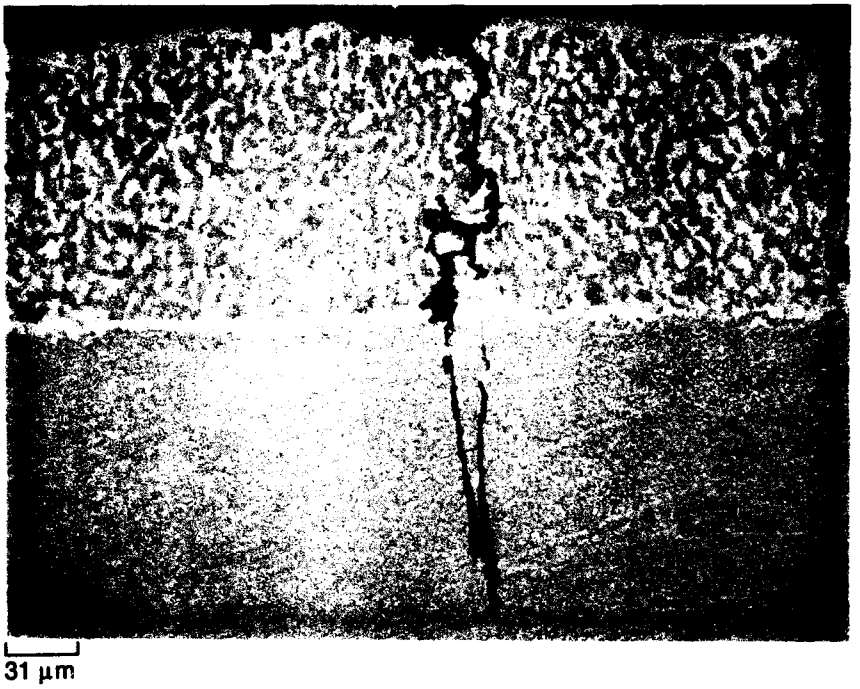

FD 357829

Figure 68. Hot Section Microstructure of Quad Cycle/Shutdown TMF Specimen of PWA 1480/PWA 276 NiCoCrAlY (Cycles to Failure = 8967)

The N_f value for the overlay coating (about 9,000 vs 14,000 for the baseline quad) suggests the shutdown aggravates the TMF process. The machanism of degradation of the 275 aluminide, however, is still determined by the shape of the quad, and oxidized grain boundaries apparently do not propagate into the substrate in spite of the increased tensile loads in the shutdown step.

6.3.3 Hold Time Effects

Hold time in the TMF test cycle simulates steady-state conditions at constant engine power. In tests so far performed, hold time was imposed at maximum temperature of the cycle for the purpose of increasing coating/substrate interdiffusion. Shortened cyclic life due to the hold time was observed, but post-test metallography suggested the effect was not attributable to oxidation of the coating or to coating/substrate interdiffusion.

To supplement the original Task I experiments, isothermal holds were imposed in the cool-down portion of the quad cycle (1800°F under 11.4 KSI tensile stress). This condition is believed to be more realistic than interruption of the cycle at T_{max} and also to be potentially damaging because cracks are being pulled open at temperatures less than T_{max} but still hot enough that rates of oxidation could be significant.*

* Tensile load at T_{max} of the quad cycle is about 3 ksi. Although not at the moment predictable from basic principles, it is not inconceivable that hold times at slightly lower temperature but higher tensile stress could be more damaging than the T_{max} effect because of a stress/oxidation interaction.

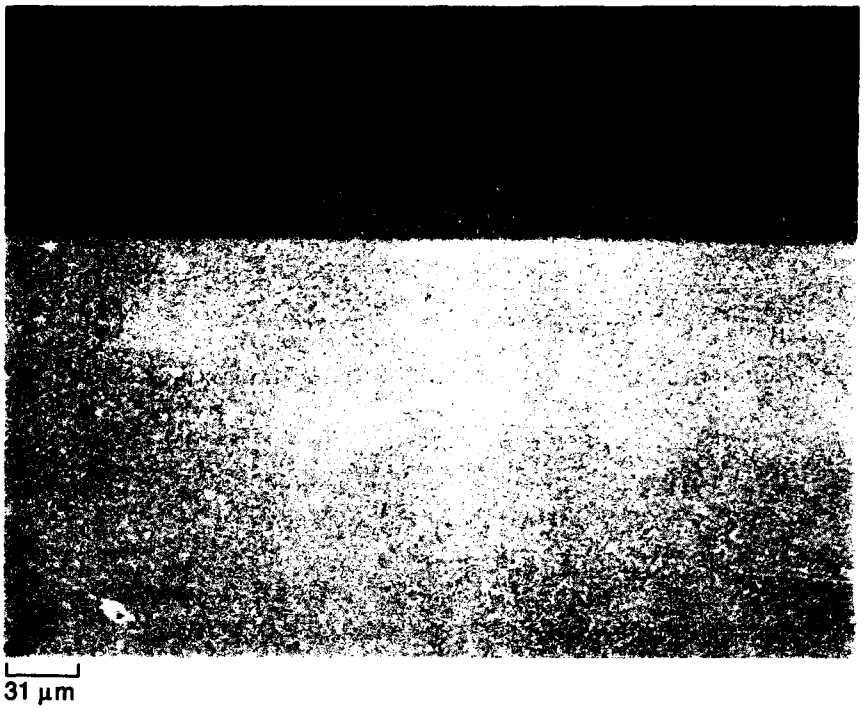

FD 357830

Figure 69. Hot Section Microstructure of Quad Cycle/Shutdown TMF Specimen of PWA 1480/PWA 275 Aluminide (Exposure Time = 4000 Cycles)

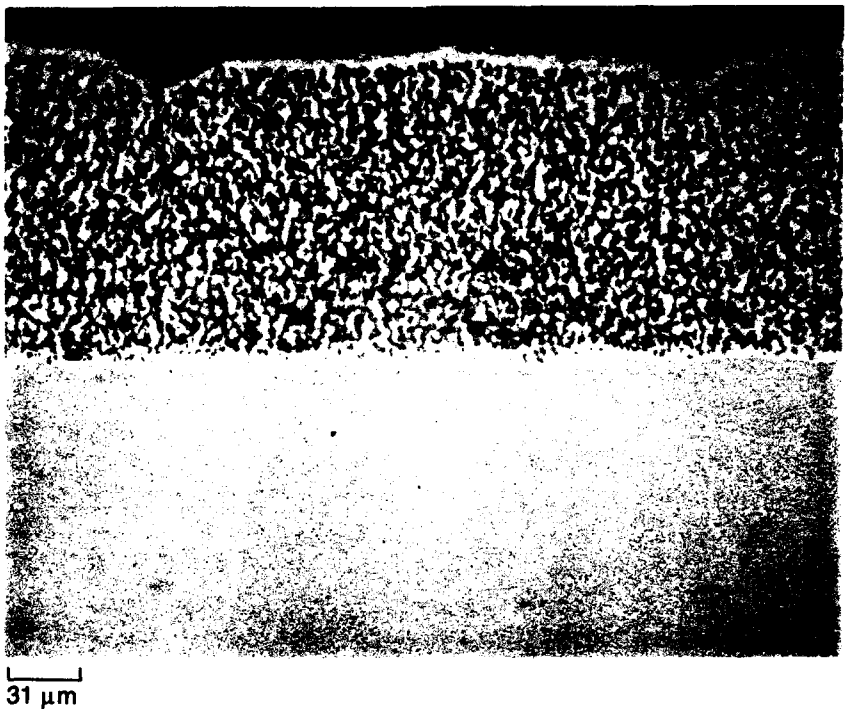

FD 357831

Figure 70. Hot Section Microstructure of Quad Cycle/Shutdown TMF Specimen of PWA 1480/PWA 276 NiCoCrAlY (Exposure Time = 4000 Cycles)

Typical results were that PWA 276 NiCoCrAlY failed in slightly shorter exposure times (approximately 10,500 vs 12,000 in the baseline quad cycle at the same temperature limits and strain range). Post-test metallography showed the center gage section was completely devoid of β-NiAl, and the uncoated ID was characterized by numerous oxide mounds and deep (150 μm oxidized cracks (Figure 71). Only one coating-initiated secondary crack propagated more than 100 μm beyond the coating/substrate interface, and the fracture profile suggested that oxidation/cracking behavior of the ID contributed to breakage of the sample.

Metallography of short-time specimens, i.e. 3000 to 6000 cycles, indicated similar microstructural features, with the extent of strain-induced oxidation perhaps being slightly aggravated by the hold time.

6.3.4 Mean Stress and Quad Cycle Shape Effects

Plans to study mean stress effects were expanded into arbitrary changes in cycle shape to attempt definition of the role of key cyclic variables. The work was considered necessary because the concept of the quad cycle was still believed to be fundamentally correct, but apparently critical details of cycle shape and/or testing speed had not been fully resolved.

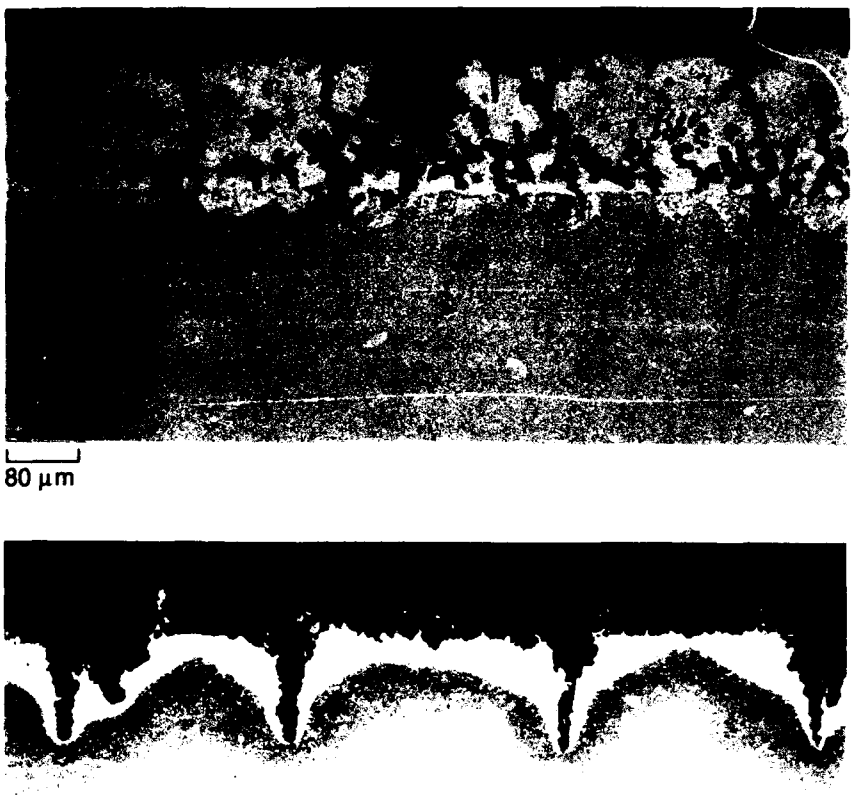

FD 357832

Figure 71. Center Gage Microstructure of Quad Cycle TMF Specimen of PWA 1480/ PWA 276 NiCoCrAlY (2-Minute Isothermal Hold at 1800°F on Cool-Down Step, Cycles to Failure = 10,520)

A key experiment was the triangular cycle sketched in Figure 72. The cycle was designed to have the same strain range and temperature limits as the quad but avoid the 1800 — 2000°F leg believed to be causing the strain-induced oxidation.

An aluminide-coated triangle cycle specimen broke in 2113 cycles, and the coating was not oxidized. In comparison, grain boundary oxidation of coatings on quad cycle specimens is noticeable after only 1000 cycles, but tests have been run up to 15,000 cycles without cracks propagating into the substrate.

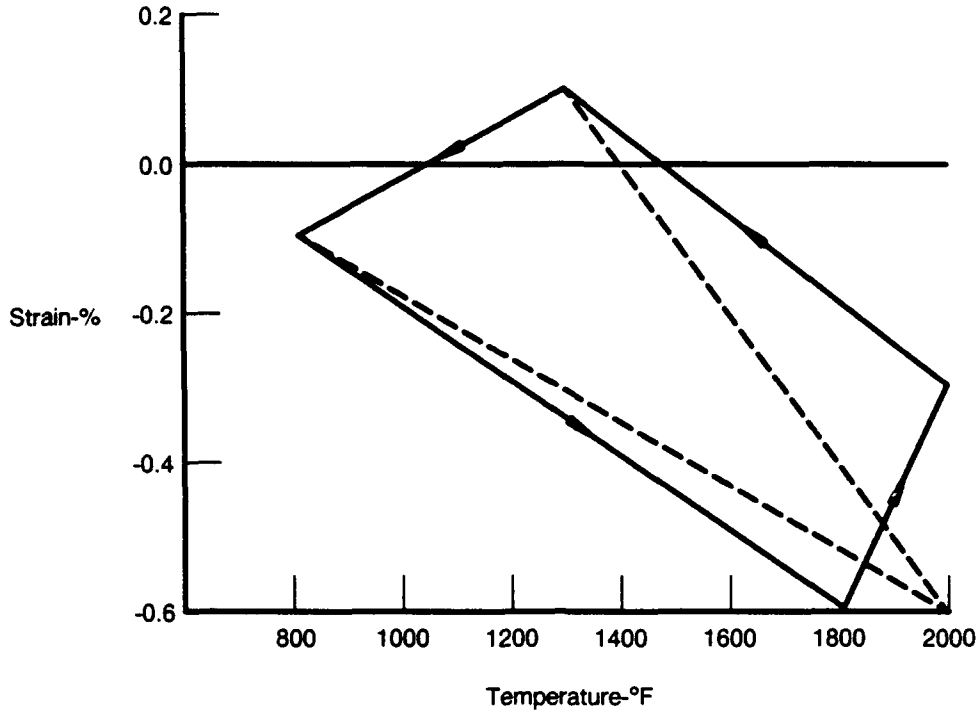

Figure 72. Strain-Temperature Diagram of Quad and Triangle Cycle

This result appears to isolate the strain induced oxidation to the high temperature Type 2 leg of the quad cycle, i.e. the portion of the quad cycle involving simultaneously increasing temperature and tensile stress. It also suggests that the length and/or temperature limits of the type 2 leg should impact both cycles to failure data and degradation microstructure.

The next arbitrary shape change was made in response to recently acquired ATEGG program heat transfer data which led to prediction of generally narrower strain/temperature cycles and higher mean strains. Figure 73, for example, is a node on the leading edge of an F100 vane where TMF cracking was encountered. A key feature of the quad cycle — namely that maximum compression is reached short of maximum temperature — is still predicted, but the section between maximum compressive strain and maximum temperature is much shorter.

A cycle reflecting the points just discussed — but retaining enough continuity with the old cycle to permit definition of shape effects — is sketched in Figure 74. Duplicate samples of aluminized PWA 1480 exposed to the narrow quad broke in 3379 and 8236 cycles respectively; the reason for the relatively large difference is not known, but the comparison with experience on the original wide quad, i.e., >15,000 cycles with severe oxidation but no substrate cracking, is still considered useful and valid.

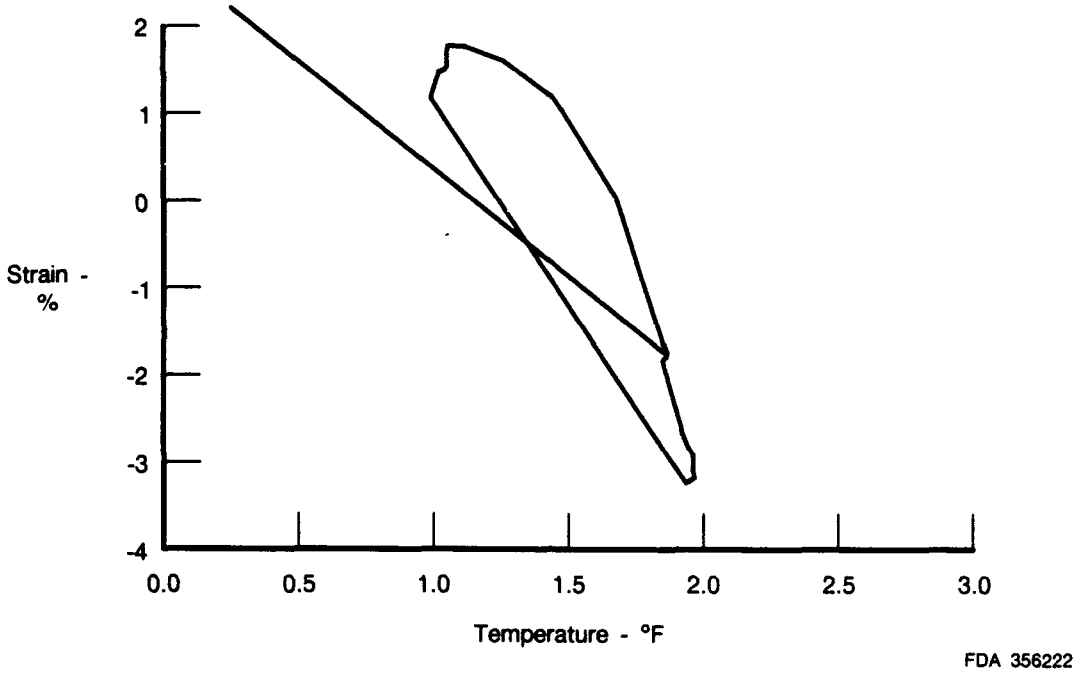

Figure 73. Strain-Temperature Cycle for Leading Edge of F100 1st-Stage Vane

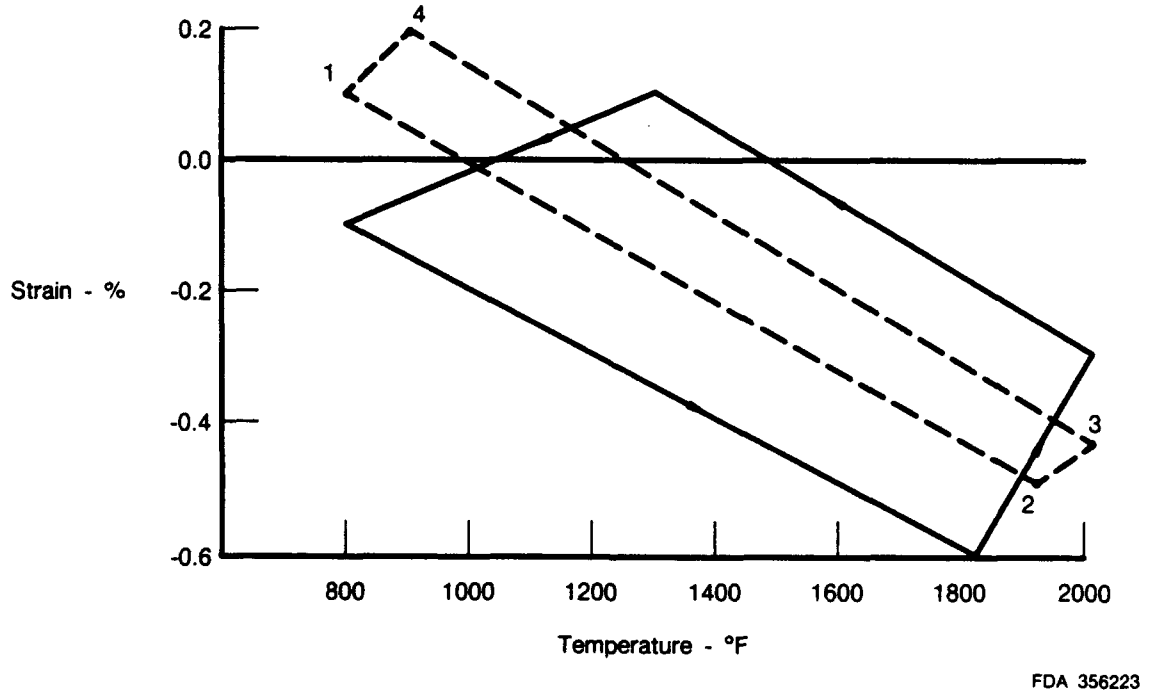

Figure 74. Original Quad and Revised Cycle With Higher Mean Strain and Narrower Shape

Microstructural degradation of the coating on the short-time sample was negligible; after 8,236 cycles there was metallographic evidence of the strain-induced oxidation morphology previously associated with the original, wide quad cycle (Figure 75).

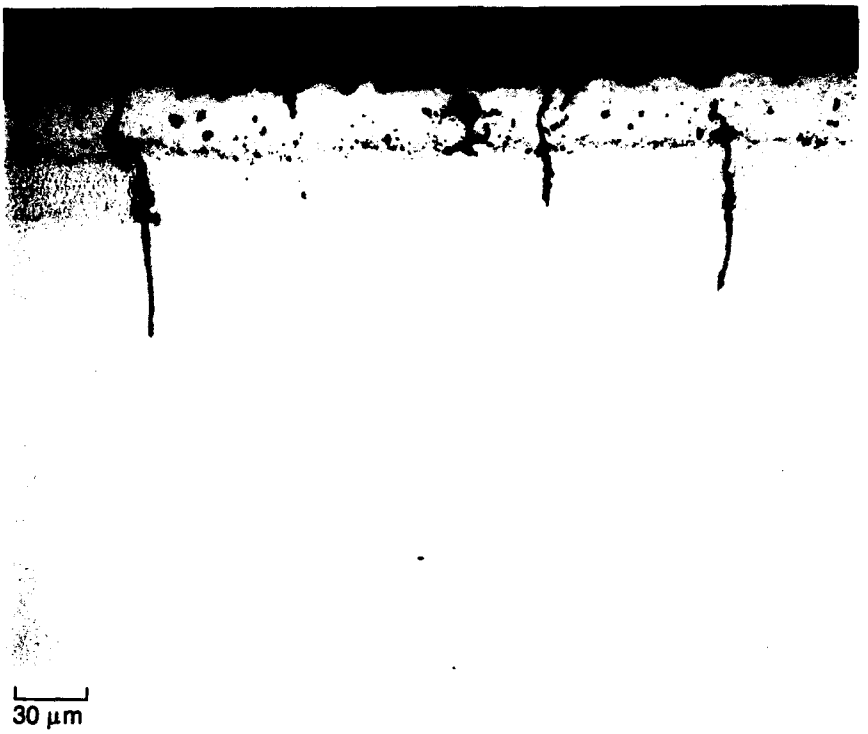

FD 357833

Figure 75. Typical Gage Section Microstructure of Modified Quad Cycle (+0.10%/800°F, −0.50%/1900°F, −0.45%/2000°F, +0.20%/900°F) TMF Specimen of PWA 1480/PWA275 Aluminide (Cycles to Failure = 8,326 at 4 cpm)

A series of systematic shape changes was made by modifying high-temperature strain, i.e., moving point 2 or point 3 in Figure 74. Strain/temperature end-points (adjusted slightly to reflect measured fitting of the wave forms on the TMF rig) and N_f data are summarized in Table 3. Note in the table that 4B through 7B are increasing width of the cycle by moving point 3 to higher tensile strain, while 6C vs 6B involves a temperature change at maximum compression.

Table 3. *Quad Cycle Shape Effects; PWA 1480/275 Aluminide*

Quad #	*Point 1*	*Point 2*	*Point 3*	*Point 4*	*Nf*
Type 1	+0.10%/800°F		−0.60%/2000°F		4594
4B	+0.10%/800°F	−0.50%/1930°F	−0.45%/2000°F	+0.20%/860°F	3779 8326 4566
5B	+0.10%/800°F	−0.50%/1930°F	−0.40%/2000°F	+0.20%/860°F	3526 4971
6B	+0.10%/800°F	−0.50%/1930°F	−0.35%/2000°F	+0.20%/860°F	9331 7553
7B	+0.10%/800°F	−0.50%/1930°F	−0.30%/2000°F	+0.20%/860°F	8418 6160
6C	+0.10%/800°F	−0.50%/1600°F	−0.35%/2000°F	+0.20%/860°F	5587

R19528/10

Although scatter in the data is wider than desirable, the tendency for longer cyclic lifetime with increasing width of the cycle, i.e., type 1 and 4B through 7B, seems established.

Figure 76 compares the typical gage section microstructure of the Type 1 sample with the quad 5B which failed in approximately the same number of cycles. Selected areas would support the argument that grain boundary oxidation is more prevalent in the quad, although the difference is not striking.

Grain boundary oxidation in one of the wider quad samples (7B) is shown in Figure 77. The attack is not nearly as severe as in the original quad, but the nature of the grain boundary oxidation appears similar.

Lastly in this group of experiments, quads 4B through 7B were run for 4000 cycles for documentation of microstructures exposed for identical time-at-temperature; the samples are illustrated in Figure 78. None had cracks extending into the substrate, and the structure of one of the samples (7B) indicates a processing or testing anomaly. Nevertheless the photos appear consistent with the hypothesis of increasing grain boundary oxidation with widening of the cycle.

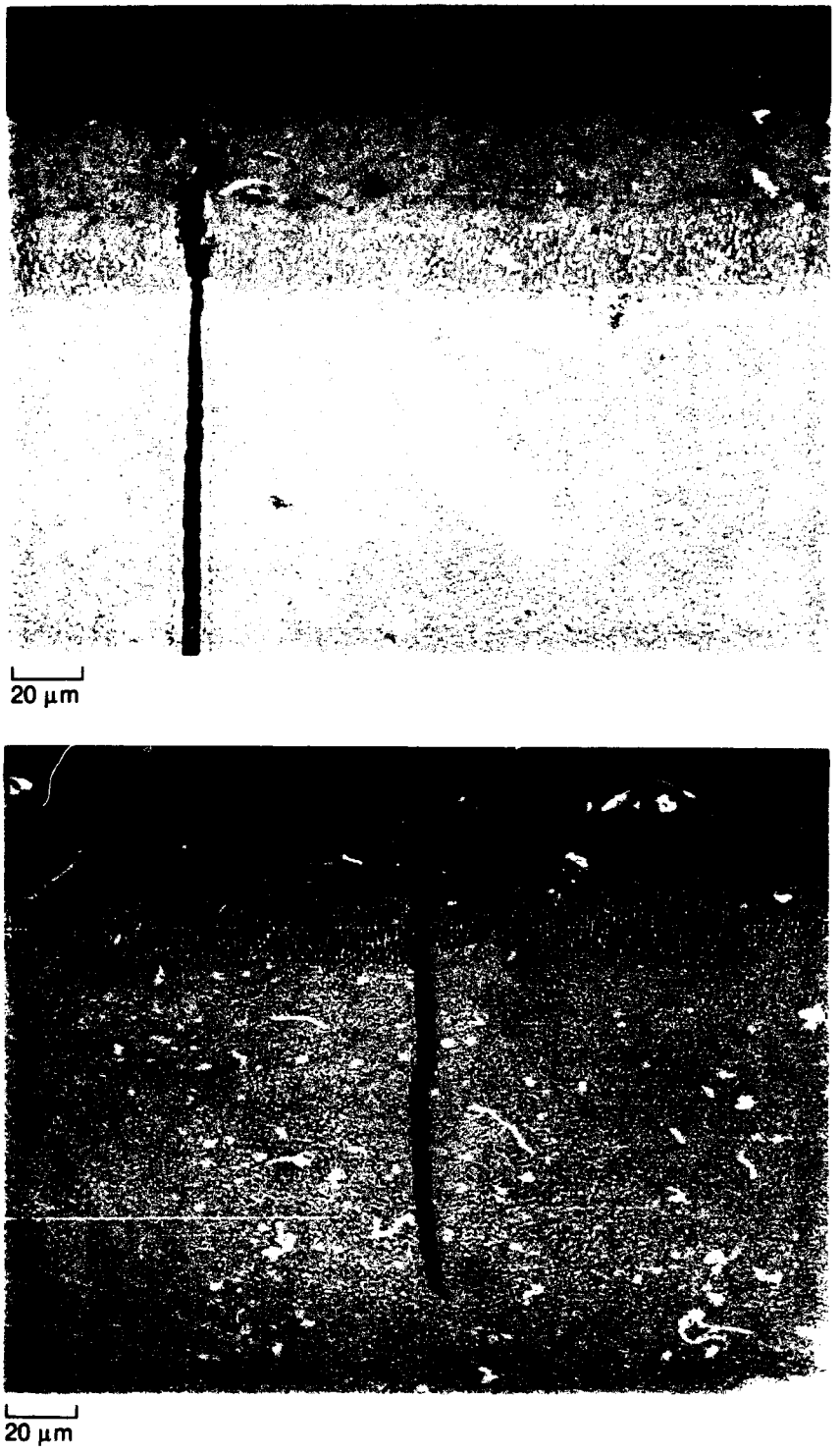

Figure 76. Microstructure of Narrow Quad (Top) Versus Type 1 TMF Sample With Same Temperature Limits and Strain Range (N_f for Narrow Quad = 4971 Cycles; for Type 1, 4954 Cycles)

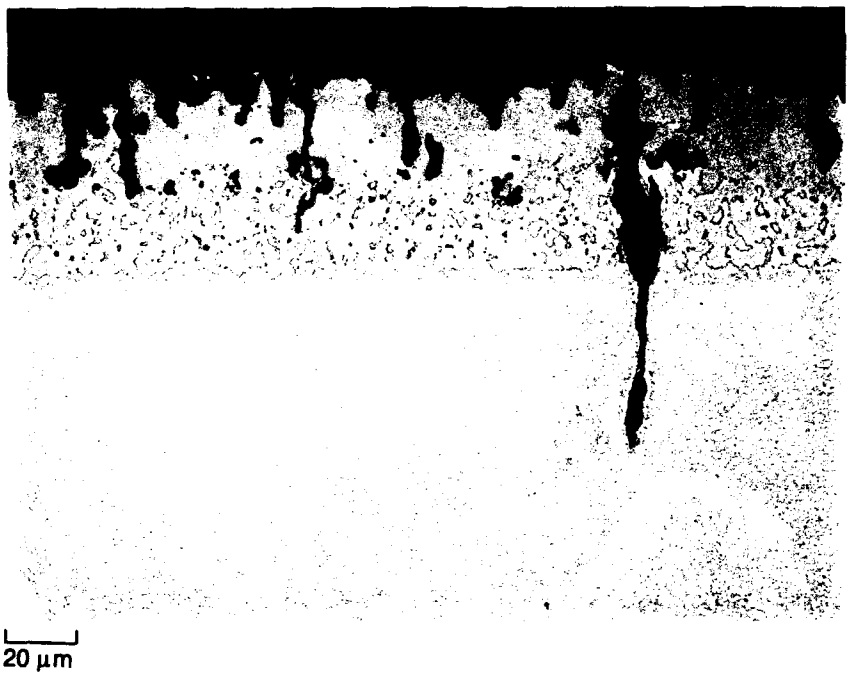

FD 357835

Figure 77. Microstructure of Modified Quad (7B in Table 3) TMF Sample (N_f = 8,418)

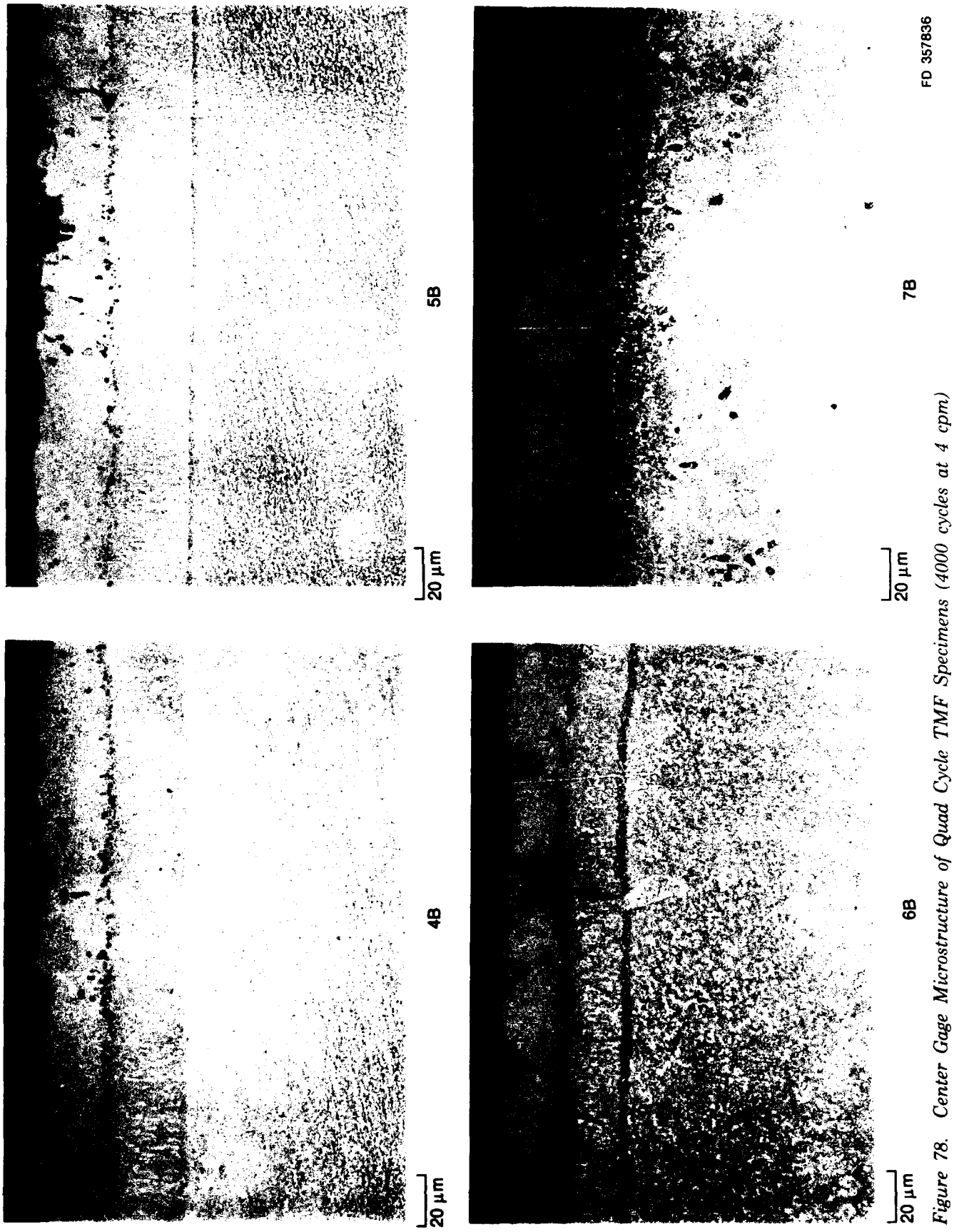

Figure 78. Center Gage Microstructure of Quad Cycle TMF Specimens (4000 cycles at 4 cpm)

SECTION 7.0
LAYERED COATINGS

7.1 OBJECTIVE

Evaluated in this task were a strain isolating system and thin sputtered ceramics over PWA 276 NiCoCrAlY. The former was intended to arrest surface-initiated cracks; the latter, to reduce the TMF-generated rumples which appear to be the precursor of TMF cracks in NiCoCrAlY.

7.2 BACKGROUND AND APPROACH

7.2.1 Strain Isolation Layers

A design approach toward improving the fatigue resistance of an overlay coating is the introduction of a compliant layer between the coating and the superalloy substrate as shown in the schematic diagram of Figure 79. The microstructure of the compliant layer is characterized by a substantial volume fraction of oxide particles or non-interconnected voids which reduce the effective elastic modulus and tend to arrest any cracks which initiate in the oxidation resistant surface layer.

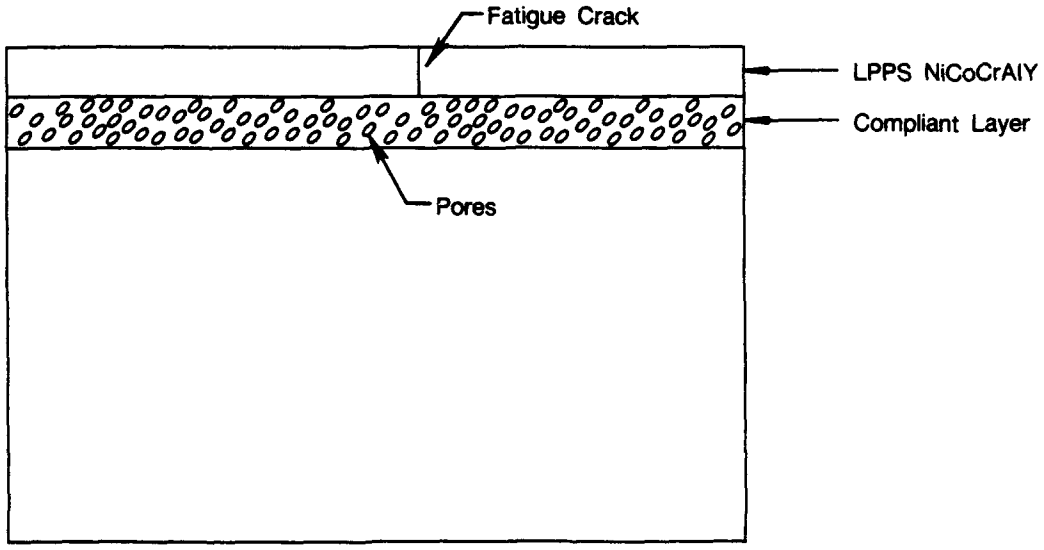

Figure 79. Schematic Diagram of Strain Isolator Concept for Design of Fatigue-Resistant Overlay Coating

Possible techniques for depositing the compliant layer include plasma spraying in air, plasma spraying at low pressures with coarse powder, and plasma spraying at low pressures with a polyester fugitive which would be subsequently removed in a post-coating heat treatment.

7.2.2 Ceramic Overlayers

Application of thin ceramic overlayers was carried out by sputtering, and quad cycle TMF tests were performed to evaluate the effectiveness of the overlayer.

7.3 RESULTS AND DISCUSSION

7.3.1 Strain Isolation Layers

Cycles to initiation/failure data from this task are not interpretable, due primarily to coating adherence problems. Coating separation was often evident from nonuniform heating and cooling during the TMF cycle, and this problem precluded effective temperature control during test as well as meaningful post-test metallography.

Figure 80 for example, shows a type 1 specimen which was stopped after 900 cycles because of visual observation of nonuniform temperature cycling (the discontinuity at the coating/substrate interface interferes with heat flow). Numerous cracks already extend through the coating. Indeed the cracks are stopped when the coating separates from the base alloy, but such a situation is unlikely to be of either practical or mechanistic interest.

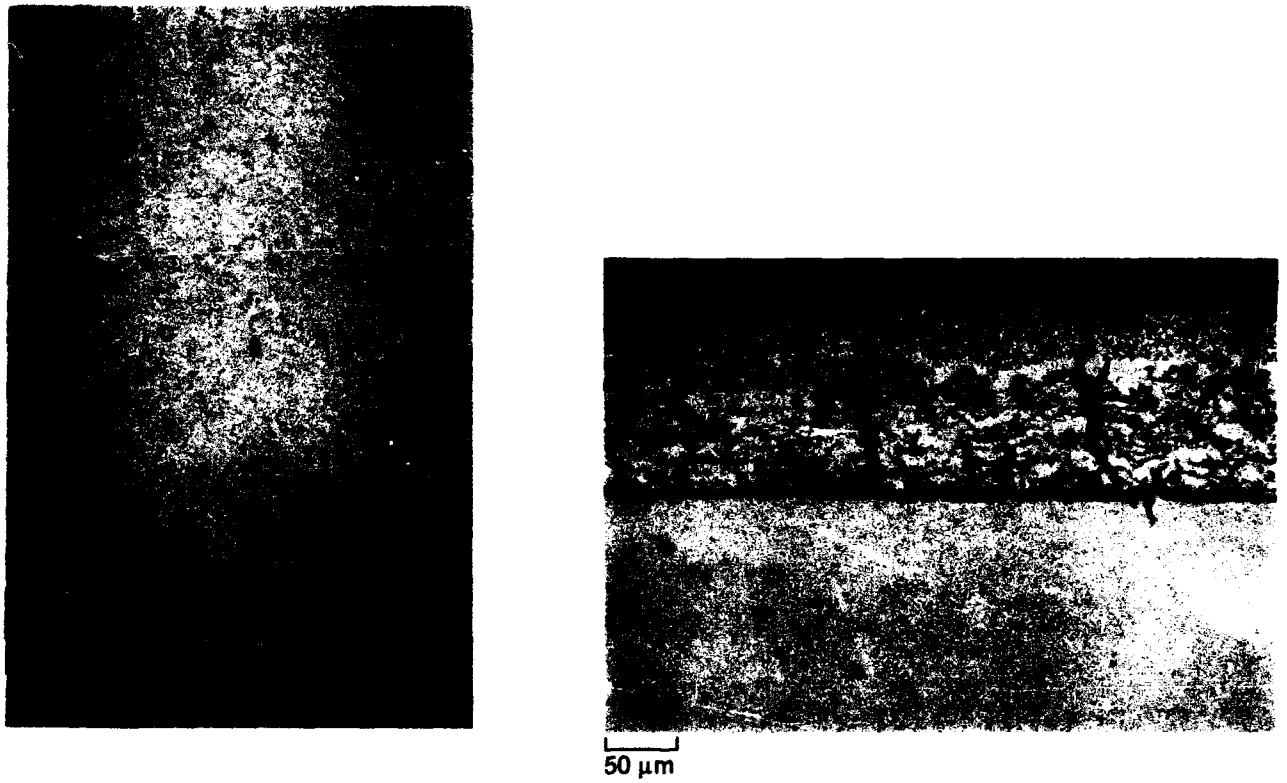

Figure 80. Surface Condition and Gage Section Microstructure of Strain Isolator Coating After 900 Type 1 Cycles at 0.7% Strain Range.

A specimen run to failure in a Type 1 test is illustrated in Figure 81. Many cracks are stopped because of interfacial separation, but adherence in localized areas is apparently sufficient for many others to propagate into the substrate.

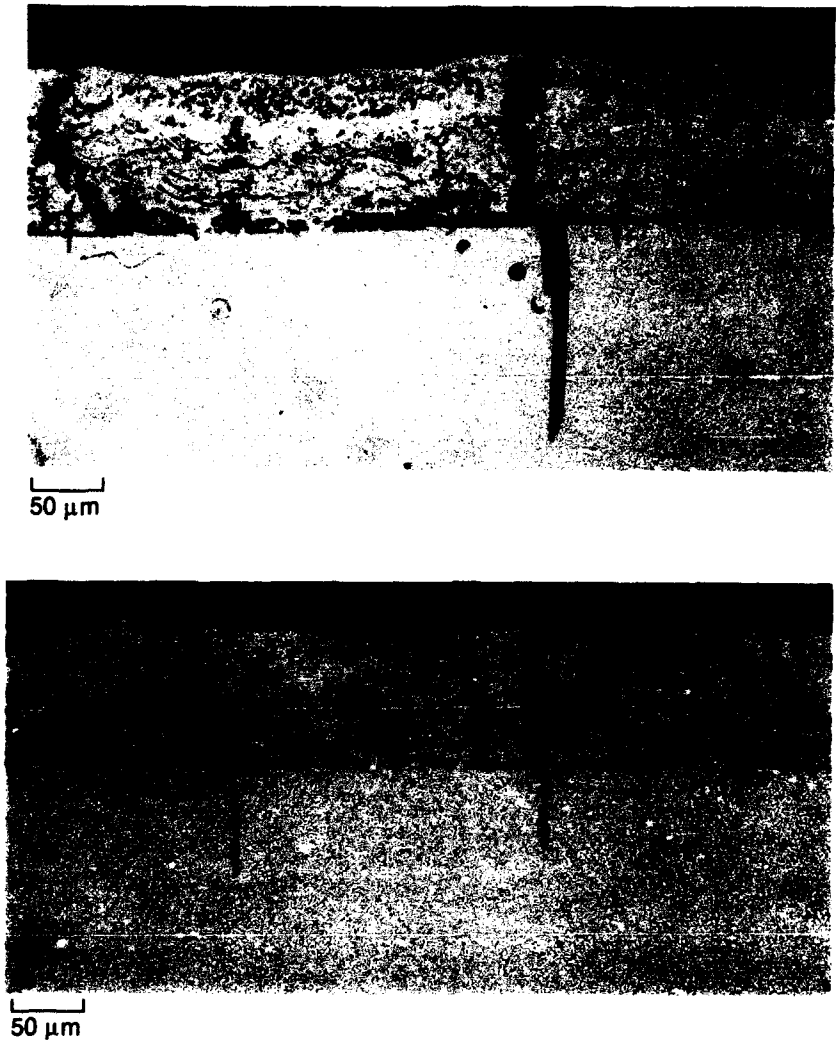

Figure 81. Typical Microstructure of Two-Layer Strain Isolator Coating (Type 1 TMF Cycle, 800-2000°F, N_f = 3179 at 2 cpm)

As expected from previous results, quad cycle specimens were run to much longer exposure times. Except for debonding, however, there was no evidence that cracks were effectively arrested, and coatings usually fell off when the samples were cut for metallography.

7.3.2 Ceramic Overlayers

Thin layers of Al_2O_3 (estimated thickness: 1-2 µm) were sputtered onto lathe-polished PWA 276 NiCoCrAlY for testing in quad TMF cycles. Surface rumpling, as judged by visual inspection and longitudinal cross sections, appeared slightly diminished, but numerous ring cracks developed in the ceramic and propagated into the metallic coating. There was no improvement in cycles to failure values.

SECTION 8.0
GENERAL DISCUSSION AND CONCLUSIONS

This section attempts a broad, general interpretation of the significance of some of the results in this program and their implication on fundamental understanding and further research into high temperature fatigue behavior. The general conclusions fall into the following major areas:

8.1 ROLE OF COATING OXIDATION AND COATING/SUBSTRATE INTERDIFFUSION

A basic premise in the original formulation of this program was the hypothesis that initiation of TMF cracks might be related to time-dependent changes in composition and microstructure of overlay coatings. Accordingly, it was postulated that TMF cracks initiate in the coating because mecahnical properties of the as-deposited coating material degrade as the composition (and, consequently, the morphology and volume fraction of the phases in the microstructure) of the coating is altered by oxidation and interdiffusion.

The proposed tests, however, did not relate crack initiation or specimen failure data to coating oxidation or coating/substrate interdiffusion. Type 1 cycles caused initiation and propagation of coating cracks long before metallographically discernable surface oxidation and significant alteration in thickness or microstructure of the coating and interdiffusion zone was noted. In the opposite direction, a cycle which aggravated coating oxidation was identified, but the nature of TMF cracking of overlay coatings was not affected, and aluminide coatings were so severely oxidized that the coating was completely destroyed without propagating any TMF cracks into the substrate material.

Since the temperature limits and strain ranges employed in the testing program are still considered realistic, these results imply that TMF behavior — at least that of current generation MCrAlY coatings (and similar Ni-Cr-Al compositions) on Ni-base superalloys — is a mechanical behavior problem which is not significantly affected by bulk coating oxidation or coating/substrate interdiffusion. For the diffusion aluminides, overall durability and failure mode of the coating/substrate system appears more strongly dependent on cycle shape effects. The magnitude of these effects is difficult to quantify; its nature and direction are that open cycles (i.e. a quad as opposed to the straight line Type 1) increase the relative importance of oxidation processes (versus the TMF cracking without noticeable coating oxidation in Type 1 cycles).

8.2 TYPE 1 VERSUS QUAD-SHAPED CYCLES

Important differences between Type 1 and quad cycles were identified and appear to be qualitatively understood. More difficult, however, is the judgement of which cycle is more useful, both as a research tool and as an indication of relative engine performance and failure mechanism.

The argument for Type 1 is simplicity and faster testing time. Considering typical scatter in fatigue data and the need for extensive testing to establish statistical confidence, testing time is a major consideration in the scheduling and economic feasibility of TMF research and design data generation.

If Type 1 is cheaper and faster, an argument for the more complex and time- consuming quad cycle must be based on better relevance to engine experience or definition of mechanistic effects which are not revealed in Type 1 tests. In the former area, it appears that the quad cycle as run in this program reproduces at least somewhat a critical item of engine experience — namely, that TMF cracks in overlay coatings invariably propagate into the substrate, while

cracks in diffusion aluminides sometimes stop at the interdiffusion zone. The microstructural correlation of engine hardware and quad cycle TMF specimens is not perfect, but the marked difference in overlay versus aluminide coatings in Type 1 versus quad cycles still appears to indicate that the quad cycle better simulates engine conditions and demonstrates a critical difference in behavior of aluminide versus overlay coatings which is not observed in Type 1 testing.

Whether or not there is a fundamental mechanistic difference between quad and Type 1 cycles probably depends on the type of coating. For overlay coatings of composition and microstructure similar to PWA 276 NiCoCrAlY, the quad cycle induces a unique oxidation morphology in the form of preferential consumption of the β-NiAl phase (leaving holes in an otherwise unoxidized coating). In spite of this microstructure, however, crack initiation is still related to surface rumpling, i.e., cracks initiate in the valleys of the rumples. For a given strain range and temperature limit, the severity and amplitude of rumpling produced by quad versus Type 1 cycles are not strikingly different. Also, for realistic test conditions, coating cracks initiate in the quad cycle long before the β-NiAl phase is completely consumed. Hence, it appears that neither the mechanism of crack initiation nor the tendency for propagation of coating cracks into the substrate are significantly influenced by oxidation processes in the quad cycle.

Strain-induced oxidation also occurs in quad cycle testing of aluminide coatings, and there is a more striking difference between Type 1 and quad cycles in that the coating is completely destroyed prior to crack formation in the substrate. High strain range Type 1 tests, for example, fail in less than 5000 cycles, and there is no metallographic evidence of surface or grain boundary oxidation (Figure 71). After much shorter exposure times, however, the quad cycle causes oxidation of virtually all of the grain boundaries in the hot section (Figure 69). Longer exposure times in the quad cycle promoted severe coating degradation, but no TMF cracks progagated into the substrate (Figures 68 and 70).

8.3 SHUTDOWN STEPS

It seems almost axiomatic that a shutdown step is an increase in severity of test conditions. Indeed, in the case of quad cycle testing of PWA 276 NiCoCrAlY, N_f values were lower than data of corresponding cycles without the shutdown step. The nature of surface rumpling and development of rumples into TMF cracks was still the same, however, so it is difficult to envision a fundamental change in mechanism due to the shutdown step.

In the case of aluminide coatings, the effect of the shutdown step was probably masked by the severe coating degradation induced by the quad cycle. The dominant factor for the range of variables studied in this program was obviously the shape of the quad; neither the failure mechanism nor the number of cycles to coating spallation were significanly impacted by shutdown steps in the cycle shapes examined.

8.4 HOLD-TIME EFFECTS

Basically, there are three possible mechanisms of a hold-time effect: (1) loss of load-bearing cross section due to coating/substrate interdiffusion and bulk surface oxidation, (2) time-dependent dislocation motion in the stressed substrate material, and (3) oxidation at the crack tip. The first of these is self-explanatory; the second or third could induce crack growth during the isothermal hold and/or affect the value of da/dn on the next cycle.

Hold times imposed at T_{max} of the quad cycle were found to decrease N_f values (Section 4.2.4.5), but the effect was clearly not attributable to coating oxidation or coating/substrate interdiffusion. Surface oxidation and loss of cross section were negligible, and the life-limiting TMF cracks were much deeper than the interdiffusion zone.

REFERENCES

1. Rau, C.A. Jr., A.E. Gemma, and G.R. Leverant: Thermal Mechanical Fatigue Crack Propagation in Nickel and Cobalt-Base Superalloys Under Various Strain-Temperature Cycles. Fatigue at Elevated Temperatures, ASTM STP 520 (1973) pp. 166-178.

2. Linask, I and J. Dierberger: A Fracture Mechanics Approach to Turbine Airfoil Design. Paper No. 75-GT-79, Gas Turbine Conference and Products Show, Houston, TX, March 1975.

3. Strangman, T.E. and S.W. Hopkins: Thermal Fatigue of Coated Superalloys. Ceramic Bulletin 55, No. 3 (1976) p. 304.

4. Halford, G.R. and S.S. Manson: Life Prediction of Thermal Mechanical Fatigue Using Strain Range Partitioning. Thermal Fatigue of Materials and Components, ASTM STP 612, D.A. Spera and D.F. Mowbray, Eds., American Society for Testing and Materials, 1976, pp. 239-254.

5. Strangman, T.E. and S.W. Hopkins: Thermal Fatigue of Coated Superalloys. Ceramic Bulletin 55 (1976) pp. 304-310.

6. Strangman, T.E.: Ph.D. Thesis, Univ. of Connecticut, 1978.

7. Fujimo, M and S. Taira: Effect of Thermal Cycle on Low Cycle Fatigue Life of Steels and Grain Boundary Sliding Characteristics. Proc. Third International Conf. on Mechanical Behavior of Materials, Cambridge, UK (1979).

8. Warren, J.R. and B.A. Cowles: Thermal Mechanical Fatigue Screening Method for Gas Turbine Engine Applications. Paper No. AMMRC MS 82-4, Presented at Army Symposium on Solid Mechanics, Bass River, MA (1982).

9. DeLuca, D.P. and B.A. Cowles: Fatigue and Fracture of Advanced Blade Materials. AFWAL-TR-84-4167.

10. Barkalow, R.J., R.J. Hecht, and R.L. Shamakian: Advanced Coating Research and Development. AFWAL-TR-83-4086, February 1985.

11. Wilson, D.A. and J.R. Warren: Thermal Mechanical Crack Growth Rate of a High Strength Nickel Base Alloy. ASME paper No. 85-GT-12.

12. Bain, K.R.: The Effect of Coatings on the Thermomechanical Fatigue Life of a Single Crystal Turbine Blade Material. Paper No. AIAA-85-1366, Amer. Inst. of Aeronautics and Astronautics, Presented at 21st Joint Propulsion Conf., Monterey, CA, 1985.

13. Sellers, R.R.: Control of Gas Turbine Power Transients for Improved Turbine Airfoil Durability. Paper No. AIAA-82-1182, Amer. Inst. of Aeronautics and Astronautics, June 1982.